Improving the Acoustic Absorption of Vertical Greening Systems

By Jesse Bakker

VERTICAL OMEGA PROFILES

LOCAL IRRIGATION SYSTEM

GLASS WOOL CAVITY FILL

WATER-RESISTANT GEOTEXTILE

HELMHOLTZ RESONATOR BACKING PLATE

SUBSTRATE LAYER HYDROPONIC ROCK WOOL

CUBE INSERTS FOR PLANT ROOTING

PLANTS WITH HIGH LEAF AREA DENSITY

TUDelft Delft University of Technology
Faculty of Architecture
and the Built Environment

This page is intentionally left blank

Improving the
Acoustic Absorption of
Vertical Greening Systems

by Jesse Bakker

to obtain the degree of Master of Science
at the Delft University of Technology
to be defended publicly on 28th of June, 2021 at 13:00

ing. J. (Jesse) Bakker
Master student Building Technology
Student number 4984544
J.J.Bakker-3@student.tudelft.nl

Mentors

Dr. ir. M. (Martijn) Lugten
Building Physics & Services
Faculty of Architecture and the Built Environment

Dr. ir. M. (Marc) Ottelé
Materials, Mechanics, Management & Design
Faculty of Civil Engineering and Geosciences

Dr. ir. M. (Martin) Tenpierik
Building Physics & Services
Faculty of Architecture and the Built Environment

TUDelft Delft University of Technology
Faculty of Architecture
and the Built Environment

Abstract

Noise pollution is a growing health concern in cities, especially in busy streets with parallel reflective facades, known as urban street canyons. Here, high flows of vehicular traffic generate a broadband noise, with high noise levels in the low-frequency (LF) spectrum. In the canyons, noise decays slowly due to multiple reflections. To counter this, vertical greening systems (VGS) can be applied as multi-disciplinary solutions. Not only can these systems attenuate noise, they can also e.g. decrease the urban heat island effect and increase biodiversity. Yet, the shortcoming of VGSs is the lack of LF-absorption. Hence, the following research question was asked: "How can the acoustic absorption of vertical greening systems in urban street canyons be improved, especially for low-frequency noise?"

Four concept designs were developed consecutively, and evaluated on the basis of design criteria. These criteria included specifications on acoustic absorption, manufacturability, and durability. The final design consisted of a living wall system (LWS) based on hydroponic rock wool, with a parallel array of Helmholtz resonators integrated in its structure. This array was added to increase the LF-absorption of the VGS below 250 Hz. The Helmholtz cavity volumes were not physically subdivided, but rather filled with a locally reactive material with a low flow resistivity, to enforce propagation that is normal to the surface. Additionally, plants can also absorb sound in the visco-thermal boundary layer around their organs, depending on the leaf area density. It was found that sciophytes (shade-loving plants) had most acoustic potential due to their large leave surfaces.

Analytical, experimental, and numerical validation was performed. A Matlab script was developed that applied Delany-Bazley-Miki equations in an equivalent fluid model, and a transfer-function approach for the multi-layer complex impedance. The design yields near-unity absorption for $f>500$ Hz. The resonators extended the LF-absorption ($\alpha>0.5$) down to 80 Hz. Impedance tube and reverberation room measurements demonstrated that piercing the porous substrate layer with the Helmholtz resonator necks can yield a combined acoustic absorption. Finally, acoustic simulations showed that applying the proposed LWS to the facades in a reference urban street canyon in Rotterdam can substantially decrease sound levels, both inside the street canyon, as well as in the adjacent courtyard canyon. However, the window-to-wall ratio of the facade largely determines to what extent sound levels can be decreased, since vertical greenery cannot be applied in front of windows.

Table of contents

Discussion & Conclusion

Appendices

List of symbols and abbreviations

Symbols

α	Absorption coefficient
α_∞	Tortuosity
A	Area
c	Speed of sound
δ	Neck end correction factor
d	Layer thickness
D	Diameter
ε	Resonator porosity
f	Frequency
h	Height
i	Imaginary number
θ	Dominant angle of leaf orientation
k_o	Normal wavenumber
k_d	Complex wavenumber
λ	Wavelength
ρ	Density of air
σ	Flow resistivity
S_r	Saturation rate
r_m	Acoustic resistance
r	Radius
V	Volume
ω	Angular frequency
Ω	Porosity
Z	Normalized surface impedance
Z_c	Characteristic impedance

Abbreviations

HF	High frequency
LAD	Leaf area density
LF	Low frequency
LWS	Living wall system
MF	Middle frequency
SPL	Sound pressure level
VGS	Vertical greening system
WWR	Window-to-wall ratio
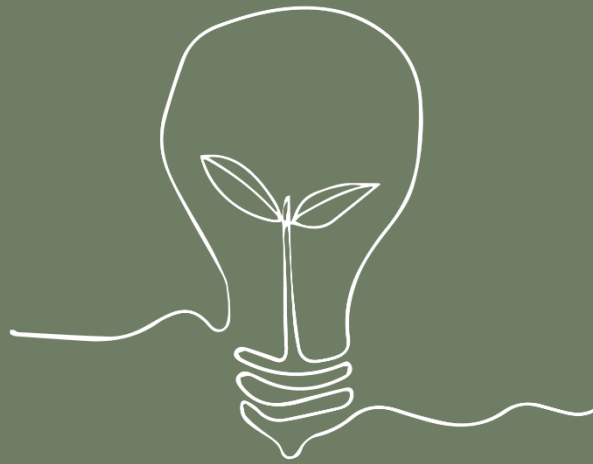
Introduction

1. Introduction

1.1. Problem statement

Noise pollution is the second largest environmental cause of health problems, after air pollution (Ribeiro et al., 2020; World Health Organization, 2011). This problem is a growing concern, especially in urban environments. One in three is annoyed by intermittent or persistent high noise levels, and the sleep quality of one of five is disturbed by environmental noise. Long-term exposure to noise contributes to stress-induced health effects, including cardiovascular diseases (hypertension, ischemic heart disease, high blood pressure), cognitive impairment in children, tinnitus, and decreased focus and mental well-being, due to interrupted sleep cycles (EEA, 2014; Halperin, 2014). Additionally, the economic implications are dire too, as the estimated social cost equal 0.4% of the EU's GDP (EU CORDIS, 2013). It is expected that urbanization will increase up to 68% by 2050 (UNDESA, 2018), consequently subjecting an increasingly larger portion of the world population to noise pollution (Pérez et al., 2018).

The primary source of noise in cities is vehicular traffic, e.g., cars, trains, trams, and motorcycles (Den Boer and Schroten, 2007; Shield and Dockrell, 2008). This noise generally contains acoustic energy across a broadband spectrum, most of which is perceivable by the human ear (Hygge, 2003). Since vehicle speed is typically low in cities (i.e. $v \leq 50$ km/h), most noise emission is caused by fuel combustion in engines, and vibrations in the transmission and exhaust. Constant idling and acceleration magnify the noise emission, causing peaks in the sound levels for low frequencies, down to 50 Hz. Even though the A-weighting decreases the significance of low-frequency sound levels, the applicability of the weighting on traffic noise is disputed. This is because humans react to sound on a highly subjective manner (Porges, 1977). Hence, low-frequency noise is perceived to be more annoying than high-frequency noise (Leventhall et al., 2003).

Facades in cities are made of acoustically reflective materials, such as concrete and glass (Davis et al., 2017). When such facades flank a road on both sides, it is known as an urban street canyon (Vardoulakis et al., 2003). Noise in the canyon reflects multiple times, which causes long decay times. This increases the overall sound pressure levels in the vicinity of the canyon (Ding et al., 2013). Architects and engineers can reduce the multiple scattering characteristics by adding absorptive materials to the existing facades. This can be achieved with artificial cladding, e.g., by application of perforated panels or slotted bricks. However, the application of vertical greening systems (VGS) has most potential. These systems are multi-disciplinary solutions that not only absorb sound, but also improve air quality, increase biodiversity, and diminish the urban heat island effect (Ottelé et al., 2011; Perini et al., 2011). A comparison between VGSs and classic sound absorbing materials is given in Table 1. The diverse qualities of vertical greening make it an integral solution for multiple environmental challenges in urban streets.

	Absorbs sound	Improves air quality	Increases biodiversity	Diminishes urban heat island	Improves thermal insulation	Improves district value	Positively affects health
Normal facade sound absorbers	✓	X	X	X	X	X	X
Vertical greening systems	✓	✓	✓	✓	✓	✓	✓

Table 1 - Comparison of advantages of normal SAMs and VGSs

Acknowledging the potential of reducing urban noise using vegetation, the EU launched the HOSANNA project in 2009 (Holistic and Sustainable Abatement of Noise by Optimized Combinations of Natural and Artificial Means). The project brought about an impulse on research on practical vegetative solutions for the urban environment. From all the performed research on this topic, it becomes clear that VGSs generally attenuate only well for frequencies above 250 Hz (Davis et al., 2017). Hence, a major shortcoming is the limited low-frequency sound absorption (see Figure 1). Secondly, the quality of vertical greening to attenuate sound in the higher frequency range mainly depends on the system's vegetation species and substrate composition, but there is no integral overview on what combination of vegetation and substrate is the optimal acoustical choice.
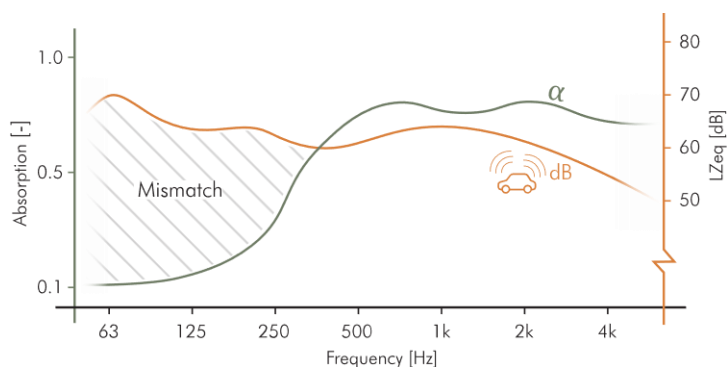
Figure 1 - The mismatch between VGS absorption and linear traffic noise levels

Summary

- Noise pollution is a large and growing health problem in cities.
- Vehicular traffic generates considerable low-frequency noise. However, this is commonly obscured by the A-weighting, and low-frequency noise is most annoying.
- This noise decays slowly in highly reflective urban street canyons.
- Vertical greenery is a multi-disciplinary solution that can be applied as a sound absorbing material
- Design optimalization must be done, because current vertical greening systems are not designed for broadband sound absorption, especially not in the low-frequency spectrum.

1.2. Research aim & objectives

The main scientific objective of this graduation research is to increase the acoustic absorption of VGSs for frequencies below 250 Hz. The secondary scientific objectives of this research include:

- Increasing the overall acoustic absorption of VGSs, including middle and high frequency sound.
- The implementation of resonators in a VGS.
- The improvement of methods to predict the combined effects of VGSs and Helmholtz resonators.

From a societal perspective, this research may lead to a reduction of sound levels in urban areas. This leads to healthier cities, an improved well-being, and more urban comfort.

1.3. Research questions

The main research question:

" How can the acoustic absorption of vertical greening systems in urban street canyons be improved, especially for low-frequency noise?

To main question was divided into several research questions. These questions can be grouped around a literature study, around the design process, and around the research validation:

Sub-questions regarding the literature study:
1. How do vertical greening systems abate sound?
2. What are the key indicators which determine acoustic absorption of the substrate layer?
3. What are the key indicators which determine acoustic absorption of the plant layer?
4. What sound absorber systems are suitable for low-frequency sound absorption?

Sub-questions regarding the design process:
5. How can resonators be integrated into the structure of a vertical greening system?
6. How can the absorption effects of the resonator and the porous substrate be combined?

Sub-questions regarding the validation:
7. To what extent does the design attenuate a broadband frequency spectrum in acoustic experiments?
8. To what extent does the design attenuate a broadband frequency spectrum in acoustic simulations?

1.4. Reading guide

Every sub-question will be answered in a separate chapter. First, chapter 2 will explore the literature about vertical greening and acoustics. Secondly, chapter 3 will zoom in on the acoustics of the substrate. Then, the acoustic absorption of plants will be discussed in chapter 4. Chapter 5 gives an overview of potential low-frequency absorbing systems. Chapters 6 & 7 describe the design process. In chapter 7, the final design is also validated analytically, experimentally, and numerically. Finally, a discussion and conclusion will be given in chapters 8 & 9.

1.5. Methodology

The graduation project was predominantly a process of quantitative research. This type of research is typically characterized by performing experiments and numerical validation to answer the main research question. The main structure of the research is shown in Figure 2.
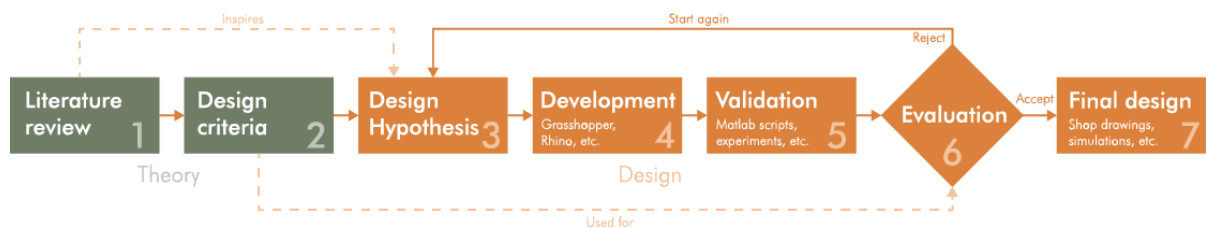
Figure 2 - Method flowchart

1.5.1. Literature review

Relevant literature was reviewed throughout the research process. This was a type of qualitative desk research. The study focused primarily on peer-reviewed articles, but also on books and non-peer-reviewed publications. Acoustic handbooks and PhD theses were consulted as sources on theoretical acoustics. Regarding literature on VGS and acoustics, a large portion of the literature research was written before the commencement of the graduation period. This work is still unpublished and was written under supervision of the main tutors. To find relevant literature, various databases were used, including Delft University of Technology's (TU Delft) library, Researchgate and Google Scholar. Additionally, still unpublished work which was presented at the Forum Acusticum 2020 e-congress was consulted.

1.5.2. Design criteria

Based on the conclusions from the literature study, a list with design criteria was drafted. This list was used to evaluate different concept designs. These criteria were based on the following fields:

A. **Absorption coefficient**: high absorption coefficient in a broadband frequency spectrum
B. **Manufacturability**: mass-production, design as simple as possible.
C. **Manageability**: easy transport and instalment
D. **Applicability**: confirming dimensions with existing facades
E. **Durability**: minimum of separate parts, fit in environment

The full list can be found in chapter 6.

1.5.3. Design hypotheses

To start the process of developing a concept design, an idea had to be put on paper. These ideas found their origin in the literature, and from preceding concept designs. The ideas were written in the form of design hypotheses. For example, it was found in literature that quarter-wavelength tubes would potential low frequency sound absorbers and that LWSs usually have air cavities behind the substrate. Hence, in the first design hypothesis, these two ideas were combined.

1.5.4. Design development

The concept designs were visually developed in the form of diagrams, using Adobe Illustrator 2020. Parametric models were made in in Rhino 7 using the Grasshopper plugin. Appendix II presents a full description on how these concept designs were developed. Additionally, concept designs were developed by writing scripts for Matlab R2020b. Matlab allows for complex matrix manipulations and is therefore well-suited for the purposes of computing acoustic impedance values. The script was continuously improved throughout the process. An overview for the used methods per concept design is given in Table 2.

Concept design 1	Concept design 2	Concept design 3	Concept design 4	Final design
Rhino and Grasshopper were used to manually place geometry. This was linked to a Matlab script	Rhino, Grasshopper, and Matlab were used. Geometry was generated using an algorithm	Matlab scripts were written and 3D-printed test pieces were experimentally tested in an impedance tube	Matlab scripts were written. Visualizations were made using Lumion and Adobe Illustrator.	Matlab script was finalized. Also, reverberation room measurements and simulations were performed

Table 2 - Overview of concept design methods (see Appendix II for a full description)

1.5.5. Analytical validation

A Matlab script was written to predict the acoustic absorption of the designs (Appendix I). The Delany-Bazley-Miki method was used to predict of the normalized acoustic impedance of porous media. To predict the acoustic behavior of resonators, the theory as described by Cox and D'Antonio (2016) was used. To predict the compound impedance of multi-layer systems, an equivalent fluid model in combination with a transfer matrix approach was used as proposed by Horoshenkov et al. (2013). Relating the morphological parameters of vegetation to acoustical parameters will be done by the methods presented by D'Alessandro et al. (2015).

1.5.6. Experimental validation using an impedance tube

An impedance tube was used during the design process to experimentally validate some design hypotheses. The procedure that was used is standardized as ISO 10534-2 (transfer function method). In this research, a Brüel & Kjaer (B&K) type 4206 was used. A broadband sound was generated using PULSE LabShop version 19.0.0.128, through a B&K type 3160-A-022 Output generator module and a B&K type 2735 power amplifier. A tube diameter of 100 mm was used, which had a frequency range of 50 – 1600 Hz. The objective of the experiment was to test the following parameters:

- The effect of moisture on the acoustic absorption of the substrate, and on the sound propagation in the multilayer structure (Saturation rate (S_r) based on mass ratios)
- The effect of combining the porous layer with different resonators (the extent of sound transmission through the porous layer)
- The effect of adding a small cavity between the resonator and the porous layer
- The effect of adding geotextile layers to the porous layer

To determine the amount of water to be added to the rock wool for the relative saturation rates, a scale was used with an accuracy of 1 g. The following equations were used to determine the saturation levels (Horoshenkov et al., 2011a):

$$S_r = \frac{\theta}{\Omega} \quad \text{and} \quad \theta = \frac{V_w}{V_t} \qquad\qquad (1.1 \text{ \& } 1.2)$$

Where S_r is the saturation rate, θ is the volumetric water content, Ω is the porosity of the sample, V_w is the water volume, and V_t is the sample volume. The saturation rates are presented in Table 3. The rock wool sample had a thickness of 40 mm, and a radius of 51 mm.

Rock wool sample	Sample vol. [cm³]	Water vol. [cm³]	Θ [%]	Sr (%)
0 (control)	314.16	0	0	0
1 (winter)	314.16	62.8	20	21
2 (summer)	314.16	219.9	70	74
3 (driving rain)	314.16	282.7	90	95

Table 3 - Saturation levels for impedance tube measurement

For the porous layer, several cylinders of hydroponic rock wool were cut out (Cultilene), with a thickness of 40 mm and a diameter of just over 100 mm. Similarly, circular cutouts of water-resistant geotextile (Gronest Aquabreathe) were cutout. Regarding the Helmholtz resonators, a design was made in Rhino using Grasshopper (Figure 3). The resonators were 3D-printed using an Ultimaker 3. A modular system was designed where different lids could be attached to a single resonator cavity. These lids were designed as the different Helmholtz neck configurations. The lids were attached using six M3x50 bolts and nuts. To ensure an air-tight seal, a ring gasket for the Helmholtz resonators was made out of dishcloth. The resonator configurations were:

- Resonator with a short neck (equivalent to a small plate thickness)
- Resonator with a lateral orifice using the offset perforated plate
- Resonator with a lateral orifice using the offset perforated plate and lateral insert.
- Resonator with long neck (pierces the porous layer)

The impedance tube measurement set-up is shown in Figure 4.
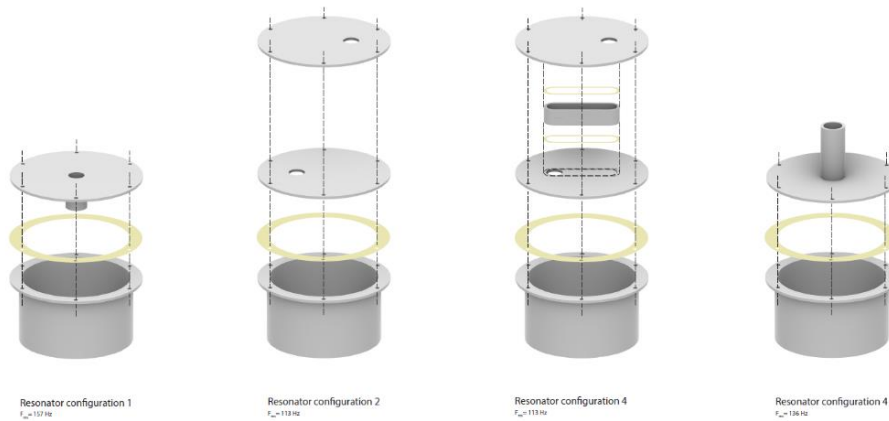
Figure 3 - Geometry for 3D-print Helmholtz resonators
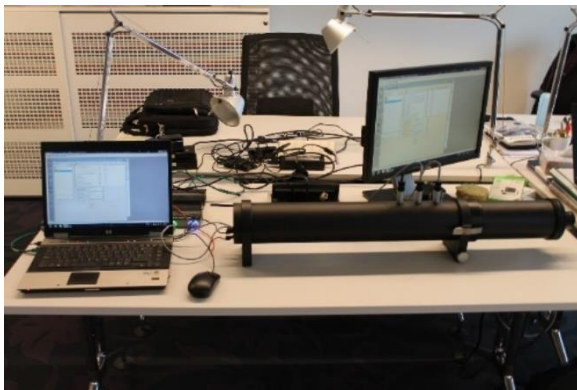
Figure 4 - Impedance tube measurement set-up

Figure 5 - Reverberation room measurements

1.4.7. Experimental validation using the reverberation room

The reverberation room at the Faculty of Applied Sciences of Delft University of Technology was used to experimentally measure the absorption coefficient of the VGS design (Figure 5). This room has a volume of 200 m² and complies to ISO 354:2003 (ISO, 2003; Tenpierik, 2015). The equipment used was:

Tool	Type
Source	Norsonic dodecahedron omni-directional loudspeaker NOR276
Receiver	Norsonic Precision Sound Analyser NOR140
	Norsonic Microphone NOR1125
Amplifier	Norsonic Pre-amplifier NOR1209
	Norsonic power amplifier NOR280
Interface	Behringer UCA222 USB interface
	Windows 7 machine running Matlab R2010bsp1 32bit
	Matlaus: custom Matlab script

Table 4 - Reverberation room equipment

In the Matlaus script, a RT < 9.6 sec was selected (sound levels in and around the measurement area are carefully controlled), with a PRA of 2+2 sweeps (4 sweeps were generated, of which two would be used for the measurement). The amplifier was set to -35 dB(A). The frequency spectrum was 80-1000 Hz, in 1/27th octave bands. In total, 15 prototype modules were made (Figure 6):

- Thermal rock wool plates (split to 50 mm) were cut into squares of 600x600 mm
- In these rock wool plates, 25 through-holes of ∅19 mm were drilled on a square lattice
- 9 mm MDF plates were similarly cut into squares of 600x600 mm, with the same holes
- ¾" PVC electrical tubes were cut to lengths of 59 mm, and were deburred
- These tubes were inserted in the holes of the MDF plates, flush to the back, and glued in place
- The rock wool plates were slid over the protruding tubes
- Glass wool plates (split to 50 mm) were cut into squares of 600x600 mm
- 12 mm plywood planks of 110 mm high were cut to fit around the setup boundary

This design combines the HF-absorption of the rockwool and the LF-absorption of the Helmholtz resonators, consisting of a neck of PVC tube and a cavity filled with glass wool. 15 modules equal a total surface area of 5.4 m², with 375 Helmholtz resonators. All resonators were predicted to resonate at 120 Hz.
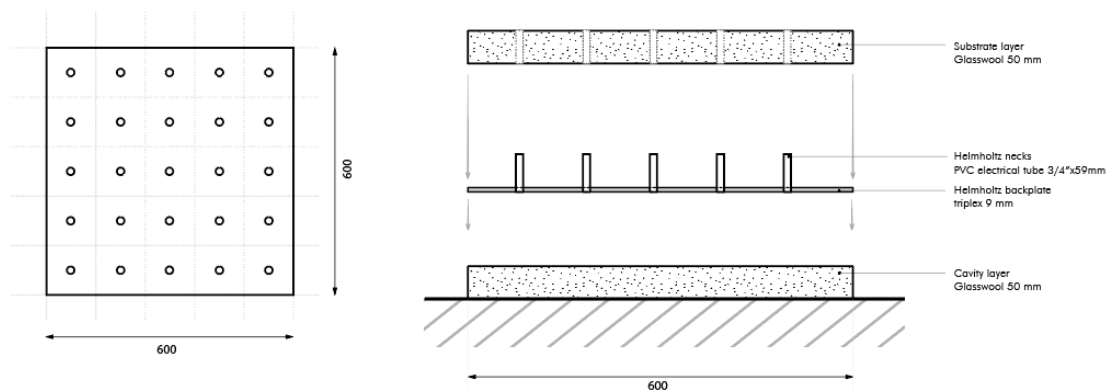
Figure 6 - Prototype module top and side view (exploded)

The following experimental set-up was used, forming various design configurations:

- Scenario 0: Control test (no sample)
- Scenario 1: Place all modules
- Scenario 2: Cover all resonator necks with painter's tape
- Scenario 3: Remove painter's tape, and remove cavity fill
- Scenario 4: Add cavity fill back in, and offset the boundaries slightly

For each configuration, six receiver positions were used and a single source position, see Figure 7. The reverberation times (RT20) were averaged, and used as a single input variable in the Sabine equation. The air absorption was accounted for, by taking measurements of the room temperature and relative humidity.
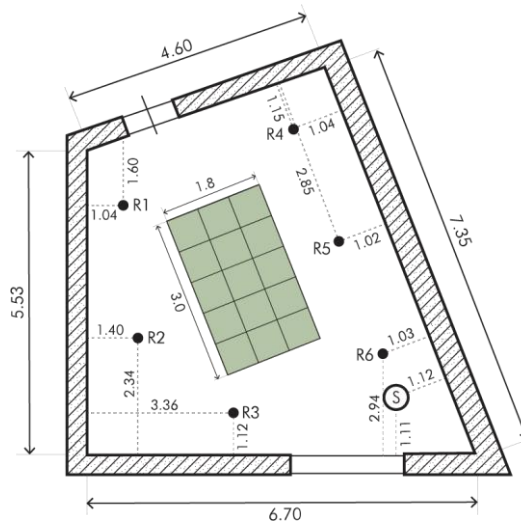
Figure 7 - Reverberation room set-up

1.5.8. Case study

To study the acoustic potential of the design in reality, a case study location was selected, and acoustic simulations were carried out. A reference street canyon was selected, and modelled as a computer model using SketchUp Pro 2018. Planes with different absorption coefficients were organized in different layers. The street profile was modelled after the Stadhoudersweg in Rotterdam, The Netherlands (51°55'50.1"N 4°27'34.4"E). This profile is an example of an urban street canyon with a high traffic flow, with an adjacent courtyard canyon. The aerial view is illustrated in Figure 8. The facades are depicted in Figure 9. Three variations on this model were simulated, as described in Table 5.

Figure 8 - Aerial view of the canyon (Google, 2021)

Figure 9 - Facade view (Google, 2021)

Model		Used software	Objective	Reason
A	Two adjacent canyons (street canyon and courtyard canyon)	Olive Tree Lab Suite 4.4 (OTL)	To research to what extent the application of LWSs to the street canyon walls affects SPLs behind obstacles	OTL can handle second order diffraction better
B	One canyon (street canyon) with WWR[1]=50.7%	CATT-Acoustic V9 (CATT-A)	To research to what extent the application of LWSs to the street canyon walls affects SPLs on the street.	Quick and reliable SPL prediction and auralization (Puczok, 2007)
C	One canyon (street canyon) with WWR=28.7%	CATT-A	To research the effect of a smaller WWR. More wall area allows for more placement of LWS. The total window area was reduced from 269.1 m^2 to 152.5 m^2	WWR can vary between 0.25-0.90 in Europe (Goia, 2016). Hence, it is an important parameter

Table 5 - Overview of simulated models 1) WWR = Window-to-wall ratio

A cross-comparison between configurations with and without facade greenery was made, based on the sound pressure levels at the receivers. An overview of all models and variations is given in Table 6.
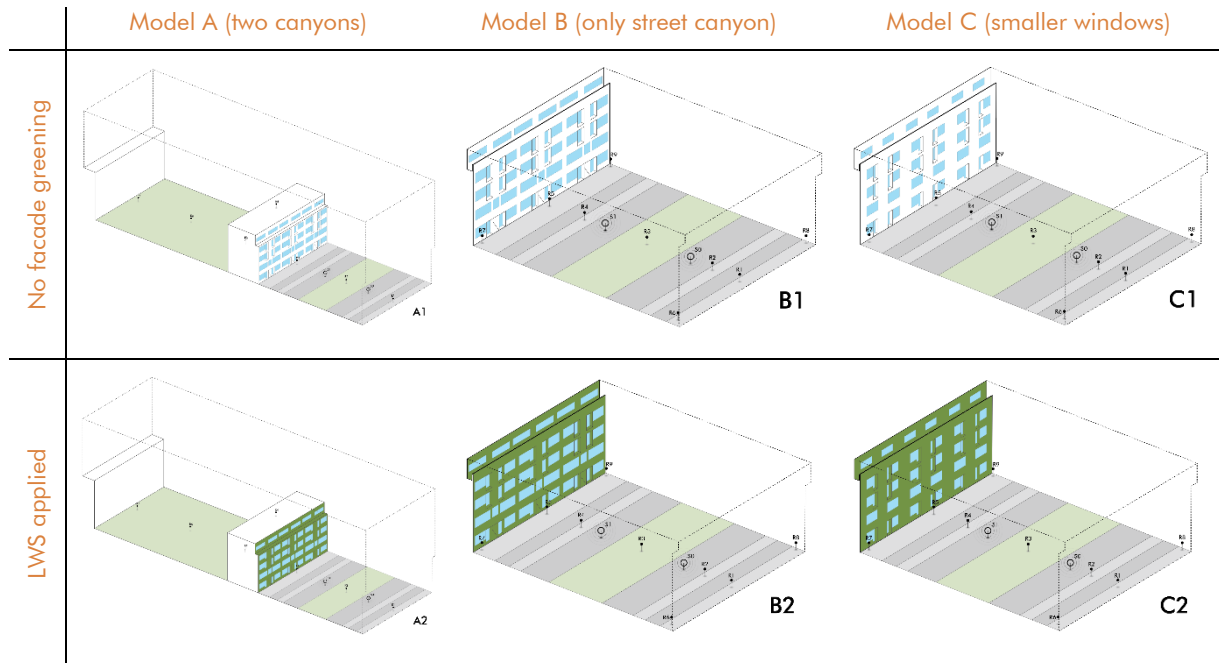
Table 6 - Matrix of models and variations

For all models, the absorption and scattering coefficients in Table 7 and Table 8 were used (based on Van der Linden et al. (2011):

	Absorption coefficients in 1/1 octave bands [Hz]					
Material	125	250	500	1000	2000	4000
Asphalt	0.03	0.07	0.10	0.04	0.05	0.05
Grass	0.10	0.20	0.40	0.70	0.80	0.80
Concrete	0.02	0.03	0.03	0.03	0.04	0.07
Glass	0.10	0.06	0.04	0.03	0.02	0.02
Masonry brick	0.05	0.04	0.02	0.04	0.05	0.05
PML[1]	1.00	1.00	1.00	1.00	1.00	1.00
Acoustic LWS[2]	0.57	0.78	0.98	0.80	0.92	0.99

Table 7 - Absorption coefficients used in the simulation

1) Perfectly Matched Layer, an artificial boundary that absorbs 100% of acoustic energy, to simulate an infinitely deep plane

2) Absorption coefficient based on analytical results from Matlab script (Appendix I)

	Scattering coefficients in 1/1 octave bands [Hz]					
Material	125	250	500	1000	2000	4000
Asphalt	0.10	0.10	0.10	0.10	0.10	0.10
Grass	0.10	0.10	0.20	0.20	0.30	0.30
Concrete	0.10	0.10	0.10	0.10	0.10	0.10
Glass	0.05	0.05	0.05	0.05	0.05	0.05
Masonry brick	0.20	0.2	0.20	0.30	0.30	0.30

PML	0.00	0.00	0.00	0.00	0.00	0.00
Acoustic LWS	0.20	0.30	0.40	0.50	0.50	0.60

Table 8 - Scattering coefficients used in the simulation

The scattering coefficients were assumed, based on the regularity of the material's surface. The positions of the sources and receivers are described in Table 9:

Object	Simulation A (2 canyons)			Simulation B+C (1 canyon)		
	X	Y	Z	X	Y	Z
Source 0	16.38	11.00	1.20	16.38	11.00	1.20
Source 1	16.38	27.60	1.20	16.38	27.60	1.20
Receiver 1	16.38	1.50	1.60	16.38	1.50	1.60
Receiver 2	16.38	19.50	1.60	16.38	6.70	1.60
Receiver 3	16.38	38.50	1.60	16.38	19.05	1.60
Receiver 4	16.38	46.50	17.5	16.38	31.66	1.60
Receiver 5	16.38	54.60	1.60	16.38	38.50	1.60
Receiver 6	16.38	77.30	1.60	1.00	1.00	1.60
Receiver 7	16.38	100.00	1.60	1.00	39.00	1.60
Receiver 8				31.76	1.00	1.60
Receiver 9				31.76	39.00	1.60

Table 9 - Source and receiver positions

For the sources in the CATT-A simulations, the research results from Can et al. (2010) on vehicular traffic in urban street canyons were used. For the OTL simulations, omni-directional broadband source characteristics were used. For cross-comparison, only the relative differences are relevant. Hence, the source characteristics are not included in this report.

Comparative simulations were performed. First, the street canyons with regular masonry brick facades were simulated. In the second step, the masonry brick in the street canyon was replaced with acoustic LWS material. The following settings were used:

Catt-A		OTL	
Setting	Value	Setting	Value
Algorithm	2, based on diffuse ray split-up	*Reflection order*	3
Number of rays	200000	*Max. path length*	1000000
Air absorption	RH 50%, 20°C	*Max. excess attenuation*	65 dB
Head direction	Stage	*Diffraction*	First and second order
Diffraction	First order		
Receiver direction	Stage		

Table 10 - Simulation settings

1.4.9. Evaluation

The performances of the concept designs were compared to the list of design criteria. When the designs did not sufficiently satisfy the requirements, a new design hypothesis was made. An overview of these evaluations can be found in chapter 6.

1.5.10. Final design

The best performing concept design was elaborated into a final design. For the final design, the following products were delivered:

- Shop detail drawings and installation drawings
- 3D visualizations
- Material choice justification
- Selection of plant species
- Thermal insulation calculation
- Weight and dimensions

Literature review

2. Acoustic attenuation by vertical greening systems

This chapter will answer the first sub-question on how vertical greening systems abate sound. To answer this, this chapter will discuss the following topics:

- Terminology and advantages of vertical greening systems (2.1)
- Design criteria for healthy vertical greenery (2.2)
- Review of literature on acoustic absorption of plant-soil systems (2.3)
- Review of literature on vertical greenery system configurations (2.4)

2.1. Introduction to vertical greening systems

A vertical greening system (singular: VGS; plural VGSs) is a systems which applies a living cladding system to a building facade (Ottelé, 2011). Such claddings use plants as a self-regenerating building envelope. There are many definitions on facade greening, which more or less accord to Köhler's (2008) description: "Greened facades are typically covered with woody or herbaceous climbers, either planted into the ground or in planter boxes in other structures to anchor plants, that can be developed into modular systems attached to walls to facilitate plant growth without relying on rooting space at ground level".

VGSs have many qualities (Moya et al., 2019; Ottelé, 2011; Perini et al., 2011; Pommier et al., 2014):

- Improvement of air quality by filtering airborne particulates and gaseous pollutants from the air such as carbon dioxide (CO_2), nitrogen dioxide (NO_2), and Sulphur dioxide (SO_2). Through photosynthesis, the vegetation can convert CO_2 into oxygen (O_2) and biomass, while NO_2 and SO_2 are converted into nitrates and sulphates in the tissue of the plant, respectively.
- Increasing biodiversity in urban environments, e.g., by attracting birds, bats, and insects
- Diminishing of the urban heat island effect by a plant's absorption of insolation, to accommodate its biological functions, such as photosynthesis, transpiration, evaporation, and respiration. Additionally, the building mass is shaded so that it accumulates less heat
- Improving thermal insulation, as the still standing air in between the facade and the VGS presents favorable boundary conditions for convection
- Indirectly improving the economic value of a neighborhood by improvement of the aesthetic and social aspects in the neighborhood
- Therapeutically reduce stress levels and positively affect human health
- Acoustic attenuation of incident sound energy

Terms as green facades, living walls, vertical greenery systems, bio-walls, active living walls, may all be popularly used as synonyms; however, these systems can vary substantially. Ottelé (2011) has defined a clear overview in the terminology of VGSs. A clear distinction can be made between vegetation that roots in the ground and vegetation that roots on a hydroponic system, i.e., containers of (artificial) substrates. Vegetation that roots in the ground, climbs up by directly using the roughness of a facade or indirectly using

a suspended structure. A system that roots in hydroponic systems is known as a living wall system (LWS). The latter systems generally contain low-growing herbaceous or woody plants. Such systems need irrigation and nutrient supply. An overview is given in Table 11 (based on Mir, (2011); Ottelé (2011); Wagemans (2016)).

	Vertical greening systems (VGSs)							
	Rooted in ground		Not rooted in ground (hydroponics)					
	Green facades		Green facades		Living wall systems (LWSs)			Other
System	Regular green facade	Suspended green facade	Planter box green façade	Suspended planter box green facade	Mineral wool LWS	Felt geotextile LWS	Planter box LWS	Bio-receptive facade
Type	Direct	Indirect	Direct	Indirect	Indirect	Indirect	Indirect	Direct
Substrate	Soil	Soil	Soil	Soil	Hydroponic rock wool	Laminated felt pockets	Hydroponic substrate/soil	Concrete
Vegetation	Self-climbing plants	Self-climbing plants	Self-climbing plants	Self-climbing plants	Herbaceous plants / shrubs	Herbaceous plants / shrubs	Herbaceous plants / shrubs	Mosses
Structural material	Facade masonry	Mesh / plastic / wood structure	HDPE (1) / galvanized steel (2) planter box	HDPE (1) / galvanized steel (2) planter box / mesh	Steel / aluminium profiles / geotextile	Steel / aluminium profiles / laminated felt	Steel / aluminium frame / plastic boxes	Concrete / composite
Costs €/m^2	30-45	40-75	100-150 [1] 400-500 [2]	100-150 [1] 400-500 [2]	750-1200	350-780	400-600	-
Irrigation	Pre-cipitation	Pre-cipitation	Irrigation system	Irrigation system	Irrigation system	Irrigation system	Irrigation system	Pre-cipitation
Planting density	< 4 / m^1	< 4 / m^1	< 4 / m^1	< 4 / m^1	< 27 / m^2	< 25 / m^1	< 30 / m^1	N/A
System weight	> 5.5 kg / m^2	> 5.5 kg / m^2	> 5.5 kg / m^2	> 5.5 kg / m^2	40-60 kg / m^2	100 kg / m^2	> 150 kg / m^2	N/A
System thickness	200 mm	200 mm	200 mm	200 mm	< 400 mm	< 350 mm	< 450 mm	N/A
Main advantage	Cheapest & simplest system	No moisture problems	Control over substrate	Control over substrate	Light-weight LWS	Cheap LWS	Durable LWS	Distinctive use of plant species
Main dis-advantage	Possible facade damage (moisture)	Limited suitable plant species	Possible facade damage (moisture)	Limited growth height	Expensive LWS	Un-sustainable LWS	Heavy LWS	Unsuitable for most facades

Table 11 - Overview of VGS types

2.2. Criteria to design a healthy vertical greening system

The attitude towards vertical greening is not always positive, since some greening systems are not properly designed and die. A healthy greening system is essential to guarantee the advantages listed in chapter 5.1., including acoustic absorption. This following risks have to be regarded when designing a VGS (Gunawardena and Steemers, 2020):

- Thermal and moisture stress

    The applied vegetation species in a VGS must be suitable for the climate in which the system is deployed. A VGS can fail when the climatic circumstances exceed the tolerances of the vegetation species, since irrecoverable injury can occur. Species must be selected that can handle atypical temperatures and humidity, such as extra cold and dry winters and heatwaves.

- Light-exposure

    The lighting and shadowing of a vertical greening installation should be thought through. For example, shade-loving plants should not be exposed to too much insolation on south-facing facades, since this can cause plant stress

- Mechanical stress

    wind affects the plant stress levels. Low wind speeds can reduce irradiation-induced heat stress by advection of heat in the vegetation layer. Alternatively, high wind speeds can induce a mechanical stress on the vegetation. It can cause limited growth, a reduced leaf count, and a greater radial growth. Wind stress can occur especially at higher elevations, due to turbulent flows at the system's edges and apexes. Too much wind can reduce the humidity in the vegetation, consequently drying out the plant tissue.

- Hypoxic and nutrient stress

    LWSs need an irrigation system that provides the vegetation with water and essential nutrients, such as phosphorus (P), magnesium (Mg), calcium (Ca), and potassium (K), in varying ratios (Perini et al., 2011). Watering frequency depends on the system, e.g., a felt-based system needs a high watering frequency of 3 - 5 times a day, while a soil-based system needs only watering 1 - 2 times a day. Irrigation programs can change to adjust per season, since the winter demand is lower. Also, precipitation sensors account for natural watering, and additional irrigation volumes are adjusted. Water risks include wintertime frost damage, spillage, leakage, and oversupply. Oversupply of irrigation can be fatal, since the hypoxic stress can induce rot in the roots, wilting, and overall reduced growth. Lastly, the application of synthetic pesticides can aggregate in the wastewater and thus a toxicity is indicated in the irrigation system output

2.3. Research on acoustics of plant-soil systems in vertical greenery

The still unpublished literature review from Bakker, Lugten, & Tenpierik has condensed a large number of results on VGS acoustic absorption in a single graph (Figure 10). The absorption coefficient graphs are grouped to distinguish the major factors which influence the measurement results. For example, the reverberation chamber absorption coefficient results tend to increase above $\alpha > 1$, since the random incidence in such a setup deals with edge scattering. Meanwhile, impedance tube measurement results tend to be overall far lower absorption coefficients, since this method uses only small samples of vegetation and normal incidence. A collection of leaves becomes increasingly more complicated and thus behaves differently on a bigger scale. Another factor that influences the absorption coefficient graphs, is that the experiments represent different types of vegetation species, substrate compositions, and have applied various source frequency spectra.
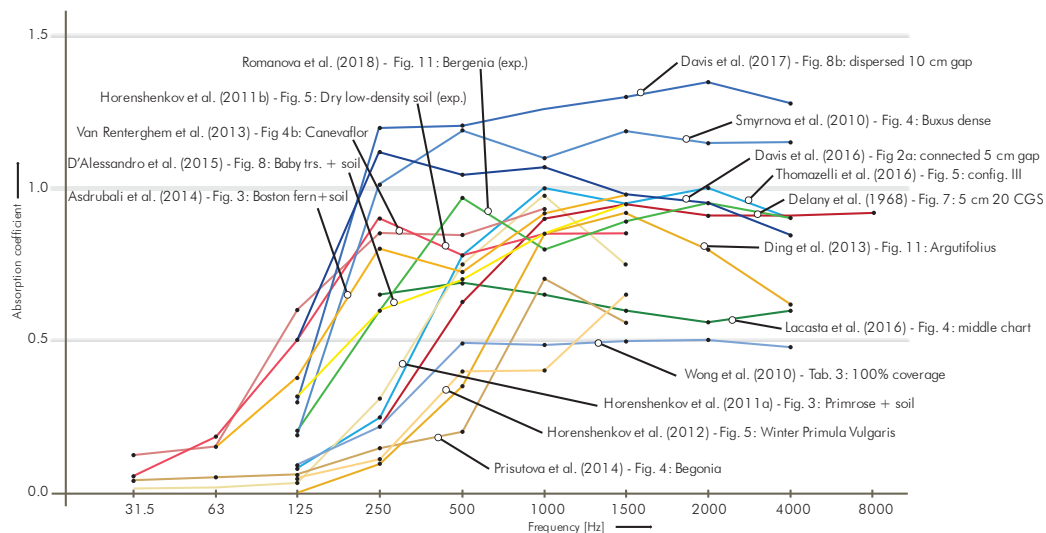

Figure 10 - A selection of absorption coefficient results from the unpublished literature review from Bakker, Lugten, & Tenpierik. *Blue* graphs are reverberation chamber results of densely planted systems, *yellow* graphs are impedance tube results of soil-plant systems, *red* graphs are impedance tube results for substrates, and *green* graphs are in-situ measurement results.

The measurement results of all researches listed in Figure 10 seem to agree on the fact that VGSs act as porous absorbers. This entails that such systems absorb well for higher frequency sound and absorb poorly for lower frequency sound. The increase in absorption coefficient from low to high frequencies does not occur linearly, but instead, steeply climbs towards a peak in the 250 - 500 Hz range, and from there climbs with a slight slope further towards a higher absorption coefficient. In the higher frequencies, slight negative and positive discontinuities result from unpredictable interferences by the vegetation layer.

Notable studies on plant-soil systems are the following:

Asdrubali et al. (2014) have researched the acoustic behavior of several plant species, including ferns, baby tears, and ivy on a fibrous substrate, in both impedance tubes and in a reverberation chamber. They found that the substrate is the main absorber in soil-plant systems, and vegetation increases absorption if planted very densely. In case of the very densely added fern samples in the diffuse field experiment, the absorption

coefficient increased by 25% relative to the substrate absorption coefficient for the frequency spectrum 800-1600 Hz. The vegetation is of lesser contribution to sound than the substrate, so the acoustic performance of vegetation is generally expressed as an increase of the absorption coefficient relative to the bare substrate absorption coefficient.

Ding et al. (2013) conclude that for green walls, the substrate absorbs most of the sound energy, and the addition of a leaf layer positively influences the absorption characteristics. These changes typically occur for frequencies higher than 250 Hz. For the purposes of this research, a natural porous soil was substituted by melamine foam. The plant species were Japanese andromeda, scarlet wonder, primrose, and Corsican Hellebore. The experimental results were the input for a numerical model, which predicted that the addition of a leaf in front of a porous substrate increases the absorption coefficient for 500-2000 Hz, has no effect for frequencies below 250 Hz, and decreases the absorption coefficient for high frequencies (above 2 kHz).
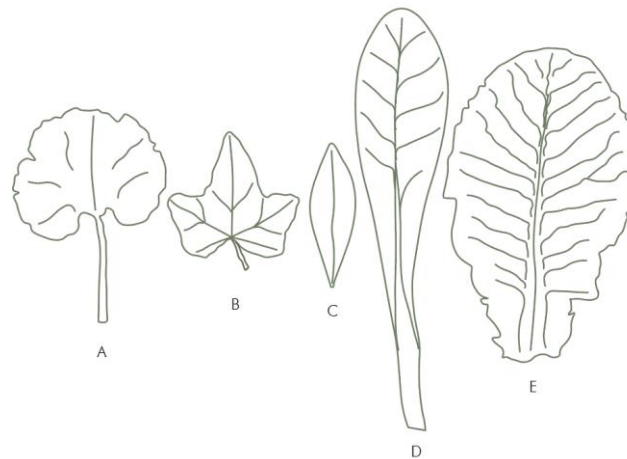

Figure 11 - Researched plant species by Horoshenkov et al. (2013). (A) Geranium, (B) Ivy, (C) Japanese Andromeda, (D) Summer Primrose, (E) Winter Primrose

Horoshenkov et al. (2013) have researched the acoustic behavior of several low growing plant species in combination with different substrates (Figure 11). Important differences between the plant species were the average leaf area, the number of leaves on the specimen, and the dominant angle of leaf orientation. For example, the Japanese Andromeda shrubs had an average leaf area of 4.8 cm^2, an average leaf number of 360 per plant, and a dominant leaf angle of 30°($\pm$20°), while the common primrose (winter) specimens had leaves with an average area of 54.8 cm2, on average 19 leaves per plant, and a dominant leaf angle of 72°($\pm$15°). A combination of experimental and numerical results show that the winter primrose leaves, having the highest leaf area density (159 m^{-1}) and a large dominant angle of leaf orientation, had the best noise attenuating performance. Adding a layer of this vegetation species to a bare light-density substrate increases the absorption coefficient up to 80% for frequencies below 400 Hz and a 15-20% increase for frequencies above 800 Hz. Adding vegetation to a substrate increased the absorption coefficient for almost every test, and also for almost all frequencies.

Wong et al. (2010) have researched the acoustic performance of green walls in-situ and in a reverberation room. In this laboratory setup, a wooden frame structure was built which held Boston fern samples in pots. Plant coverages of 100%, 71%, and 43% were tested. The wooden frame was consequently significantly exposed at the 43% plant coverage. It was found that the reverberation time was tremendously reduced for dense vegetation, most notably between 200 - 1000 Hz. Also, the vegetation coverage determines the amount of reduction of reverberation time. They argue that the substrate absorbs most of the lower frequencies, while the vegetation absorbs mostly the higher frequencies. However, for frequencies lower than 250 Hz, only small differences were found.

Smyrnova et al. (2010) researched the absorption properties of various plant species by application of a P-U probe and in a reverberation chamber. The P-U probe is a device that measures both the air pressure and particle velocity, the product of which makes up the sound intensity. The plant species included pansy, primrose, and Buxus, the samples of which were potted and placed on the floor. All plants decreased the reverberation time, most notably for frequencies higher than 250 Hz. Densely planted Buxus (16 pots/m^2) seemed to have a consistently high absorption coefficient between 400 - 5000 Hz.

D'Alessandro et al. (2015) researched the acoustic absorption of Boston fern and baby tears in combination with a light-density coconut fiber soil. Impedance tube measurements show that the fern on soil gives an absorption peak at around 400 Hz with absorption coefficients of about 0.7, and this increases up to 0.9 above 1200 Hz. The absorption of merely the ferns (without soil) has a significantly lower absorption coefficient, not exceeding 0.3. This confirms that the substrate, absorbing up to 80% of sound energy, is the main acoustically absorbing medium in a soil-plant system. The experimental results were input in an equivalent fluid model, to deduce the theoretical tortuosity and flow resistivity of the samples. This model could very accurately predict the acoustic behavior of the samples, however for Baby tears, having more complex variability of leaf inclination, a larger mean error of up to 4.4% was calculated.

Thomazelli et al. (2016) have researched the acoustical behavior of a geotextile system filled with light-weight coconut fiber substrate and turtle vine samples, both in a reverberation room as well as in-situ. The substrate had a porosity of 87%, which is highly porous for natural soils, and is even comparable to the absorption of glass wool. In the laboratory experiment, the geotextile bags were placed on the ground, both with and without substrate and vegetation. The latter configuration had both the lowest reverberation time and the highest absorption coefficient (near-unity for f > 1 kHz). In the in-situ experiment it was found that the fully equipped green wall (including substrate and vegetation) had the highest measured absorption coefficient.

2.4. Effect of VGS configurations on acoustics

The many variations on vertical greening configurations result in various acoustic performances. Also, the size and strategic placement of the vertical greening systems on facades has an effect on the noise attenuation performance. Since there is no standard configuration of vertical greening systems, these factors must be addressed.

2.4.1. Acoustic transmission

The degree of 'openness' in a vertical greening system, i.e., uncovered surface area through which incident sound can freely pass, must be prevented as much as possible. When researching the acoustic influence of an absorber in a free field, its performance is usually expressed as an insertion loss: the reduction in decibels as a result from inserting the acoustic intervention.

Wong et al. (2010) have performed a well-referenced in-situ research of eight different vertical greening systems. Variations in these systems were differences in substrate thickness, plant height, and either a mesh system or a shelved module system. The insertion loss results were compared to the measurements of an empty control wall. The vertical greening systems with the overall lowest insertion losses generally had small leaved plants and considerable gaps through which sound could freely pass. Insertion losses of up to 4.0 dB at 800 Hz were measured. The best performing vertical greening systems had dense and broad-leaved plants in substrate-filled containers, having insertion losses of up to 8.4 dB at 630 Hz and 8.8 dB at 4kHz. In some cases, unexplainable negative insertion losses were measured. In other cases, high insertion losses were measured as a result of having climber vegetation which rooted in large planting pots at ground level. Overall, an important conclusion was that the impenetrability of a vertical greening system was key to a high insertion loss.

Similarly, Pérez et al. (2018) argue that the connection between vertical greening system modules determine the overall acoustic insulation to a large extent. Small fissures can transmit sound through the system, whereas fully sealed joints would improve the acoustic insulation. Also, acoustic bridges must be prevented, which can occur in systems that are directly connected to a facade. Adding an air cavity and using poorly transmitting anchors creates a physical separation, ultimately increasing the insertion loss.

Adding to this, Davis et al. (2016) have researched the effect of connecting or dispersing modular vertical greening system elements in a reverberation chamber. The effect of either connecting or dispersing the elements resulted in no significant differences on the absorption coefficient. This shows that large gaps in such configurations do not affect the absorption coefficient.

2.4.2 Air cavity behind vertical greening systems

Several studies have shown that physically separating the VGS from the aback wall can increase low-frequency sound absorption. Standing waves occur in urban street canyons and in reverberation rooms, where the wave peaks of greatest sound particle velocity occur at fixed distances from the wall, i.e., at one-

fourth the wavelength. This is the distance from the wall where most acoustic energy is carried, therefore being the most strategic position to acoustically insulate. Rather than increasing the thickness of the absorbing layer to diminish the distance to the first peak, offsetting the absorbing layer is more efficient, since less material is needed. This is illustrated in more detail in chapter 3.2.5.

In the study of Davis et al. (2016), the influence of adding air cavities of different thicknesses VGS modules was researched in a reverberation room. The air cavities seemed to increase absorption for lower frequencies, shifting the curve towards the lower end of the frequency spectrum.

This is in accordance with the study of Thomazelli et al. (2016), who have researched a geotextile LWS in-situ, filled with substrate. Offsetting the system by 20 mm by raising it on wooden slats has increased the absorption coefficient below 630 Hz, most notably around 300 Hz.

Also, a large-scale in-situ research from Wong et al. (2010) had an interesting finding of a vertical greening system which was offset 8.5 cm from the back wall. The insertion loss had a small peak of 3 dB at 150 Hz. Other researched vertical greening systems did not have this offset, and consequently had no similar significant peak in low-frequency sound insulation.

2.4.3. Placement of vertical greening systems on a facade

Sound waves may not stay within the street canyon, but can propagate to nearby adjacent street canyons. A distinction can thus be made between a source canyon and a receiver canyon. To reach the receiver canyon, a sound wave has to propagate over the roof edges, where diffraction will occur. At these diffraction boundaries, the sound energy is distributed in a large number of angles. Consequently, less acoustic energy is received by a point receiver in the receiver canyon (Van Renterghem and Botteldooren, 2009). Figure 12 illustrates this effect. When diffracted waves diffract again, we speak of second order diffraction. This occurs when sound propagates around e.g. a building.
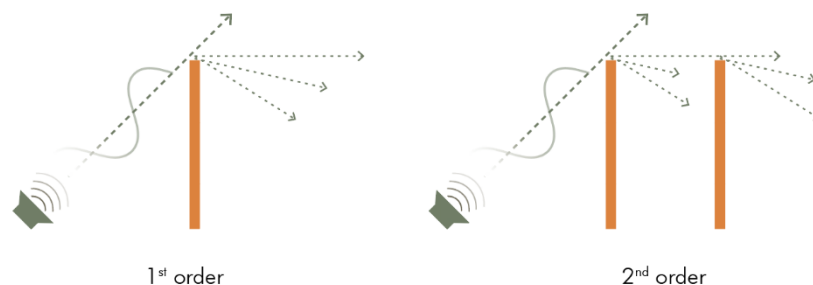
1st order   2nd order

Figure 12 - First order and second order diffraction

These diffraction effects are key in the research of Van Renterghem et al. (2013). They research the influence of vertical greenery and green roofs on diffraction and propagation in these scenarios. A reference geometry consisting of two adjacent urban canyons were modelled, separated by six-story buildings (Figure 13). Twenty-one different envelope greening combinations were considered. The authors argue that the

application of VGS to the upper floors of the city street canyons are most efficient in mitigating the noise propagation toward the adjacent courtyard. Adding vegetation to the lower floors on the source side therefore increases the insertion loss only marginally in this case. Adding vegetated roof screens as small noise barriers to the roof edges increased the insertion loss by altering the refraction over the roof edge. It does not seem important whether to place these screens on either the source or receiver roof edges, however, placing them at both roof edges gives a much larger insertion loss: larger than the addition of the separate effects. For the courtyards, it was found that as much vegetated area as possible yields the best acoustical results. This is simply because increasing surface absorption decreases the reverberation in the confined courtyard.
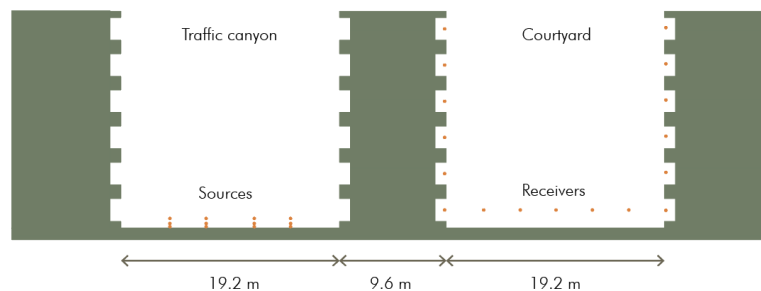

Figure 13 - Urban canyon and adjacent courtyard model used in the research of
Van Renterghem et al. (2013)

Similarly, inclined green roofs can also influence diffraction and propagation to adjacent canyons. Hence, the effect of adding green roofs to various roof shapes has been researched (Van Renterghem et al., 2013). From the results it can be derived that when a roof is tilted perpendicular to the noise propagation, a larger interaction zone is introduced. Reducing the roof angles over which sound propagates gives rise to a softer diffraction edge because the turbulence is less pronounced. Complex roof shapes, such as a saw-tooth factory-style roof shape, gives a good acoustic performance when combined with green roofs, because the irregular morphology has a significant influence on the noise propagation. On the contrary, adding green roofs to depressions in the roof shape does not add any value to the insertion loss, since sound is not forced to interact with the absorbing surface.

The research of Guillaume et al. (2015) is in accordance with the research of Van Renterghem et al. (2013). They too have performed a numerical study on the effect of vegetation on sound levels in urban street canyons. A canyon of infinite length and of four floors height with window depressions was modelled, on which various vertical greening systems and green roof combinations were applied, with varying green coverage ratios. The upper floors of the treated facades had the most impact on reducing the sound pressure levels and the decay times.

2.5. Conclusion

The theory summarized in this chapter can answer the first sub-question: "How do vertical greening systems abate sound?"

- Vertical greening systems (VGS) is an umbrella term that includes a wide variety of systems where greenery is applied to a facade. A clear distinction can be made between vegetation that roots in the ground (green facades), and vegetation that roots on a hydroponic system, such as in containers or in mineral wool (living wall systems or LWS).
- It is proven that vertical greenery acts as a porous absorber. Low frequency sound (f<250 Hz) is not absorbed, while near-singular absorption is found for higher frequencies. Keeping this in mind, normal VGS can be optimized for acoustic absorption of mid- to high frequencies.
- Firstly, it is essential to maintain a healthy VGS to guarantee well-developed greenery. Therefore, a VGS must be carefully designed and properly maintained. Some design keys are:
    - Species must be selected that can handle extra cold and dry winters and heatwaves
    - Shade-loving plants should not be placed on a south-facing facade
    - Periodic maintenance task prevents crown domination, uprooting, and vegetation fall-out.
- Secondly, the configuration of the VGS can be optimized for minimizing the insertion loss.
    - The impenetrability of the VGS through which incident sound cannot freely pass yields a higher insertion loss.
    - Small fissures and acoustic bridges decrease the impenetrability of a VGS, as these factors can transmit sound through the system
    - Adding an air cavity can increase the low-frequency absorption performance. Shifting the porous material towards a quarter of the sound wavelength increases the visco-thermal interaction.
- Ideally, a VGS configuration is as impenetrable as possible and transmits no sound to the rigid backing. A VGS needs plant species that fit in the environment, and needs to be carefully maintained.

3. Acoustic attenuation by the substrate layer

In the previous chapter it is shown that vertical greenery can absorb sound in different ways. Essentially, VGSs consist out of two layers: the substrate layer and the plant layer. The substrate layer is the base medium in which the plants can root. This medium is always porous, and can therefore absorb sound. In fact, the substrate can to absorb up to 80% of the incident sound energy above 1000 Hz (Asdrubali et al., 2014; D'Alessandro et al., 2015). This chapter will discuss the following topics:

- Requirements for a substrate (3.1)
- Key criteria for visco-thermal absorption (3.2)
- The effect of moisture content on the acoustic absorption of substrates (3.3)

3.1. Requirements for a substrate

When considering the growth of a plant, the substrate is the foundational layer, forming the base for plant growth. The substrate must be able to accommodate the needs of the part of the plant that remains underground: the root (Esau, 1953). The following functions take place in the substrate:

1. The substrate should be able to supply moisture and nutrients to the absorbing organ of the root.
2. The substrate should be able to accommodate nutrient storage in the plant's roots. Hence, the substrate should not be rigid, but should be able to expand.
3. The substrate is the anchorage in which the plant develops many lateral branches to increase the friction between the root surface area and the porous substrate.

Although a natural soil is the most obvious type of substrate, it is accepted that plants do not necessarily need soil, but merely mechanical support and water with essential nutrients (Remael, 2014). Patrick Blanc, a pioneer in the development of living wall systems was inspired by more than 2500 species that grow on rocks and tree trunks. Ultimately, whenever mechanical support and essential nutrients are provided, plants can root in any inert structure. The plant growth technique using inert media is known as hydroponics (Ramsey and Ungerleider, 2008). Examples of particulate hydroponic substrates are perlite, pumice and vermiculite. Rigid hydroponic materials include rock wool, glass wool. Fibrous (in)organic materials could be polyurethane, polystyrene, and polyethylene. The advantage of rigid layers is that these media do not need a constituting container. The advantage of particulate media is that these usually have a better drainage capability (Ramsey and Ungerleider, 2008). The efficiency of hydroponic substrates is demonstrated in greenhouses, where it is common practice to use hydroponic soils to have a better control over the plant growth, prevent fungi, and improve water retention and aeration (Figure 14). Artificial substrates of glass wool or rock wool and beds of perlite particles are commonly applied in these contexts (Ramsey and Ungerleider, 2008).

Alternatively, hydroponic materials can be used as a combination with potting soil to form quasi-hydroponic substrates. Perlite is a well-used hydroponic particulate material that can be used as an artificial vegetation

bed or be mixed-in with other (fibrous) soils to increase porosity and pore size distribution, while also countering the over-time compaction of a soil. Pore sizes can be carefully controlled, and are usually within the range of 0.5 - 5 mm. Perlite is resistant to aqueous corrosion, has high water retention of up to five times its own weight, and has minimal impact on the pH values of the solution. Similarly, polymer gel particles or vermiculite pearls are water-absorbing particles that are added to soil to absorb moisture without reducing the porosity of the soil. Since the polymer gel / vermiculite pearls take in most of the water, no moisture can aggregate and clog the soil's pores.

Figure 14 - Amaryllis growth in a substrate layer of perlite (own image)

3.2. Visco-thermal absorption by porous substrates

The substrate acts as a porous absorber that can attenuate an incident sound wave by visco-thermal absorption (Davis et al., 2017). In a nutshell, this means that the friction between air and all the pore walls attenuates the incident sound energy. The key factors in visco-thermal absorption are: flow resistivity, pore size distribution, tortuosity, and the Delany-Bazley method.

3.2.1. Flow resistivity

The substrate should be a porous material which contains air gaps in its medium. The degree to which a material contains these air gaps, is known as its porosity. Soils usually have porosities of 10-40% (Rossing, 2007). As a sound wave meets a porous material, a pressure must be exerted to force the air in the material's pores. The ease with which that can occur is characterized by the flow resistivity σ [Nm^{-4}s or rayls m^{-1}] (Rossing, 2007). This resistance against airflow is caused by friction. Air is a viscous fluid and undergoes viscous drag in the boundary layers at the pore walls of a porous absorbing material. These frictional viscous forces convert the sound energy into heat, therefore being able to effectively absorbing a significant amount of the incident sound energy (Cox and D'Antonio, 2016; D'Alessandro et al., 2015; Ding et al., 2013).
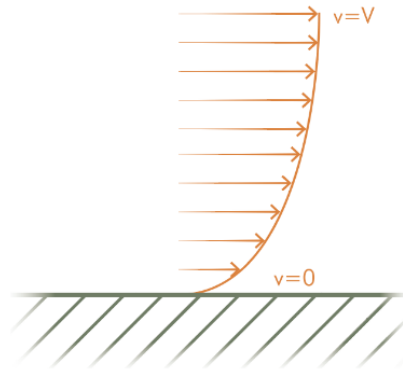
Figure 15 - The viscous boundary layer, V=bulk velocity

When a sound wave propagates near the pore wall in a porous material, a gradient in flow velocity can be observed as a thin layer of viscous fluid near the surface (Figure 15). Air molecules that are directly adjacent to the boundary have zero velocity, due to viscous friction (drag) in the fluid. This condition is known as a no-slip boundary condition, and it is caused by the adherence of fluid to the boundary (Gommer, 2016). Conversely, air molecules some small distance away from the boundary can flow freely, in other words, having a frictionless flow, as is quantified by the fluid's bulk velocity (V) (Godbold, 2008). The distance between the stationary and freely flowing layers of fluid is a build-up of flow velocity and is known as the viscous boundary layer. In this boundary layer, the relative motion between air molecules produces vortices, which are turbulent chaotic flows in the fluid. Ultimately, the sound energy is converted to heat energy by viscous friction in this turbulence, and the losses are significant even for small boundary layers. The size of a viscous boundary layer is generally smaller than 0.25 mm.

For more turbulent propagation, pores should be interconnected, similar to a labyrinth through which the air can propagate deeply into the medium (Cox and D'Antonio, 2016). The number of interactions between the sound wave and the pore boundaries can hereby be maximized. Hence, the interconnectedness of pores, known as open porosity, is fundamental for visco-thermal absorption.
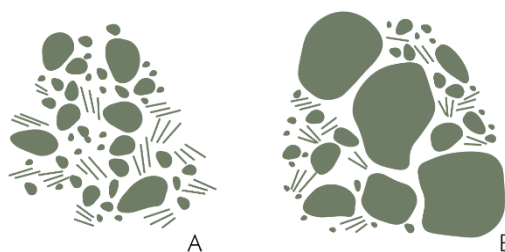
Figure 16 – Uniform (A) and variable (B) pore sizes

3.2.2. Pore size distribution

A soil is not expected to have uniformly sized pores, both in length and in diameter (Figure 16). The pore size distribution describes the variation of pore sizes of a material, which can be determined by its texture (EU CORDIS, 2013). For example, the addition of perlite and polymer gel to a fibrous substrate can create meso-pores (Horoshenkov et al., 2011a). These are pores with a diameter larger than 1 mm, which can

significantly widen the absorption spectrum (Godbold, 2008). A wide distribution of pore sizes controls the acoustical properties, as various diameters capture a wider frequency spectrum. The same increased pore size distribution is caused by a forest floor: a humus layer of partially decomposing vegetation, composed of decayed plant matter and loose soil (Ding et al., 2013; Van Renterghem et al., 2015). A forest floor does not appear in green wall systems the same way as it does in forests, since leaves do not accumulate that much in green wall systems. However, it can theoretically be expected the plant rooting disturbs the substrate surface and increases its pore size distribution.

3.2.3. Tortuosity

The substrate should not be just porous (Figure 17), but the pores should also be interconnected (Figure 18). This is known as open porosity. Materials with a high open porosity have interconnected pores, similar to a labyrinth. When a sound wave enters this labyrinth, it cannot simply travel straight to the other end of the material, but it has to propagate via a more chaotic path. Through a very twisty and complex path, the propagation vector of the acoustic wave is constantly affected, resulting in an inertial air flow. The complexity of this propagation path can be expressed as the tortuosity (Cox and D'Antonio, 2016; Gommer, 2016). Tortuosity can in the simplest case be thought of as the ratio of the porous material thickness to the actual path length of an acoustic wave which is constantly internally reflected (EU CORDIS, 2013).
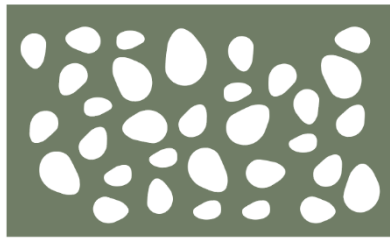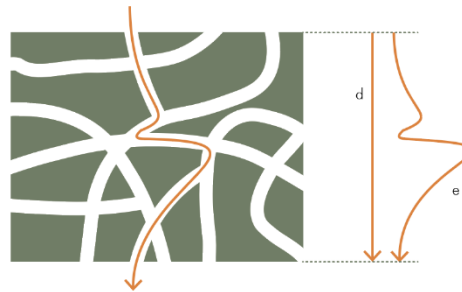
Figure 17 - Closed porosity

Figure 18 - Tortuous propagation. d=direct path, e=effective path

3.2.4. Relationship between flow resistivity and acoustic impedance

Since a high flow resistivity is resisting the flow of air, it dissipates a fraction of the sound energy, consequently absorbing sound. Porous materials therefore have an acoustic impedance at their surfaces which is related to their flow resistivities. This relationship between flow resistivity and acoustic impedance is researched in the study of Delany and Bazley (1970). They have conducted a large number of experimental measurements to find flow resistivity values for a wide variety of porous absorbers. Since the flow resistivity is frequency-dependent, the only inputs needed to retrieve the characteristic impedance of porous material, is its flow resistivity and the frequency, see equations 3.1 and 3.2.

$$Z_c = \rho c \left[1 + 0.0497 \left(\frac{f}{\sigma} \right)^{-0.754} - i0.0758 \left(\frac{f}{\sigma} \right)^{-0.732} \right] \tag{3.1}$$

$$k = \frac{\omega}{c} \left[1 + 0.0858 \left(\frac{f}{\sigma} \right)^{-0.7} - i0.169 \left(\frac{f}{\sigma} \right)^{-0.595} \right] \tag{3.2}$$

Where Z_c is the characteristic impedance, k is the complex wavenumber, ρc is the characteristic impedance of air, f is the frequency, σ is the flow resistivity, and ω is the angular frequency. The Delany and Bazley equations are widely used in prediction models. However, the model works in a limited frequency range and is only valid for isotropic homogenous materials with porosities near unity (Martens et al., 1985). Natural materials generally have a lower porosity and are mostly anisotropic. Hence, the Delany and Bazley model has poor predicting performance for these scenarios. Specifically, Miki (1990) points out that the real part of the characteristic impedance becomes negative for low frequencies, which must be a positive-real function. Miki (1990) has therefore suggested modifications to the coefficients and the degrees in the Delany-Bazley equations. This model as modified by Miki can very convincingly predict the acoustic behavior of vegetative systems (Horoshenkov et al., 2013). Even more recently, additional research is carried out by Komatsu (2008), and improved the accuracy of the Delany-Bazley-Miki model even more by introducing natural logarithms in the equations. These equations are omitted in this report. To predict the normalized surface impedance of the porous layer Z_1, the following equation can be used:

$$Z_1 = -i\, Z_p \cot(k_d \cdot d)$$ (3.3)

Where Z_p is the characteristic impedance of the porous layer, k_d is the complex wavenumber (both Z_p and k_d following from the Delany-Bazley-Miki method), and d is the thickness of the porous layer, which is equivalent to the cavity depth. To predict the frequency-dependent absorption coefficient α, the absolute value of the normalized surface impedance Z_1 has to be taken:

$$\alpha = 1 - \left|\frac{Z_1 - \rho c}{Z_1 + \rho c}\right|^2$$ (3.4)

3.2.5. Substrate thickness

As the thickness of the substrate layer, increases, so does the chance of interactions between incident sound and pore walls. Davis et al. (2017) concluded that a substrate thickness of 80 to 100 mm seemed to be an optimal soil thickness that yields a good overall absorption performance. Most studies on green walls apply a substrate with a thickness of 100 mm. While theoretically the absorption coefficient for lower frequencies increases for a greater thickness (Delany and Bazley, 1970), it was found by Yang et al. (2013) that a substrate thicker than 50 mm showed only a marginal increase in the absorption coefficient for frequencies above 1000 Hz.
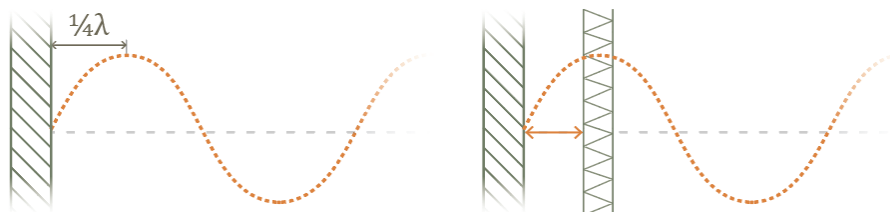

Figure 19 - Optimal placement of absorptive material at the quarter wavelength

When rigidly backed, full absorption takes place where the incident sound wave contains the most energy, which is at one quarter the wavelength off the wall (Gommer, 2016). Here, the particle velocity is maximized and thus allows visco-thermal absorption attenuates sound energy most effectively (Figure 19). However, sound absorbing layers generally have a thickness in the order of magnitude of several centimeters. Consequently, porous absorbers can usually not contain the pressure maximum of the indecent wave in their structure (Godbold, 2008). It is for this reason that the acoustic absorbing performance of porous materials is limited to sound waves of small wavelengths, i.e., of high frequencies (Cai et al., 2014).

3.3. Effect of moisture content on acoustic absorption

The moisture content in a porous substrate affects its absorption coefficient (Horoshenkov et al., 2011a; Van Renterghem and Botteldooren, 2014). Soil moisture is essential for successful plant growth, but conflicts with sound absorption by reducing the soil porosity. Water infiltration swells absorbing soil particles, which clog the pores and prohibit incident sound from entering the porous medium (Van Renterghem and Botteldooren, 2014). Also, the meniscus of water coats soil particles, consequently aggregating them by capillary forces and decreasing soil permeability.

The amount of reduction of absorption coefficient is linked to the degree of saturation, and is therefore more pronounced for lower-porosity soils (Figure 20) (Horoshenkov et al., 2011b). A high-density clay soil with smaller pores (40-60 μm diameter) is more quickly saturated and has more easily clogged pores due to stronger capillary forces. Adding the same amount of moisture to a light-density fibrous soil has far less pronounced negative effects on the absorption coefficient (Horoshenkov et al., 2014). When a little bit of water is externally added to the substrate, it will most likely only enter a few millimeters because of the absorption of the particles in this top layer (Horoshenkov et al., 2011a). Since the pore size distribution varies with depth, a multi-layer model must be devised with different values for the non-acoustic parameters.

Figure 20 - Light-density coir substrate and high-density clay-based soil (Horoshenkov et al. 2011b)

Van Renterghem and Botteldooren (2014) have researched the influence of rainfall on the acoustic properties of a green roof. A mineral substrate XF200 of 70 mm thickness, used in an extensive green roof with various sedum species (cover ratio 65%) was experimentally tested in-situ. Both natural precipitation and artificial wetting were applied. The results showed a difference in sound attenuation between the dry state and a nearly saturated state of up to 10 dB. The sound diffracted differently for an increased moisture content in the frequency range of 250 - 1250 Hz. For lower frequencies, the increased moisture content made no impact, since the absorption was low anyhow.

Horoshenkov et al. (2011a) have researched the influence of moisture on the acoustical properties of different types of substrates. A light-density substrate made from coconut fibers, perlite, and polymer gel was compared to a high-density clay-based soil. Substrate samples were placed in an impedance tube of 100 mm diameter (1.57 L soil specimen), after which 100 cm^3 water was added. The results show a significant sevenfold reduction in absorption coefficient for the high-density soil, essentially reducing the absorption coefficient to around 0.1 for the entire measured frequency spectrum (100 - 1500 Hz). The light-density soil also shows a reduction of absorption, however this is only up to 1.5-fold and for frequencies exceeding 200 Hz (Figure 21). The large differences can be explained by the stronger capillary forces in the small pores of the low-permeable clay-based soil, which make the surface into a strong reflector. Additionally, the polymer gel particles in the light-density substrate absorbed a large portion of the moisture, which enables the deeper pores to remain largely unaffected. Thus, a pore size stratification (layering) must be modelled in such cases. Overall, the light-density soil has a great absorption coefficient, similar to fiberglass.
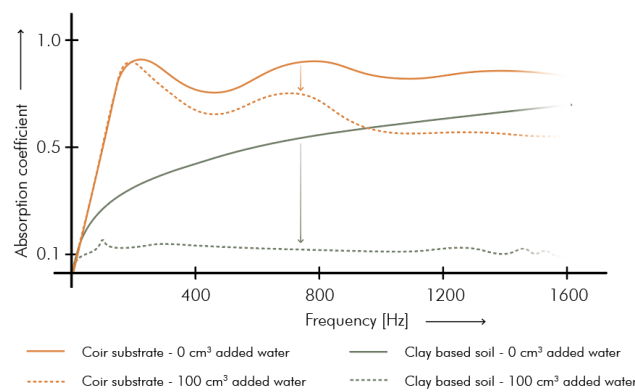

Figure 21 - Effect of moisture on substrate absorption coefficient as measured by Horoshenkov et al. (2011a)

3.4. Conclusion

The theory summarized in this chapter can answer the second sub-question: "What are the key indicators which determine acoustic absorption of the substrate layer?"

- The substrate is the layer which provides mechanical support and essential nutrients to the plant. Plants can therefore root in any inert structure which satisfies these conditions (hydroponics). This has many advantages, including an improved retention of water and better control over the plant growth.
- Substrates are porous materials and absorb sound by visco-thermal absorption. As a sound wave meets the pores, a pressure must be exerted to force the air into the medium (flow resistivity). The resistance against airflow is caused by viscous friction. Basically, the air 'sticks' to the pore walls, in a region known as the viscous boundary layer. Friction is converted into heat, and this is how acoustic energy is absorbed.
- Delany and Bazley have developed a model that relates the flow resistivity to the acoustic impedance of a porous material. The impedance is the resistance of a medium to bringing its particles in vibration, and relates to the absorption coefficient.
- The more interconnected and twisted the pores are, the higher the flow resistivity. Also, a thicker layer can therefore absorb a lower frequency sound.
- Additionally, moisture in the substrate is essential for successful plant growth, but conflicts with sound absorption by reducing the soil porosity. Water infiltration swells absorbing soil particles, which clog the pores and prohibits sound from entering the pores.
- Ultimately, considering the acoustics of porous materials, a substrate can be made more acoustically absorbing. The layer should be very porous, and should be able to remain porous when moisture is added. For potting soil, hydroponic particles such as perlite can be added to counter the over-time compaction. Alternatively, inert materials can be used, such as mineral wools. An important condition is that the pores should be interconnected and tortuous. Closed porosity materials, such as Styrofoam, are therefore not suitable for sound absorption, nor for plant rooting.

4. Acoustic attenuation by vegetation

Although the substrate is usually accountable for a major part of the incident sound absorption, the vegetation in greenery systems also has the potential to attenuate a portion of the sound to which is it subjected. The first studies on acoustic absorption by vegetation were published in the 1970s and 1980s, such as the study of Bullen and Fricke (1982), who researched the propagation through belts of trees. Over the years, it has become clear that plants can attenuate sound in different ways, which greatly depends on the morphological parameters of the species. This chapter will discuss the following topics:

- How mechanical vibration of leaves attenuates sound above ~2000 Hz (4.1)
- How visco-thermal absorption attenuates sound below ~2000 Hz (4.2)
- How scattering sound can also attenuate sound (4.3)

4.1. Plant leaf vibration

The leaf is the main lateral organ attached to the stem, either appearing as a lateral outgrowth (e.g. in some vascular plants) or as branch-system (e.g. in ferns) (Esau, 1953; Haupt, 1953). The leaf is primarily allocated for the process of photosynthesis. Plant tissue itself does not absorb sound waves (Bucur, 2006), as the outermost layer (epidermis) of a leaf is continuous for mechanical support and to contain water inside the vascular tissue.

The leaf typically has a flattened structure, known as a lamina. When referring to the surface of a leaf, the upper surface is termed the adaxial side, and the back side of the leaf is termed the abaxial side. Plant leaves can absorb incident sound by converting sound energy into heat when the leaves mechanically vibrate as a sound wave hits a leaf (Tang et al., 1986). Compliant oscillations of the leaves and stems occur at certain resonant frequencies, which can be expected when the incident wavelength is equal or smaller than the leaf dimension (Romanova et al., 2019). For example, in a study of Martens et al. (1985), a peak in sound attenuation was found for 4 kHz incidence (λ = 80 mm), which correlates with the transverse dimensions of the tested ivy leaves.

Martens and Michelsen (1981) have researched the plate vibration damping of different types of leaves using laser vibrometry. This method ensured that no mechanical load was applied to the leaves, possibly influencing the resonant properties. The plant species tested were leaves from privet, birch, hazel, and oak trees. The results show that leaves behave as linear mechanical systems, resonating with velocities of $1e^{-5}$ to $3 e^{-4}$ m/s, which is 1-3 orders of magnitude smaller than the air particle velocities. Even though the sound attenuation by a single leaf is small, the number of leaves on the scale of an entire plant is large. The more leaves on a plant, the more vibration damping effects (Horoshenkov et al., 2011b).

Tang et al. (1986) also researched tree leaf vibration, but using accelerometers on different positions of the leaf specimens. It was found that leaves have many vibrational modes (i.e., leaves resonate at different

frequencies), but are broadly grouped into two distinct clusters. The cluster of vibration excitations at 2.5 - 3 kHz were associated with leaf resonance along the direction of the main stem (longitudinal), while the second cluster of vibration excitations at 8 - 10 kHz is believed to be associated with the resonance along the width of the leaf (transverse), at the broadest section (Figure 22). These transverse and longitudinal vibrations are of different magnitudes and out of phase, consequently annihilating the sound energy in the leaf tissue.
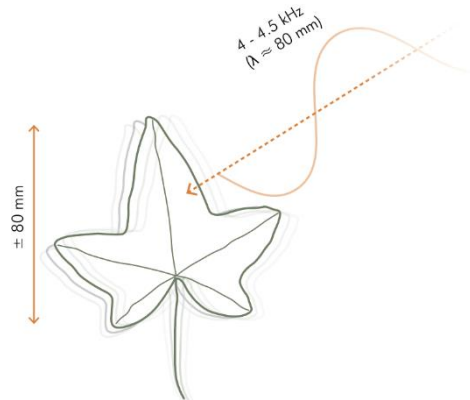

Figure 22 - Ivy leaf vibration as mentioned by Martens et al. (1985b)

Pérez et al. (2018) and Martens et al. (1985) argue that the mass of the plant leaf also influences its resonant properties. The thickness of the epidermis (outermost protective layer) determines for a large part the mass of the leaves (Esau, 1953). Plants that find their origin in relatively moist habitats (mesomorphic plants) have a thin epidermal layer, since the vascular tissue does not have to contain a large amount of moisture (Esau, 1953). On the other hand, plants that come from dry habitats (xeromorphic plants), e.g. aloe, cacti, and agave, have thick or even lignified epidermis, for the vascular tissue to contain a large water buffer. Xeromorphic plants therefore generally have a higher mass and oscillate for lower frequencies. Hence, when considering compliant vibrations, it is important to select a plant species with substantial biomass, and wait for a proper development of the foliage. Generally, broad leaved plants have a better sound attenuating performance. The shape of a leaf does not influence its acoustic performance as much as its dimensions Pérez et al. (2018).

Horoshenkov et al. (2011b) have found that when adding vegetation to a substrate, the increase of absorption is maximum at a frequency which depends on the leaf area. Hence, the smaller the leaf area, the higher this frequency. This implies that different leaf dimensions resonate at different frequencies.

4.2. An equivalent fluid model

The most obvious acoustic phenomenon occurring when a sound wave meets a plant layer, is the visco-thermal absorption. A method that can be used to be able to predict the visco-thermal absorption of a plant layer is known as an equivalent fluid model. In poroacoustics, porous media are modelled in homogenized ways using this model.

4.2.1. Modelling a plant-soil system in an equivalent fluid model

A layer of vegetation contains large voids of air. Therefore, the layer can be approximated as a porous medium which can absorb incident sound by viscous friction (Rossing, 2007). The visco-thermal absorption in soil-plant systems can be predicted using an equivalent fluid model (Prisutova and Horoshenkov, 2014). In such a model, both the substrate and vegetation layers can be represented by uniform porous media with a specific flow resistivity, porosity, tortuosity, pore size distribution, and layer thickness. In other words, the rigid-frame porous medium can be approximated by a parallel array of capillary tubes in which an equivalent fluid passes, having a characteristic impedance and complex wavenumber (Horoshenkov et al., 2013). The vegetation layer has a relatively low flow resistivity and high porosity, compared to the substrate (Romanova et al., 2019).

The Miki model (1990) can very convincingly analytically predict the acoustic behavior of such a two-layer system. D'Alessandro et al. (2015) have found absorption coefficient discrepancies of 0 - 0.9% between Miki's model and impedance tube measurements of fern samples. For Baby tear samples, having a more complex morphology, larger discrepancies of 3.7 - 4.4% were found. In an equivalent fluid model, non-acoustic parameters represent vegetation morphology semi-empirically (D'Alessandro et al., 2015). Vegetation has many morphological parameters, including leaf thickness, leaf weight, leaf dimensions, leaf angle, number of leaves on the plant, plant height, and plant volume. The leaf area density (LAD) is used to compare the total leaf area to the equivalent column of air that a plant inhibits (Horoshenkov et al., 2013) (Figure 23). It is also known as the (adaxial) leaf area per unit volume (Aylor, 1972). The LAD includes the three-dimensional nature of the canopy (height and width), and is therefore a more descriptive term to express canopy density, compared to the LAI (Kenney, 2000; Lin and West, 2016).
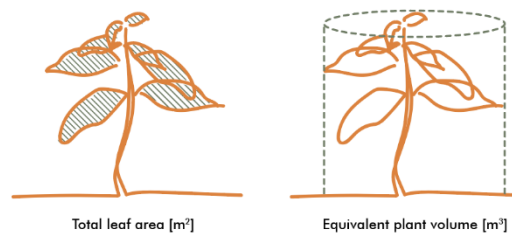

Total leaf area [m²]   Equivalent plant volume [m³]

Figure 23 - Leaf area density determination

The leaf area density LAD is used in all literature regarding the equivalent fluid model for approximating acoustic absorption, such as the well-referenced studies such as the works from D'Alessandro et al. (2015) and Horoshenkov et al. (2013). Related factors, such as the Leaf Area Index, cannot be used in their equations. The relation between a plant's morphology and non-acoustical parameters flow-resistivity, tortuosity, and porosity can be approximated using the equations 4.1 – 4.6, presented by D'Alessandro et al. (2015). The tortuosity α_∞ is directly related to the dominant angle of leaf orientation θ:

$$\alpha_\infty = \cos\left(\frac{\theta_f}{2}\right) + 2\sin\left(\frac{\theta_f}{2}\right) \qquad (4.1)$$

The equivalent volume occupied by the plant sample V_p is determined by:

$$V_p = a_p \cdot h_p \tag{4.2}$$

where h_p is the height of the plant sample and a_p is the plant footprint area:

$$a_p = \pi \cdot d^2/4 \tag{4.3}$$

where d is the diameter of the used plant pot or equivalent circular footprint area. The leaf area density of the plant sample is determined by:

$$LAD = \frac{(n_f \cdot a_f)}{V_p} \tag{4.4}$$

Where n_f is the number of leaves on the sample and a_f is the mean area of the sample's leaves. The flow resistivity σ of a vegetation layer depends on the leaf area density LAD and the dominant angle of leaf orientation θ. Eq. 4.5 is used for θ > 70° and eq. 4.6 is used for θ < 40°:

$$\log_{10} \sigma = 0.0083\, LAD + 1.413 \quad \text{or} \quad \log_{10} \sigma = 0.0067\, LAD + 0.746 \tag{4.5 \& 4.6}$$

Horoshenkov et al. (2013) has altered the Delany-Bazley-Miki equations to account for the equivalent porosity Φ and tortuosity α_∞ of a plant layer:

$$Z = \frac{\sqrt{\alpha_\infty}}{\Phi}\left[1 + 0.07\left(\frac{f}{\sigma}\right)^{-0.632} + i0.107\left(\frac{f}{\sigma}\right)^{-0.632}\right] \tag{4.7}$$

$$k = \frac{\omega\sqrt{\alpha_\infty}}{c}\left[1 + 0.109\left(\frac{f}{\sigma}\right)^{-0.618} + i0.160\left(\frac{f}{\sigma}\right)^{-0.618}\right] \tag{4.8}$$

4.2.2. Transfer-matrix approach for multi-layer impedance

When considering a multi-layer system, the combined impedance can be predicted using the transfer-matrix method. This is a mathematical approach in which each layer is represented by a matrix, in which the sound pressure and particle velocity at the boundaries are used (Berardi, 2013). Consider a two-layer system, e.g. the vegetation layer backed by the substrate layer. In this case, the combined surface impedance can be predicted using the following equation (Horoshenkov et al., 2013; Vér and Beranek, 2006):

$$Z_t = Z_{c;p}\frac{Z_{s(n)} - Z_{p(c)}\tanh(ik_p d_p)}{Z_{p(c)} - Z_{s(n)}\tanh(ik_p d_p)} \tag{4.9}$$

Where $Z_{p(c)}$, k_p, and d_p represent the plant layer characteristic impedance, complex wavenumber, and layer thickness, respectively, and $Z_{s(n)}$ represents the substrate layer *normalized surface* impedance. In case a layer contains different material properties along its planar surface, e.g. in case of a perforated layer, or when a substrate is very locally irrigated, the acoustic impedance of that layer Z_x can be predicted using the following equation to determine its compound impedance:

$$\frac{1}{Z_x} = \frac{1}{Z_y \varepsilon_y} + \frac{1}{Z_z \varepsilon_z} \qquad (4.10)$$

Where Z_y and ε_y are the acoustic impedance and area fraction of the first medium on the planar surface, and Z_z and ε_z are the acoustic impedance and area fraction of the second medium on the planar surface:

$$\varepsilon_y = \frac{A_S}{A_y} \qquad \text{and} \qquad \varepsilon_z = 1 - \varepsilon_y \qquad (4.11 \text{ \& } 4.12)$$

Where As is the surface area of the sample, and Ay is the surface area of the specific medium on the planar surface of the sample. If the second layer in the two-layer system is a compound surface, substitute Z_p for Z_x in equation 4.9.

4.2.3. Leaf area

Plants with a higher leaf area density absorb more incident sound energy and have broader frequency range (Azkorra et al., 2015; Horoshenkov et al., 2014). The leaf area density can be determined by comparing the total leaf area on a plant to the equivalent column of air the plant inhibits. Plant species that find their origin as growing on the floor of dense forests, so-called sciophytes, have developed larger leaf surfaces to increase their insolation needed for photosynthesis (Esau, 1953). These low-light conditions are sometimes accompanied with a low water supply, and some plants have adapted to survive these additional stresses. Since photosynthesis is a process that takes place on the adaxial leaf surface, sciophytes have optimized their growth by growing a larger leaf surface area, and a thinner leaf compared to heliophytes (sun-tolerant plants). Since solar energy is conserved in sciophytes, the plants grow slowly and damaged plant organs are usually not replaced. Due to the specialized function of the leaf for photosynthesis, the organ predominantly contains primary tissue and lacks storage tissues (Esau, 1953). Therefore, the organ cannot grow unrestrictedly. The leaf generally does not have the capability to restore its tissue, when exposed to harmful external conditions such as wind. Consequently, leaves are limited in size, mass, and lifespan.
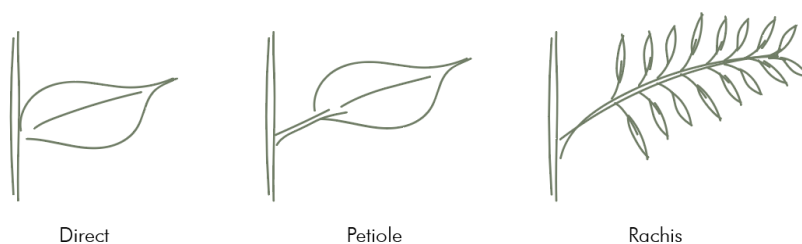

Direct   Petiole   Rachis

Figure 24 - Leaf connection types

44

4.2.4. Dominant angle of leaf orientation

Plant leaves contain a network of veins of various sizes, the largest of which attach to the plant stem, either directly, by means of a petiole, or in case of compound leaves (e.g. in ferns) by a central rachis (Figure 24). The dominant angle of leaf orientation (θ) is the average angular difference between the main vein to the plant stem (Horoshenkov et al., 2013). This morphological parameter relates to the tortuosity (a_∞) of the vegetation layer. Tortuosity defines the ratio between the direct and the effective paths a sound particle takes between two points (Figure 25). In case of a porous vegetation layer, a larger leaf angle results in a longer effective path through which sound propagates. In the limit, a maximum tortuosity can be achieved for a leaf that is oriented perpendicular to the incident sound.
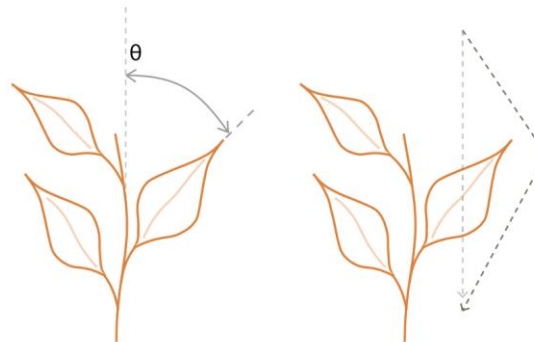

Figure 25 - Dominant angle of leaf orientation and its relation to tortuosity.
d=direct, e=effective path of propagation

Moreover, the orientation of leaves is not static but rather dynamic, as the position of the sun and its intensity can influence the orientation of the leaf. The plant can actively orient the adaxial surface to a light source, through a process called phototropism (Chamovitz, 2017). The mechanism that can move the aerial organs is controlled by specific swelling highly elastic cells (pulvinus) in the petiole. This phenomenon results in a mechanical force that can move the petiole in any direction. In addition, maximization of light absorption is not always preferred, and consequently plants can orient their leaves parallel to the sun to prevent dehydration, e.g. in times of drought. The changeability of the leaf orientation is one of the factors that complicates the reliable determination of the acoustic performance of a plant layer.

4.3. Scattering & destructive interference

A stochastic layer of vegetation can be approximated as an array of reflectors with a random probability distribution of size and orientation (Yovel et al., 2009), consequently reflecting and refracting sound, resulting in a typical scattering phenomenon. Although scattering in the vegetation layer influences the incidence vectors, it does not induce a physical loss in sound energy levels (absorption), but is rather the imaginary component of acoustic impedance, known as acoustic reactance (Tang et al., 1986). Scattering prevents the free propagation of sound and attenuates sound levels for higher frequencies (D'Alessandro et al., 2015), most notably above 2000 Hz. This depends on leaf size: the bigger the leaves, the lower the frequency from which the sound effectively scatters.

Whenever direct and the reflected sound waves interfere with each other, a local destructive interference causes sound attenuation (Azkorra et al., 2015). In vegetative scenarios, this phenomenon is commonly referred to as the ground effect, and can be caused by two phenomena. Firstly, the ground-reflected wave travels a longer distance than the direct wave. Secondly, due to interactions with acoustically soft soil, the sound wave is delayed, as well as partially impeded. On the contrary, over hard ground, the retarding effect does not apply. Wherever the two waves are of opposite phase, a cancellation effect is produced.

4.4. Conclusion

The theory summarized in this chapter can answer the third sub-question: "What are the key indicators which determine acoustic absorption of the plant layer?"

- Vegetation can attenuate incident sound in three ways: by sound-driven oscillations of leaves, by scattering, and by visco-thermal absorption in the air voids.
- For frequencies above ~2000 Hz, the mechanical vibration of leaves is the predominant attenuating factor. The resonant frequency depends on the similarity between the leaf dimensions and the incident wavelength. Also, the mass of the plant plays a role in the plant's resonance. Plant mass is mainly determined by the thickness of the outer layer of tissue.
- Additionally, plant leaves are randomly oriented and therefore scatter sound to a large extent. As a result, destructive interference attenuates a portion of the sound.
- For frequencies below ~2000 Hz, the plant can absorb sound by visco-thermal absorption. The absorption coefficient can be predicted by imagining a plant layer as a porous medium. This method is known as an equivalent fluid model. Thus, the absorption coefficient of both the plant layer and the substrate layer can be predicted using the Delany-Bazley-Miki equations. The acoustics of porous media are described in chapter 3.
- In an equivalent fluid model, the following morphological parameters of a plant can be related to acoustic parameters:
  - The plants total leaf area in comparison to the volume the plant inhibits, known as the leaf area density, relates to flow resistivity.
  - The angle of inclination of the leaf, relative to the incoming sound wave, relates to the tortuosity.
  - The biomass volume of a plant in comparison to the volume the plant inhibits, determines the porosity, and is generally above 0.95.
  - The ratio of the plant height to the plant width therefore determines to a large extent the flow resistivity.
- Plant species that are used to low-light conditions, known as sciophytes, have devolved relatively large leaves to capture as much sunlight as possible. In addition, yielding a maximum insolation entails that the plant usually orients its leaves perpendicularly to the incoming solar rays. This fact can be exploited for to yield a high tortuosity. Thus, sciophytes generally have a higher leaf area density and, consequently, have a higher acoustic absorption potential.

5. Analysis of suitable sound absorbers for integration

The previous chapters have shown that adding vertical greenery as a sound absorbing material on the facades of an urban street canyon can reduce the sound levels. However, the low-frequency absorption performance is still insufficient to attenuate road traffic noise. This can especially be seen in Figure 10. To solve this problem, a new VGS will be designed which to incorporate a separate low-frequency (LF) absorbing system. This chapter lists all potential LF-sound absorption systems.

5.1. Resonant panels

Resonant panels, also known as membrane absorbers, form mass-spring systems with a single degree of freedom that can effectively attenuate low-frequency sound waves (Godbold, 2008). Diaphragms, usually in the form of rigid panels of plywood, are mounted on an enclosed air space. In this case, the panel forms the mass and the enclosed air forms the spring. When the incident sound wave hits the panel, a compression behind the membrane occurs, which is converted into heat. The surface impedance Z can be approximated by equation 5.1 (Cox and D'Antonio, 2016):

$$Z = r_m + j[\omega m - \rho c \, \cot(kd)] \tag{5.1}$$

Where r_m is acoustic resistance as in $r_m = \sigma d_2$ m is the acoustic mass per unit area of the panel, and d is the depth of the cavity. In case of a cavity filled with porous absorbent, the spring will differ depending on the spring stiffness of the specific resilient material. The spring stiffness can be related to the Young's Modulus of the cavity material, and the membrane dimensions.

5.2. Passive destructive interference

This type of sound absorption is achieved by tubes that are specifically tuned to certain frequencies. The system captures the incident wave in two different tubes, of which one is deliberately longer than the other. The two tubes meet at a given point; hence, the two separate propagation paths intersect. This intersection is located where the two waves are in opposite phase, which cancels out the pressure difference by destructive interference. Essentially, the system is comprised of two quarter-wavelength tubes, and at their intersection, half of the wave's crests and troughs are attenuated by destructive interference. Setaki et al. (2014) has produced prototypes by means of rapid manufacturing, where paths of constant section were bent to fit into a small space.

5.3. Helmholtz resonators

5.3.1. Single resonator

Helmholtz resonators, also known as resonant cavity absorbers, act as mechanical mass-spring oscillators with a single degree of freedom (Godbold, 2008; Gommer, 2016). The air enclosed in an orifice vibrates

against the air in an enclosed volume, which acts as a spring with almost zero mass (Costa, 2016) (Figure 26). The system is set in motion by an incident sound wave at the resonant frequency. At that frequency, the resonant absorber is able to achieve an increased magnitude of oscillations, which is attenuated by visco-thermal absorption at the viscous boundaries (Godbold, 2008). Hence, rather than having a broadband absorption, resonant absorbers have an absorption peak in a narrow frequency range. The quality of such absorbers is that these perform well for low frequency sound, usually far more spatially efficient than the equivalent required thickness of a porous absorber. However, the drawback is that the absorption bandwidth is limited to a narrow region around the resonant frequency.
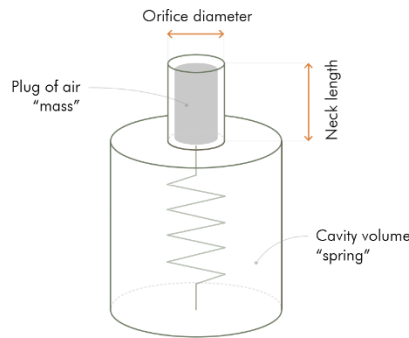

Figure 26 - Schematic representation of Helmholtz resonator

A Helmholtz resonator can be tuned to absorb for a certain resonant frequency, which is dependent on the mass and the spring stiffness, which are determined by the length and radius of the neck, and the dimensions of the cavity, respectively. Additionally, Absorption can reach levels of unity when the internal resistance is similar to the characteristic impedance of air. Kinsler et al. (1982) presents equations to approximate the resonant frequency of Helmholtz resonators (not taking into account the neck length correction):

$$f_r = \frac{1}{2\pi} \sqrt{\frac{s}{M}} \tag{5.2}$$

Where s is the equivalent stiffness of the spring:

$$s = \rho c^2 \frac{A^2}{V} \tag{5.3}$$

Where $A = \pi r^2$ is the cross-sectional area of the circular orifice (r being the orifice radius), V is the cavity volume, and M describes the mass:

$$M = \rho A l \tag{5.4}$$

Where A likewise is the cross-sectional area of the orifice and l is the length of the neck. To yield a small resonant frequency f_r, the ratio (s/M) in eq. 5.2 should be small, i.e. a large mass M as denominator and a small spring stiffness s as numerator. It must be noted that the orifice area A determines both the spring stiffness A and the mass M. The orifice area A influences the spring stiffness s, because the plug of air in the Helmholtz neck, forming the mass, oscillates and overshoots due to the inertia of the oscillating motion

(Kinsler et al., 1982). Consequently, the air contained in the Helmholtz cavity is compressed, since the cavity volume is assumed to be static. Therefore, the cavity pressure is increased by an amount that is proportional to the volume of the air column of dimensions orifice area A times height of the mass displacement ξ. Since the orifice area A has is more crucial to the spring stiffness s than to the mass M, it follows that the orifice area A should be as small as possible to yield a lower resonant frequency f_r. However, to still make the mass term M larger, the neck length L should be increased. Concluding, since the orifice area A is more significant in the spring stiffness term s, it follows that the Helmholtz resonator neck should be long and narrow to yield a low resonant frequency.

To account for air movement around the orifices of the neck, a correction factor δ is added to the neck length. The neck of a Helmholtz resonator has two ends, which means that a correction factor should be added twice. For an orifice radiating into an infinite medium, the correction factor as given by Rayleigh (Cox and D'Antonio, 2016):

$$\delta_\infty = \frac{8r}{3\pi} \tag{5.5}$$

The correction factor for an orifice radiating into a confined space is presented by Ingard:

$$\delta_2 = 0.85r \left(1 - 1.25\frac{2r}{D}\right) \tag{5.6}$$

where D is the diameter of the cylindrical cavity of volume V and r is the orifice radius. The acoustic impedance at the external orifice of a Helmholtz resonator is a complex number, since the maximum pressure may not occur at the same phase as the maximum air velocity (Gommer, 2016). The impedance of a Helmholtz resonator with a cavity filled with a porous material is given by Z_2 (Cox and D'Antonio, 2016):

$$Z_2 = \frac{1}{\varepsilon_R}(2\delta a + l)i\omega\rho + Z_1 + R_i \tag{5.7}$$

Where δ is the neck end correction (eq. 5.5/5.6), l is neck length, ρ is the density of air, ω is the angular frequency, Z_1 is the impedance above the porous layer (eq. 5.9), R_1 is the optional added resistance in the Helmholtz neck (eq. 5.11), and ε_R is the ratio between the area of the orifice A_o and the area of the resonator A_R (in the 2D front view), also known as the resonator porosity:

$$\varepsilon_R = \frac{A_o}{A_R} \tag{5.8}$$

The normalized impedance below the resonator plate, and above the porous layer is determined by Z_2:

$$Z_1 = -i\, Z_p \cot(k_d \cdot d) \tag{5.9}$$

Where Z_p is the characteristic impedance of the porous layer, k_d is the complex wavenumber (both Z_p and k_d following from the Delany-Bazley-Miki method), and d is the thickness of the porous layer, which is equivalent to the cavity depth. In case of an air-filled cavity, Z1 can be calculated using eq. 5.10:

$$Z_1 = -i\,\rho c \cot(kd)$$

(5.10)

Where $\rho{\cdot}c = Z_0$, k is the normal wavenumber and d is the cavity depth. Additionally, it is well researched that the effective frequency bandwidth can be broadened by adding viscous resistance in the neck of the Helmholtz resonator system (Godbold, 2008). This has the side effect of reducing the amplitude of oscillations, consequently reducing the absorbing peak heights. Increasing the absorption bandwidth of Helmholtz resonators in this way was researched by Gommer (2016). She concludes that the absorption bandwidth can be increased by increasing the surface area, and thereby the viscous drag, in the neck. This can be done by adding fins or by curving the neck tube. Alternatively, porous material can be added into the cavity (Godbold, 2008), which impedes the air motion by visco-thermal resistance. Figure 3.2 from Godbold (2008) shows how adding porous material reduces the peak absorption, but widens the spectrum. Additional losses in the neck can be achieved by adding a plug of porous material are characterized by the factor R_i, which can be calculated by equation 5.11 (Vér and Beranek, 2006):

$$R_i = \sigma d_n$$

(5.11)

Where σ is the flow resistivity of the porous material and d_n is the thickness of the plug in the neck. To yield the frequency-dependent absorption coefficient α, equation 5.12 can be used. The term Z2 is complex, consisting of a real and imaginary part, yet by taking the square of the complex term, the answer becomes real:

$$\alpha = 1 - \left|\frac{Z_2 - \rho c}{Z_2 + pc}\right|^2$$

(5.12)

5.3.2. Coupled resonators

For most practical purposes, it is not desired to absorb in a narrow frequency range, but rather in a somewhat broader spectrum. Broadband absorption with Helmholtz resonators can be achieved by combining a parallel array of differently-tuned systems in a panel (Dannemann et al., 2018; Randeberg, 2000). Similar to how the great number of unique keys on a piano allow a pianist to play any piece, the unique set of resonators in a parallel coupled system can absorb in a wide frequency spectrum. The combined impedance of a parallel resonator array can be calculated Z_x in eq. 5.13. (Van der Eerden, 2000):

$$Z_x = \frac{1}{\sum \frac{\varepsilon_S}{Z_2}}$$

(5.13)

Where Z_2 is the vector row of acoustic impedance of the different resonator types, and ε_S is the vector row describing the ratio between the total cavity area per resonator type (in the 2D front view), and the total sample area:

$$\varepsilon_S = \frac{n \cdot A_R}{A_S} \tag{5.14}$$

Where n is the number of resonators of the same type, A_R is the individual resonator cavity area of that type, and A_S is the total area of the sample.

5.3.3. Helmholtz perforated sheet when assuming normal incidence

An array of Helmholtz resonators is commonly applied as a perforated plate placed in front of a continuous cavity, since this is simple to construct (Cox and D'Antonio, 2016; Godbold, 2008). In this case, the mass is formed by the small column of air that oscillates in the perforation of the panel. The springs are not formed by individual enclosed volumes, but rather by invisible elementary subdivisions in the continuous cavity. Each subdivision is attributable to an orifice, and the dimensions therefore depend on the spacing of orifices (Cox and D'Antonio, 2016). The cavity does not need physical subdivision, since the air particle velocity approaches zero near the invisible boundaries of two adjacent subdivisions, due to the increasing pressure (Godbold, 2008). The resonant frequency of such systems can be tuned by the orifice spacing (relates to cavity volume), cavity depth, plate thickness, and orifice radius. All orifices may be designed with a corresponding radius, however, the absorption bandwidth of the Helmholtz resonator array can be increased by varying the orifice radii and spacing. Basirjafari (2020) combines an array of Helmholtz resonators that increase in dimensions following the Fibonacci sequence, resulting in a relatively broad absorption bandwidth. Considering the fact that the ratio between the orifice area and the cavity area determines the height of the resonant peak, an optimization can be made for the resonator dimensions.
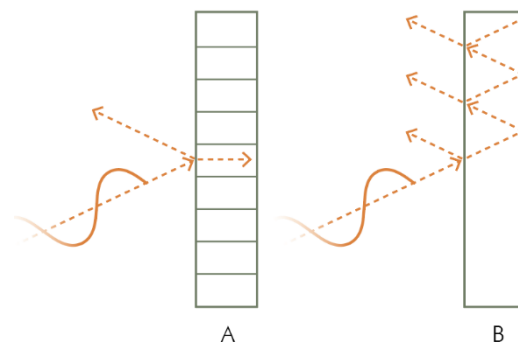

Figure 27 – Normal (A) and lateral (B) propagation in Helmholtz cavity

5.3.4. Lateral propagation

Diffuse sound fields form a challenge for perforated plates with continuous cavities. Lateral propagation occurs inside the continuous cavity for oblique or random incidence (Figure 27). The cavity subdivisions will no longer react independently (Cox and D'Antonio, 2016). The mechanical behavior of Helmholtz absorbers are non-locally reactive systems (Escouflaire, 2014). This means that acoustic energy is dissipated

by viscous friction in the boundary layer near the rigid structure. For incidence that is not normal to the resonator plane, internal propagation will occur in all directions, including in the lateral direction.

The internal propagation must be prevented to yield maximum absorption (Cox and D'Antonio, 2016). A solution would be to add locally reacting materials to the non-locally reacting system, since no lateral reaction exists in locally reacting systems (Escouflaire, 2014). Examples of locally reacting materials are porous materials. In such materials, the surface impedance does not depend on the nature of the incident wave, and normal propagation is enforced (Vér and Beranek, 2006). This occurs due to internal acoustic refraction (Cox and D'Antonio, 2016), similarly to how light 'bends' under Snell's law when entering a material with a different density. Hence, in porous materials, any oblique incidence can be redirected into normal propagation to the face of the porous layer. Thus, when considering a Helmholtz array in the form of a perforated sheet backed by a continuous air cavity, a porous layer of substantial thickness can be placed in front of the orifices, or inside the cavity. In this case, the propagation direction can be assumed to be normal to the surface.

5.4. Compound absorber

When porous materials for high-frequency absorption are combined with acoustic resonators for low-frequency absorption, we speak of compound absorbers. In such systems, the absorption bandwidth is extended. In case of Helmholtz resonators, the placement of a porous layer in front of the resonator orifices complicates the approximation of the combined acoustic impedance substantially (Mechel, 1994). For high frequencies, the mass reactance of the resonant system becomes so large that the resonator layer will approximate a rigid backing. For lower frequencies, a complicated interplay occurs. Detailed equations to determine the acoustic impedance of such systems are presented by Mechel (2008), but omitted in this report. The research presented by Park (2013) and Zhao et al. (2016) conclude that combining a resonator with a micro-perforated panel in front of the orifice can yield a combined acoustic absorption, where the resonator absorbs in the low-frequency spectrum and the micro-perforated panel absorbs in the mid to high frequency spectrum.

It is possible to place a porous layer in front of a Helmholtz resonator, as was found by research of Männel et al. (2013), Forssén and Van Der Aa (2013), and Van Der Aa (2010). Here, resonators were buried in porous asphalt to increase the low-frequency absorption of the road. It was concluded that external sound waves could reach the resonator orifices through the void matrix of the porous asphalt. Hereby it was found that the oscillating mass of the resonators was affected by the porous material.

Similarly, Blumrich and Wiedemann (2015) present a broadband compact absorber (BCA) for the application in automotive aeroacoustic wind tunnels. Thick steel plates are backed by a resilient porous foam layer to form a membrane absorber, so that the resonant frequency can occur below 100 Hz. In front of this resonator, a thick porous layer is placed to extend the high frequency absorption substantially. The

combined acoustic absorption is measured to be uniformly high between 200-4000 Hz, and slightly higher in the low frequency spectrum, between 50-200 Hz.

5.5. Quarter-wavelength tubes

Quarter-wavelength resonators operate similarly to Helmholtz resonators, in the sense that a spring vibrates against a mass in a confined container. However, the geometry of a quarter-wavelength resonator is a long, slender tube, in which spring and mass are continuously distributed (Van der Eerden, 2000). In other words, quarter-wavelength tubes act as Helmholtz resonators where the diameters of the orifice and the cavity are equal (Costa, 2016). Due to this uniform geometry, higher order modes occur in the tube, which allows for additional resonant peaks at higher octaves. The tubes can be tuned for low-frequency sound attenuation, as the resonant frequency is depending on the dimensions, i.e., length and diameter.

Effectively, a standing wave is generated at the resonant frequency and its higher modes, which internally reflects and meets the incident wave at the opposite phase (Van der Eerden, 2000). Recurring absorption peaks occur due to the oscillating mechanism, which are narrowband, similar to Helmholtz resonators (Fuchs, 2013). Viscous friction at the tube boundaries increases the absorption bandwidth slightly (Van der Eerden, 2000). To reach broadband absorption bandwidth, several quarter-wavelength tubes can be coupled, both in parallel and axially (Figure 28). (Fuchs, 2013; Van der Eerden, 2000). By varyingly tuning the systems, a broader frequency range can be attenuated with high absorption. Using this method, broadband absorption for low-frequency sound can be achieved. This system would consist of a sound absorbing panel with numerous orifices, each of which is intended to receive a specific narrow frequency range. The impedance of this panel is related to the individual impedances of the quarter-wavelength tubes and the panel porosity. It is important to evenly space the orifices apart, as interference by modes of similar resonant frequencies must be avoided (Cox and D'Antonio, 2016). This can be achieved by a manual rearrangement, so that similar tubes are not adjacent.
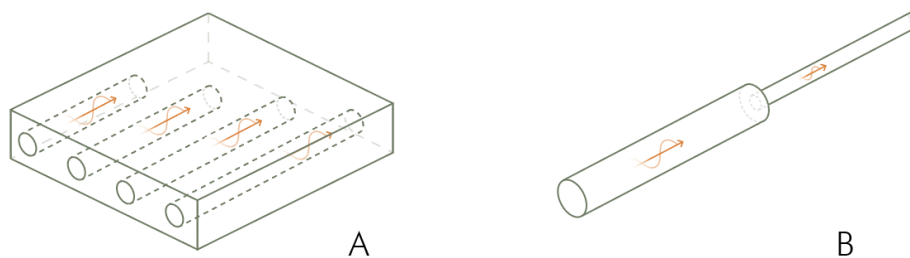

Figure 28 – Parallel (A) and axial (B) coupling different quarter wavelength tubes

The parameters of tube length and radius are the most important factors for determining the resonant frequency and absorption bandwidth (Van der Eerden, 2000). The (corrected) tube length should be equal to a quarter of the wavelength of the desired frequency. The tube radius determines the absorption

bandwidth, e.g., small radii yield higher bandwidths due to higher viscous drag. However, the absorption peaks are decreased as well, consequently increasing the needed porosity of the panel (Cai et al., 2014).

The works of Costa (2016), Cai et al. (2014), Chen et al. (2017), and Van der Eerden (2000) show that a quarter-wavelength tube can be coiled up to inhibit three-dimensional space more efficiently. By coiling up the propagation path coplanar to the constituting panel, and perpendicular on the incident wave, narrow-band acoustic absorption for an ultra-thin medium can be achieved. The tube diameter determined the thickness of the panel. Cai et al. (2014) developed prototypes by 3D-printing, and had embedded a tube with a length of 205 mm into a panel which was 9.7 mm thick, which was found to achieve near-unity absorption in the 400 Hz range. By simulating the air flow velocity in the system, they found high velocities at the entrance of the tube, and low velocities for the remainder. The plug of air near the orifice therefore sees the most viscous drag, while the remaining air acts as the spring, confirming the fact that a quarter-wavelength tube essentially is a special form of Helmholtz resonator (Gommer, 2016).

Chen et al. (2017) elaborated on the concept of coiling up quarter-wavelength tubes, by axially coupling multiple tubes in the perpendicular plane. By doing this, absorption curves can be overlapped, which broadens the absorption bandwidth. A model was simulated, which had two axially coupled tubes which were tuned to resonate at 81 Hz and 106 Hz. The results showed an absorption coefficient of 0.8 and higher for a frequency range of 76-112 Hz, reaching near-unity absorption at 81 Hz and 106 Hz. The panel thickness was 117.1 mm in this case, merely 1/38.5[th] the wavelength. A smaller-scale equivalent was subsequently 3D-printed and experimentally measured in an impedance tube. The results also showed a broadband absorption between 708 - 890 Hz, for the designed resonant frequencies of 734 Hz and 856 Hz. The panel thickness was 22.7 mm, giving a wavelength-to-thickness ratio of 21.3.

Van der Eerden (2000) argues that axially coupling of tubes of different lengths and radii indeed broadens the absorption bandwidth (Figure 29). The coupling does not have to be concentrically, necessarily. By tweaking some parameters of the axially coupled tube geometry, the local minimum can be increased.
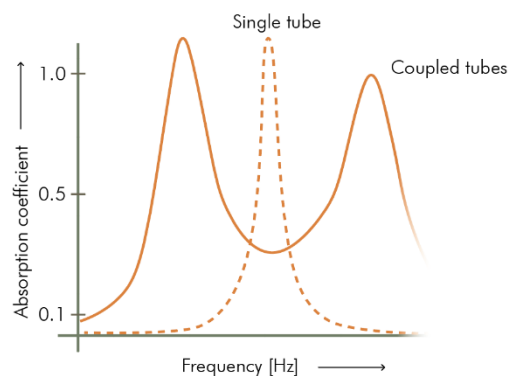

Figure 29 - Absorption curve of single versus coupled tubes (Van der Eerden, 2000)

5.6. Conclusion

The theory summarized in this chapter can answer the fourth sub-question: What sound absorber systems are suitable for low-frequency sound absorption?

Listing the acoustic absorbers has presented a range of solutions to effectively absorb sound. It is shown that resonant systems are capable to effectively attenuate low-frequency sound. These systems use heavily oscillate in specific narrow frequency bands. The systems that use this property are destructive interference tubes, resonating panels, Helmholtz resonators, and quarter-wavelength tubes.

- Interference tubes is the compound two tubes that slightly different lengths. At their ends, the tubes join, and this is exactly where the two waves are out of phase (due to path length difference).
- Resonating panels, or membrane absorbers, are cost-effective resonators. The mass of the panel vibrates against a sealed air cavity or resilient material. However, due to the simplicity of the system, the absorption bandwidth cannot be simply widened.
- The Helmholtz resonator describes a system where a plug of air vibrates against a volume of air. In most cases, the neck and cavity shape do not matter, only the dimensions do. The resonator applied in a parallel array to increase the absorption bandwidth.
- The quarter-wavelength tube is a tube that is essentially a slender Helmholtz resonator. The advantages are that the resonator can be couple both serially and axially.

The most important advantages and disadvantages of the resonating systems are listed in Table 12 (next page).
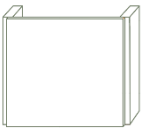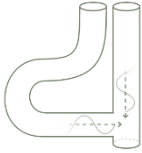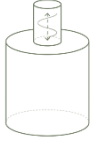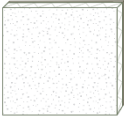
Resonant panels	Interference tubes	Helmholtz resonators	Compound absorbers	Quarter-wavelength tubes
+ Easy fabrication	+ Coiling up tubes possible	+ Well-known and well-documented	+ Broadband absorption	+ Parallel and axial coupling possible
+ Easy tuning by changing plate density	+ Easy tuning by changing tube dimensions	+ Easy tuning by changing neck and cavity dimensions	+ Relatively thin layered system	+ Coiling up tubes possible
− Only two parameters to tune the resonant system	+ Simple geometry	+ Parallel coupling possible	− More complex to predict combined impedance	+ Coplanar coiling possible
− Narrow absorption bandwidth	− Two tubes needed per resonant frequency	+ Addition of resistance broadens bandwidth		+ Easy tuning by changing tube dimensions
− Large surface area needed	− Narrow absorption bandwidth	− Narrow absorption bandwidth		+ Recurring peaks for higher order modes
	− Less efficient compared to QW-tubes			− Narrow absorption bandwidth
				− Bulky tubes for low frequency resonance

Table 12 - Overview of advantages and disadvantages per LF-absorber type

Design process

6. Design process

After reviewing the relevant literature, the design process started. First, a list of design criteria is made, based on the literature. Then, four concept designs were developed consecutively. The concept designs were developed through a process of trial and error, applying various designs that were presented in the literature. This chapter will discuss the design process:

- The design criteria (6.1)
- The choice for a certain VGS type and a certain LF-absorber system (6.2)
- The development of design concepts (6.3)
- The final design (6.4)
- Impedance tube measurement results (6.5)

6.1. List of design criteria

6.1.1. Criteria for acoustic absorption

A. The VGS design must yield an absorption coefficient that is as high as possible, ideally; $\alpha>0.7$ for all octave bands between 63-8000 Hz.

B. The primary selected vegetation species must be optimized for acoustic absorption, entailing:
- a large leaf area density (ideally: LAD > 100 m^{-1})
- large dominant angle of leaf orientation (ideally: $\Phi> 45°$)

C. The substrate composition must be optimized for acoustic absorption, entailing:
- a high open porosity ($>75\%$), also when adding moisture
- no over-time compaction
- water-resistant to driving rain

6.1.2. Criteria for manufacturability

A. The VGS design with the integrated low-frequency sound absorber system (LF-SA) must be easily mass-producible, entailing:
- The LF-SA must be extrudable or injection moldable
- The overall design must be as simple as possible, to allow for easy fabrication

B. The LF-SA is ideally as space-efficient as possible (when comparing two different systems)

C. The LF-SA should be morphologically flexible, to be able to efficiently fit into the VGS cavity

D. The resonant frequency of the LF-sound absorber should be easily tunable by morphological modification

6.1.3. Criteria for applicability:

A. The design should conform to the dimensions commonly found in existing facades. This allows for uncomplicated retrofitting of facades

B. The VGS design will be developed in terms of a single module which can be repeated horizontally and vertically on a facade

C. The VGS design must be adaptable to be applied at edges (e.g. next to windows or near the roofline)

D. The VGS is an indirect system, so that the cavity can be used to accommodate the LF-sound absorbing system
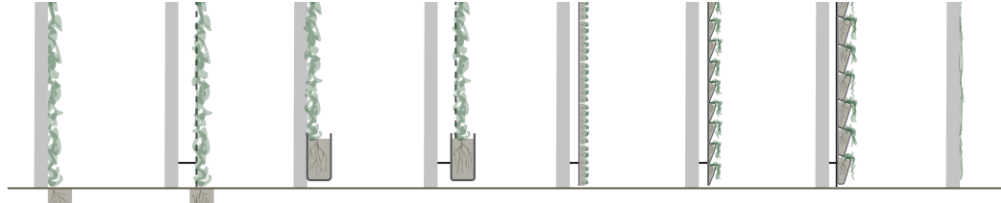
6.1.4. Criteria for manageability:

A. The VGS design should be able to be installed easily, and therefore should be light-weight enough to be able to be carried by a single person

6.1.5. Criteria for durability:

A. The VGS design should ideally have a lifetime of several decades, so that it can become a long-time investment

B. The VGS design should consist out of a minimum of separate parts, so that the structure can endure without breaking down.

C. The selected vegetation species must be suitable for application to withstand mechanical stress induced by high wind speeds or human touch and biotic stress induced by inhibiting flora and fauna, such as weeds.

D. The selected vegetation species must be suitable for the Dutch climate.

E. The selected vegetation species must be suitable for the facade orientation that is place on

F. LWS structure material criteria:

- Non-biodegradable, since the physical structure holds the vegetative system in place
- Light-weight, i.e. a low density.
- Structurally capable of handling the loads to which it will be subjected.
- Allow for large-scale production, to reduce the cost.
- Allow for production accuracy of 0.1 mm, to ensure accurate tuning.
- All materials should have a similar lifespan.
- Made from recycled material or is recyclable itself

6.2. Choice for VGS type

Chapter 2 lists all VGS types and their differences. To find the system with the most potential, a choice matrix was made (Table 13). The LWS based on mineral wool was the system with most potential for the redesign. The system has a cavity space available, has a long lifespan of several decades, and is overall a very simple system. Additionally, the system has the most exposure of its porous substrate: 100% of the substrate is exposed to the YZ-plane, which is the direction from which the incident sound wave comes. A larger amount of exposure of porous substrate means more acoustic absorption.

	Regular green facade	Suspended green facade	Planter box green façade	Suspended planter box green facade	Mineral wool LWS	Felt geotextile LWS	Planter box LWS	Bio-receptive facade
Indirect system with cavity space	0	1	0	1	1	1	1	0
Exposure of porous substrate	0	0	0	0	1	0-0.2	0.3	0
System lifespan of several decades	1	1	1	1	1	0	1	1
Simple geometry for LF-SA integration	0	0	0	0	1	1	0.5	0
Total	1/4	2/4	1/4	2/4	4/4	2.1/4	2.7/4	1/4

Table 13 - VGS choice matrix

6.3. Choice for low-frequency sound absorber

Chapter 5 lists all the potential LF-absorbers. A choice matrix was made (Table 14) Initially, based on the theory, both the quarter-wavelength (QW) tube and the Helmholtz resonator seemed to be equally suitable for integration into the VGS. The QW-tubes also have higher-order modes. Hence, the QW-tube was used in the first concept design. However, while developing the first concept, it became clear that QW-tube geometry is relatively complicated and inefficient.

	Resonant panels	Interference tubes	Helmholtz resonators	Compound absorbers	Quarter-wavelength tubes
Easy tuning of F_{res}	0	1	1	1	1
Space-efficient	1	0	1	1	1
Morphologically flexible	0	1	1	0.5	1
Broadband coupling	0	1	1	1	1
Total	1/4	3/4	4/4	3.5/4	4/4

Table 14 - Choice matrix for LF-absorber type

6.4. Concept designs

At the same time the concept designs were developed, literature was reviewed and a better understanding of the theory developed throughout the process. Hence, not all the theory listed in the literature chapters was taken into account when designing the concept designs. Table 15 shows an overview of what was known at the time of development of the concept designs, and the subsequent reasons for concept rejection.

Concept	1	2	3	4
Design hypothesis	A parallel array of quarter-wavelength (QW) can fit in the cavity space of a mineral wool LWS.	A parallel array of Helmholtz resonators can fit in the cavity space of a mineral wool LWS.	A simple layered design of a perforated plate backing the substrate layer allows for no perforations and no physical Helmholtz cavity subdivisions	Concept designs 2 and 3 are combined so that long, narrow necks pierce the substrate layer. Now, the cavity is filled with porous material to obviate physical cavity subdivision
Design & validation method	Rhino and Grasshopper were used to manually place QW tubes in the cavity. This was linked to a Matlab script	Rhino, Grasshopper, and Matlab were used. Helmholtz arrays were generated using an algorithm	Matlab scripts were written and 3D-printed test pieces were experimentally tested in an impedance tube	Matlab scripts were written. Visualizations were made using Lumion, Adobe Illustrator, and SketchUP.
Results	Not enough QW tubes could fit in the cavity space. Hence, the design yielded a poor absorption	The design yielded a fair absorption coefficient. Yet, many resonators had to be placed, perforating the substrate layer to a high degree	Although the layering concept worked, moisture in the substrate layer prohibits transmission to the resonators. Also, lateral orifices do not work, and plate perforations are not sufficient for LF resonance	This design works well, and allow for a minimal substrate layer piercing, while still yielding a good absorption curve.
Conclusion	Implementation of QW tubes in a LWS does not work, since the tubes are too bulky, and the design is too complicated for mass production.	The design could potentially work, however, it was too complicated to produce. The Helmholtz cavity array would be too heavy. Also, the high number of individual resonators meant that the substrate layer would be perforated too much	It was experimentally determined that backing the substrate layer with the perforated plate does not work well enough, because moisture in the substrate decreases absorption. Also, it does not resonate in the proper frequency range.	Integrating a small number of long, narrow necks in the LWS allows for sufficient absorption in the LF spectrum. By filling the cavity with a porous material, normal propagation is enforced, and physical subdivisions are not necessary.
Key lessons	• Adding porous materials to the tubes broadens the absorption bandwidth, but decreases the peak height • Decreasing the resonant frequency interval can increase the inflection point between peaks	• Helmholtz resonators can be designed in a way that they fit together in a modular way. • The placement of orifices can be optimized, so that they are grouped together. This allows better placement of the plants in the substrate layer	• Locally reactive materials can enforce normal propagation by acoustic refraction • Resonators can oscillate when backing a porous layer, however, the characteristics change • Designs can be scaled down to be easily measured in an impedance tube	• The size of resonators can be increased, while maintaining their absorption coefficient. This leads to a simpler design • The best way to keep a substrate porous is by irrigating as little as possible, directly at the roots.

Table 15 - Concept design development overview (Concept designs are fully described in Appendix II)

6.5. Impedance tube measurements

On the 10th of march 2021, impedance tube measurements were performed to research the potential of concept design 3. The methodology is described in chapter 1.

- Figure 30 shows the control tests for resonator configurations 1 and 4. The graphs show several resonant models, which are clearly visible. It was assumed that the first resonant peaks are the result of the actual Helmholtz action, since this peak was closest to the intended peak. The other peaks may be caused by plate resonances and air escaping through small fissures.
- Figure 31 shows the control tests for resonator configurations 2 and 3. Resonator configuration 2, the lateral orifice type, was tested using two different offsets (12 and 4 mm). The resonating peaks occur at 320 and 276 Hz, respectively. Then, the lateral insert was placed in between the two perforated plates. The first resonant peak was measured at 166 Hz.

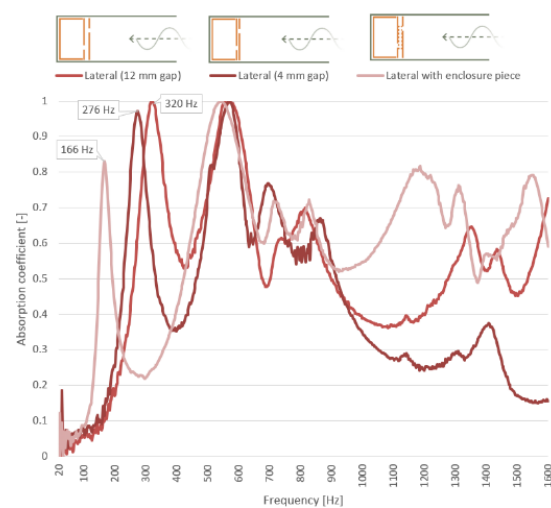*Figure 30 - Control tests for resonators with neck*

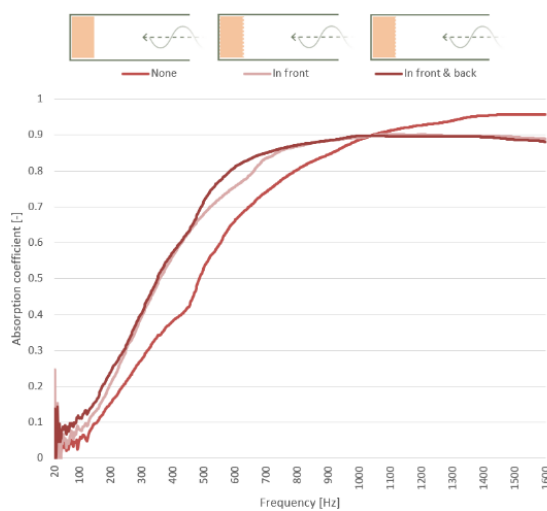*Figure 31 - Control tests for resonators with lateral orifice*

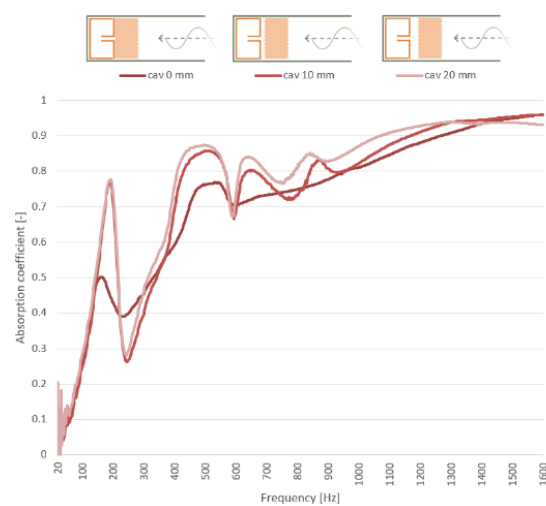*Figure 32 - Effect of adding geotextile layers to the rockwool*

Figure 33 - Effect of air cavity in between porous layer and resonator

62

- Figure 32 shows the effect of adding geotextile layers to the rock wool. The bright red line shows the absorption of the bare rock wool, which absorbs as expected. Adding a geotextile layer in front, and in front+back, slightly changes the absorption behavior. These configurations absorb lower frequencies more. For higher frequencies, the absorption decreases. For this spectrum, it can be assumed that adding geotextile layers does not substantially affect the absorption coefficient.
- Figure 33 shows the effect of adding small spacings of 10 and 20 mm in between resonator configuration 1 and the porous layer. The graph shows that adding a small cavity increases the resonant peak. There is no substantial difference in the 10 or 20 mm spacing, implying that the space needed is less than 10 mm for used orifice dimensions. Hence, it can be concluded that a BCA using a resonating mass of air, needs a small gap between the resonator and the porous layer.
- Figure 34 shows the effect of adding various amounts of moisture to the rock wool. Adding more moisture decreases the absorption. Even a small amount of water, i.e. the 21% saturation rate which is equivalent to a winter irrigation scenario, decreases the absorption coefficient from about 0.95 to 0.56 at 1600 Hz. Both the 76% Sr and 95% Sr have decreased the absorption coefficient below 0.2 for frequencies above 400 Hz. It can therefore be concluded that adding moisture to hydroponic rock wool decreases the absorption coefficient significantly. The moisture clogs the pores of the porous absorber, consequently reflecting a large portion of the incident sound. This is described in chapter 3.
- Figure 35 shows the effect of adding various amounts of moisture to the rock wool on the multilayer absorption coefficient. In these tests, the rock wool was backed by resonator configuration 1, using a small gap in between the layers of 10 mm, and two layers of geotextile. From the graph, it can be seen that any increase in saturation rate decreases the resonant peak. Therefore, the conclusion can be drawn that a decrease in the porosity of the porous layer affects the resonance performance of the resonator
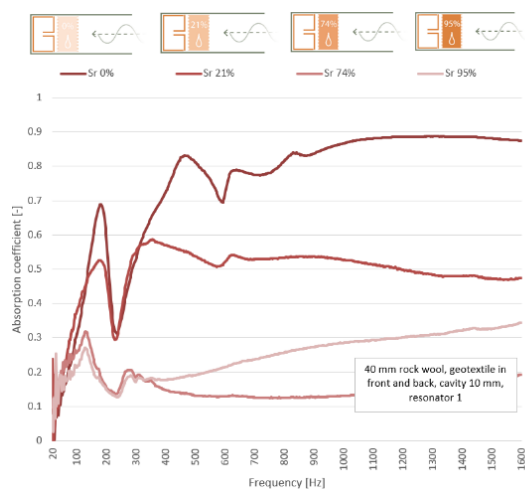
Figure 34 - Effect of moisture on acoustic transmission to the resonators
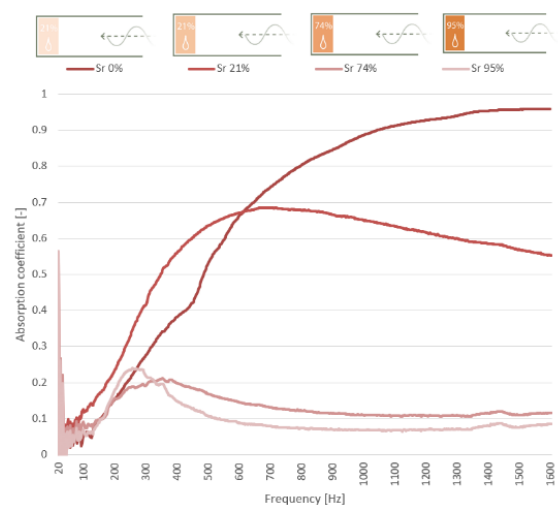
Figure 35 - Effect of various saturation ratios in the rock wool

- Figure 36 shows the effect of the four different resonator configurations, when combined with the porous layer. From the graph it can be seen that resonator configurations 1-3 have a relatively low

resonant peak of around α=0.7. Comparing this with the resonant peak of resonator configuration 4, shows that this peak is much higher, near-unity. Piercing the substrate layer with the Helmholtz neck yielded a significantly higher resonant peak, compared to other configurations. This comparative measurement shows that the resonator does not receive the incident sound wave by transmission through the porous layer. Instead, it can freely oscillate at the front surface of the multilayer structure. Hence, it can be concluded that piercing the porous layer yields better resonant oscillations.
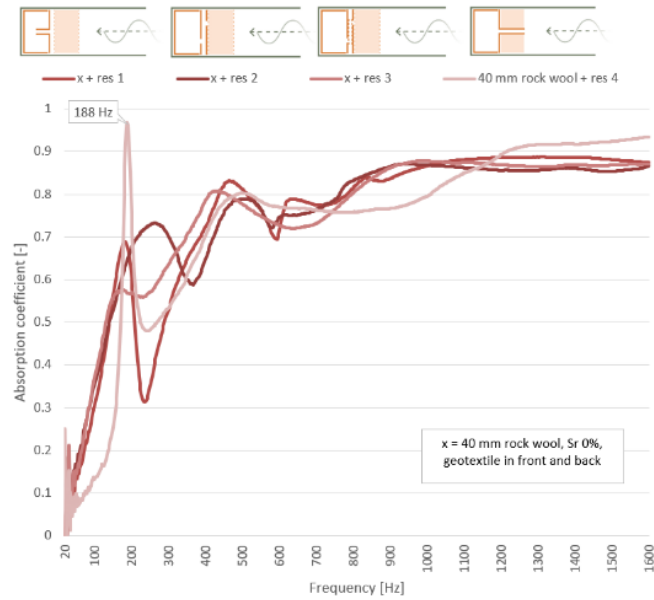
Figure 36 - Effect of resonator combinations

Figure 37 shows photos of some samples that were used in the impedance tube.

Figure 37 - Used samples. (A) multilayer setup, (B) the resonator with inward neck

7. Final design

The previous chapter has shown that various concept designs were developed consequently. The final design is an elaboration on concept design 4. Basically, the final design can be described as follows:

- A living wall system (LWS) with a substrate layer of hydroponic rock wool. In this substrate layer, cut-outs are made in which rock wool cubes fit. These cubes are the starter blocks in which the plant is grown from the seed. This system allows for efficient plant growth (commonly used in greenhouses): the plants can develop in a small cube and are only inserted in the substrate layer as soon as the module is installed.
- The substrate layer is suspended by the Helmholtz necks. These necks perforate the rock wool and suspend it by this piercing action. An acoustically open geo-textile layer wraps around the substrate and the Helmholtz resonator back plate, to bundle the layers. Also, this prevents driving rain from wetting the substrate.
- The Helmholtz necks protrude from the Helmholtz back plate. This plate backs the substrate layer, and is attached to two vertical omega profiles.
- The cavity space, behind the Helmholtz back plate and in between the profiles, is filled with glass wool. This has a good flow resistivity to enforce normal propagation, and increases the thermal resistance of the total system.
- An irrigation system is proposed, that branches into several lateral lines. These dripper lines go just above the plant roots. This allows for irrigating locally at the root. Most of the substrate layer therefore remains dry, acoustically absorbing well. The lines are pressure regulated, so water is distributed equally along all branches.

7.1. Drawings

A set of (shop) drawings is made to visualize the design:

DEF-001	Exploded view of the LWS module
DEF-002	Front views of the geotextile layer and plant layer
DEF-003	Front view of the substrate cubes and the irrigation system
DEF-004	Connection of the LWS module to the facade
DEF-005	Facade connections and flashing details
DEF-006	Helmholtz plate design
DEF-007	LWS module production
DEF-008	LWS module installation to facade
DEF-009	Installation visualization
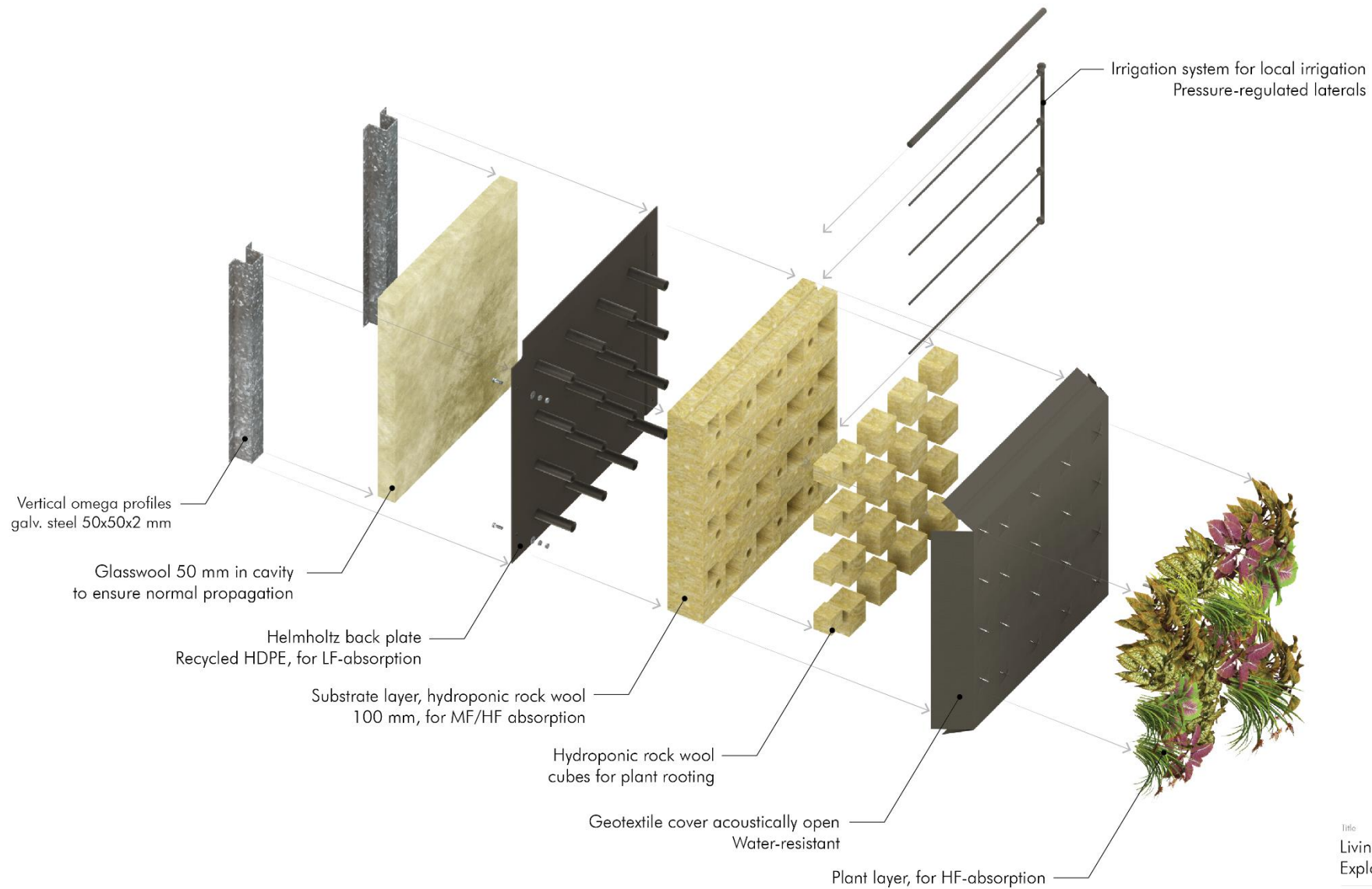
Irrigation system for local irrigation
Pressure-regulated laterals

Vertical omega profiles
galv. steel 50x50x2 mm

Glasswool 50 mm in cavity
to ensure normal propagation

Helmholtz back plate
Recycled HDPE, for LF-absorption

Substrate layer, hydroponic rock wool
100 mm, for MF/HF absorption

Hydroponic rock wool
cubes for plant rooting

Geotextile cover acoustically open
Water-resistant

Plant layer, for HF-absorption

A. GEOTEXTILE OPENINGS

150
150
150
75

92.5 137.5 137.5 137.5 37.5

600

600

LEGEND

Cut cross in geotextile at loc. of plants
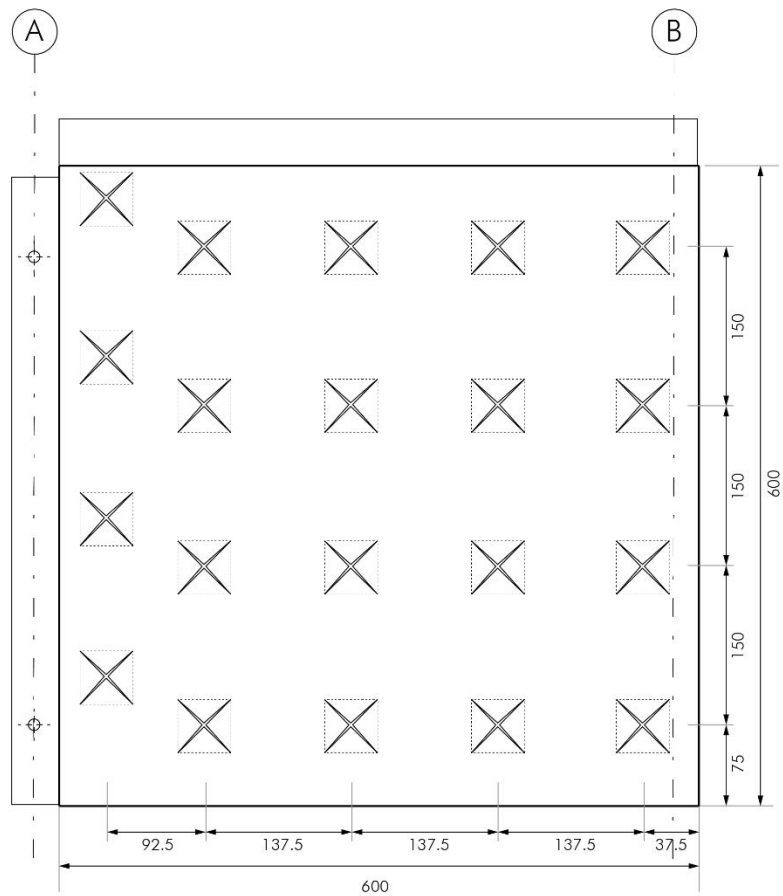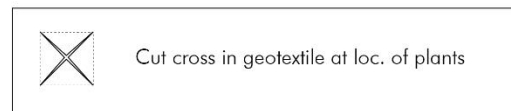
B. FRONT VIEW IMPRESSION

600

600
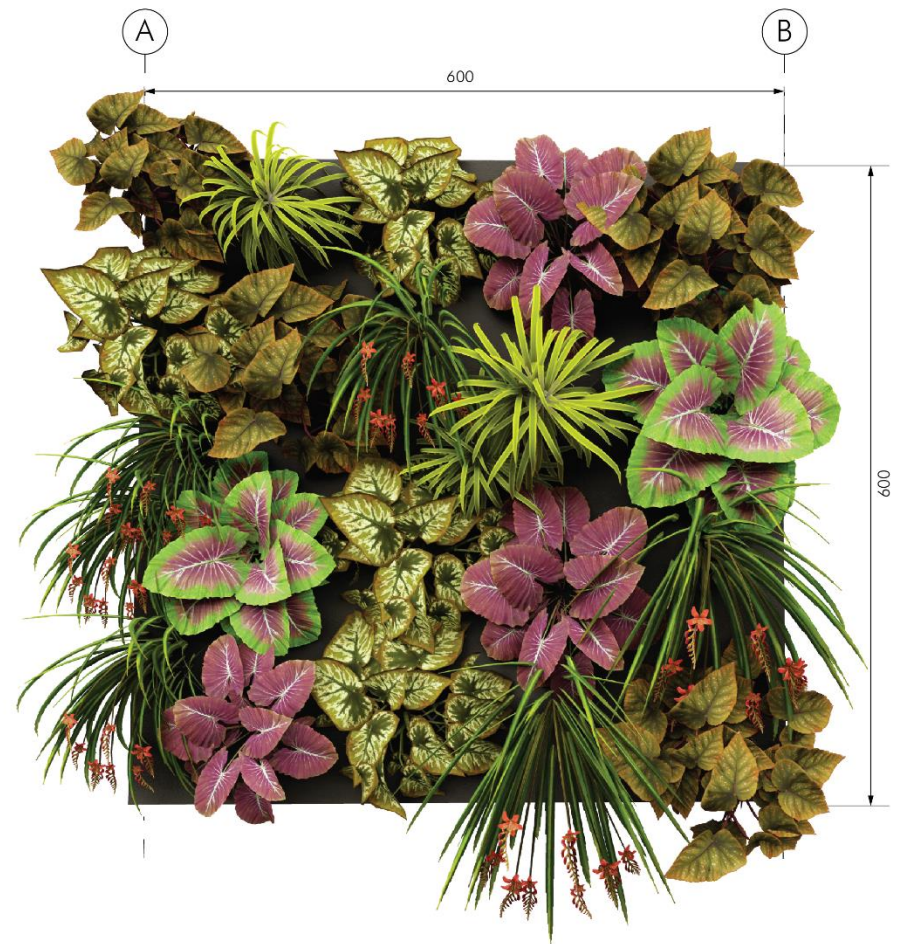
SHADE SPECIES SELELECTION

• Bergenia cardifolia
• Begonia
• Primula
• Hosta Sieboldiana
• Nephrolepis

SUN SPECIES SELELECTION

• Salvia argentea
• Impatiens walleriana
• Penagonium
• Hedera helix
• Chlorophytum

Title

Living wall system module
Geotextile & plant view

Project

Graduation studio
Optimization of VGS acoustics
Delft University of Technology - MSc4 2020-2021

Date	Scale	Phase
5-5-2021	1:5	DEF

Size	Drawn	Drawing no.
A3L	JB	DEF-002

A. HYDROPONIC ROCKWOOL CUBE PLACEMENT

A

B

B
A   A   A   A

B
A   A   A   A

B
A   A   A   A

B
A   A   A   A

150
150
150
75
600

92.5   137.5   137.5   137.5   37.5

600

50x50 mm cubes
to cover up
vertical boundary

75x75 mm cubes
to cover up
the panel

LEGEND

A	Hydroponic rockwool cube 75x75x65 mm
B	Hydroponic rockwool cube 50x50x50 mm
⊗	Helmholtz neck (which penetrates substrate layer)

B. IRRIGATION SYSTEM

Bleeder valve

ZPE Tylene 16x1.8 mm

A

Lateral 1: CNL 4 mm
B

Lateral 2: CNL 4 mm
C

Lateral 3: CNL 4 mm
D

Lateral 4: CNL 4 mm
E

ZPE Tylene 16x1.8 mm

Flow gauge

Pump

Water supply

LWS panel

LEGEND

| ○ | Emitter |
| ⊠ | Pressure compensated valve |

CONNECTION TO FACADE

A — 600 — B

550

68.8 | 137.5 | 137.5 | 137.5 | 68.8

50
3
100

600

Living wall system module layers (in-out):
• Rigid wall, facade
• Cavity fill, glasswool
• Helmholtz plate, recycled HDPE
• Substrate layer, hydroponic rock wool
• Geotextile, Gronest Aqua Breathe (vel sim)
• Plant layer

Rigid wall (facade)

Anchor M8x100 stainless steel

Thermal break plastic

Insulation fill, glasswool strips 50x50 mm

Omega profile galvanized steel 50x50x2 mm

Cavity fill, glasswool

Substrate layer 100 mm, hydroponic rock wool

Helmholtz plate 3 mm, recycled HDPE

Rockwool fill

Overlap joint, fasten with M8x25

50

50

OVERLAP JOINT
HORIZONTAL
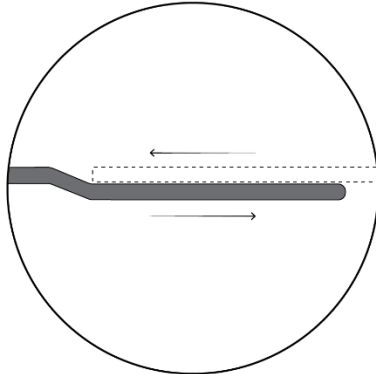
OVERLAP JOINT
VERTICAL
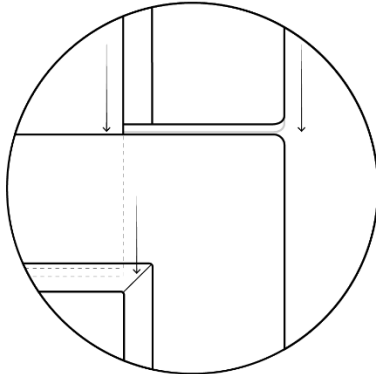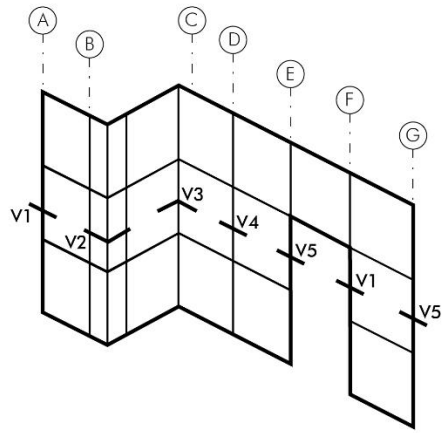
V3 Inward corner

V4 Straight

V5 Right boundary
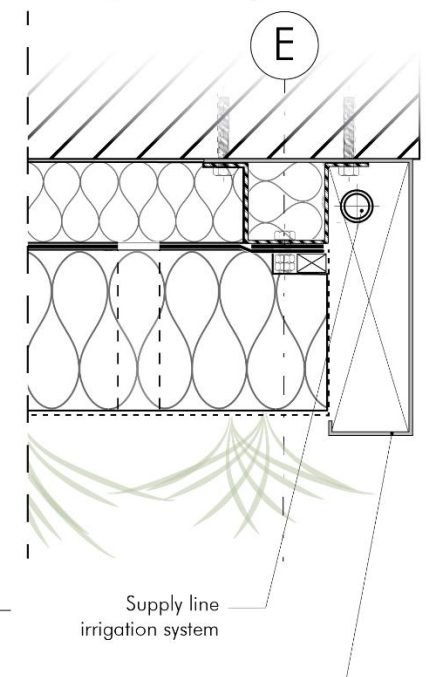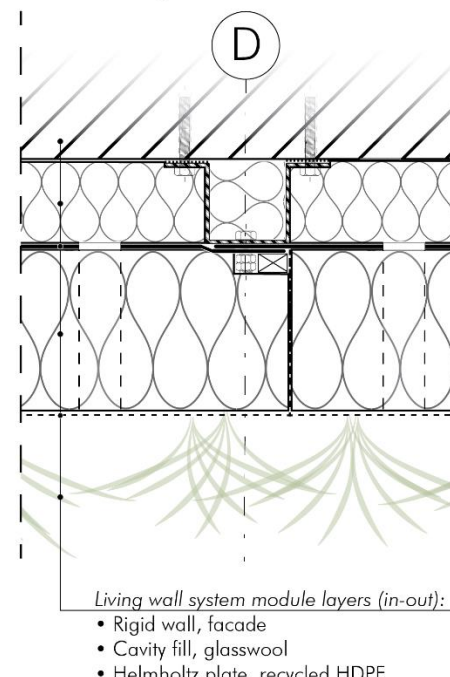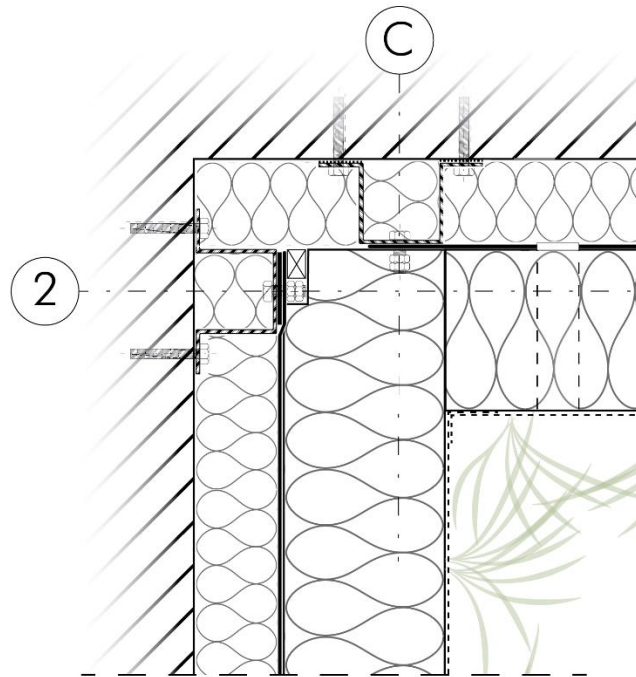
Living wall system module layers (in-out):
- Rigid wall, facade
- Cavity fill, glasswool
- Helmholtz plate, recycled HDPE
- Substrate layer, hydroponic rock wool
- Geotextile, Gronest Aqua Breathe (vel sim)
- Plant layer

Supply line
irrigation system

Aluminium flashing
powder coated in any
RAL color
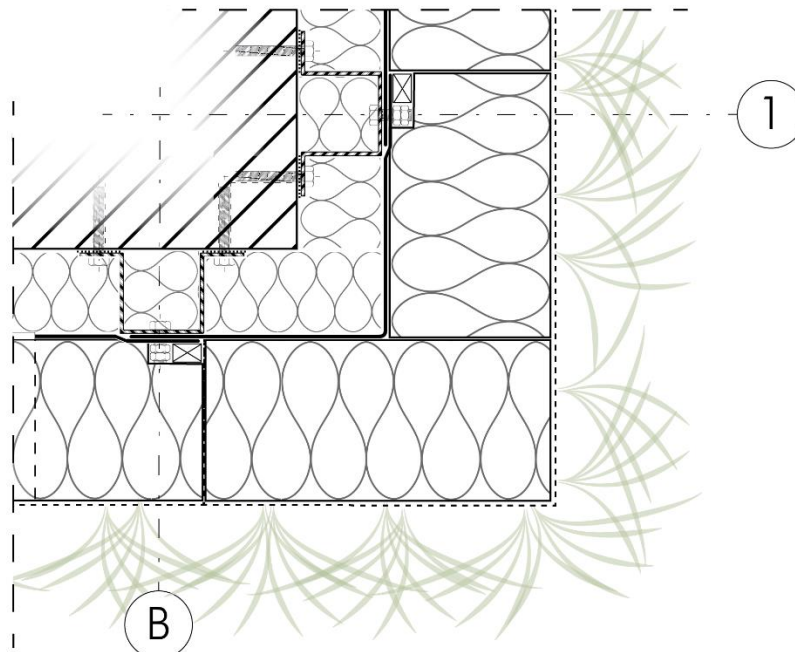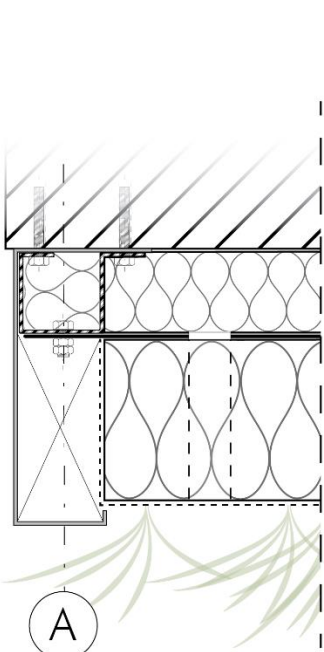
V1 Left boundary

V2 Outward corner

A. HELMHOLTZ PLATE - FRONT VIEW
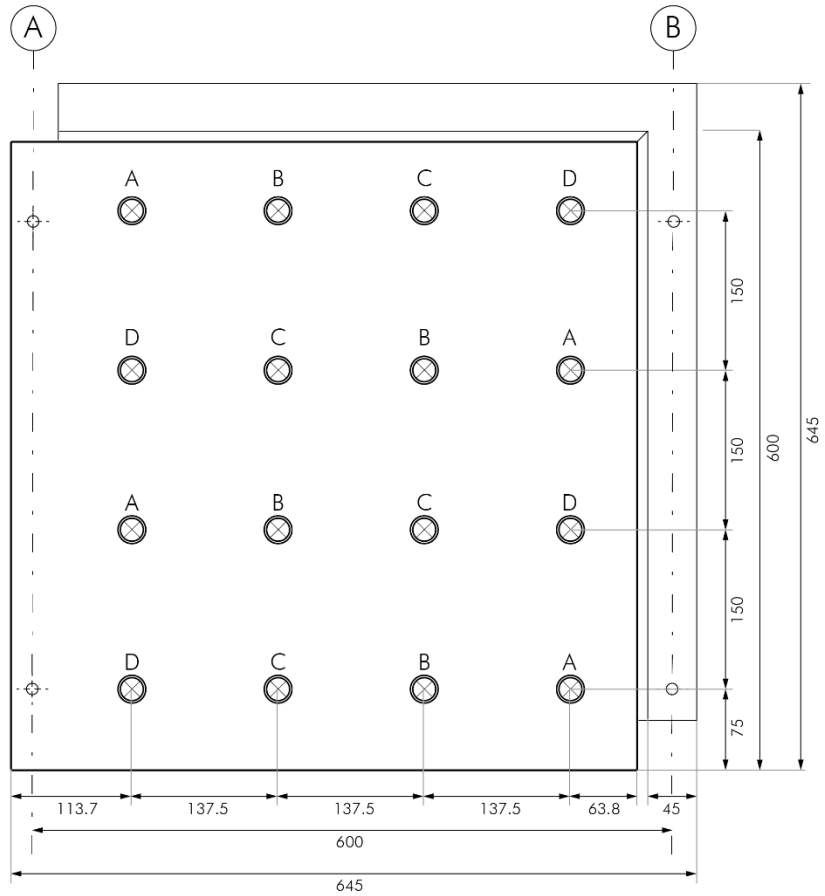
B. HELMHOLTZ PLATE - INVISIBLE CAVITY SUBDIVISIONS
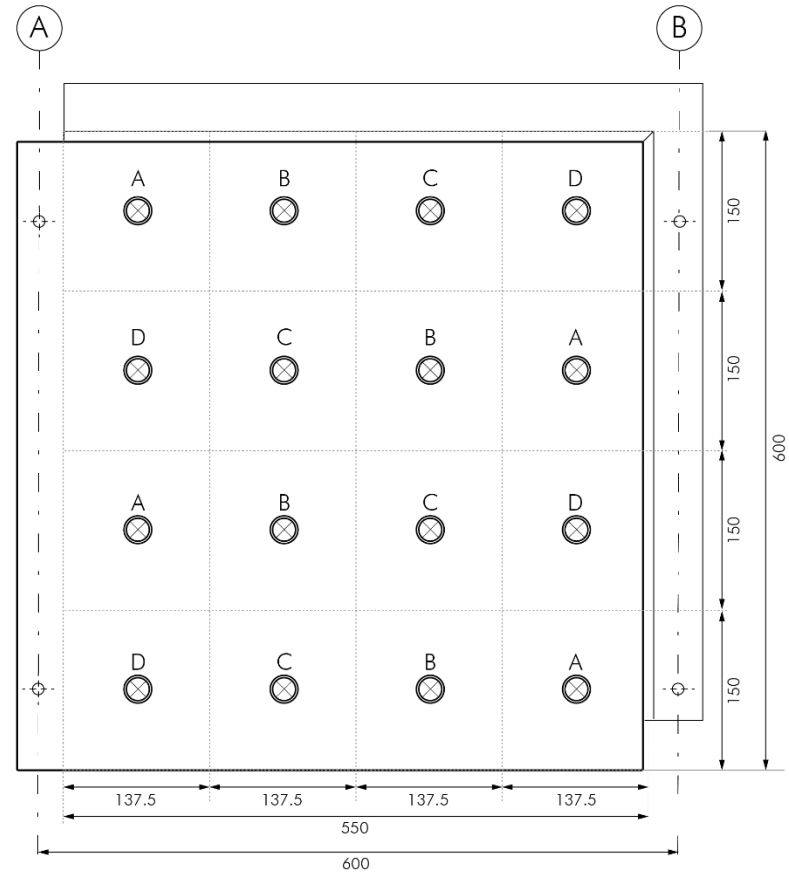
LEGEND

A	Helmholtz neck, R = 11 mm
B	Helmholtz neck, R = 12 mm
C	Helmholtz neck, R = 13 mm
D	Helmholtz neck, R = 13 mm
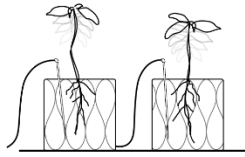
Step 1 Grow plants

Grow plants rock wool starter cubes in a plant nursery
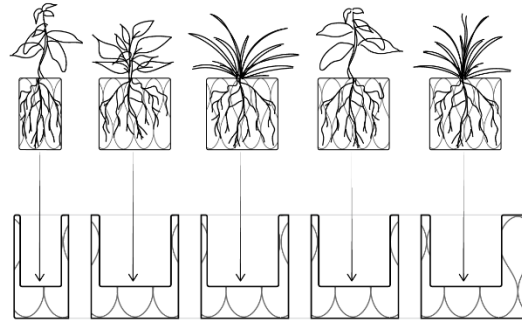
Step 2 Insert starter cubes

Insert starter cubes with developed plants of various species into the dedicated spaces in the substrate module
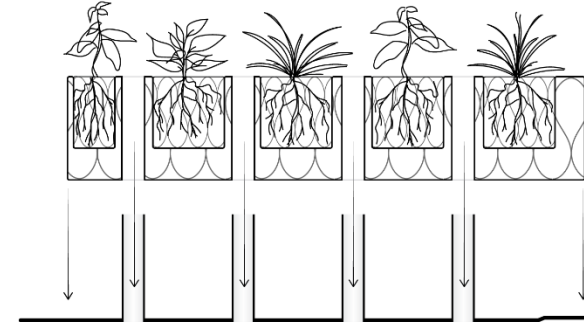
Step 3 Slide over Helmholtz plate

Slide the rock wool substrate layer over the protruding necks of the Helmholtz plates
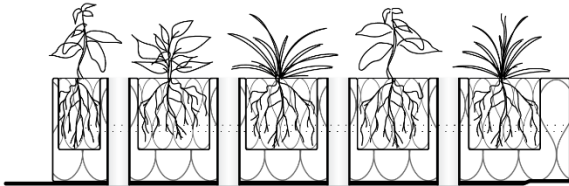
Step 4 Insert irrigation lines

Insert lateral branches of irrigation system into the module.
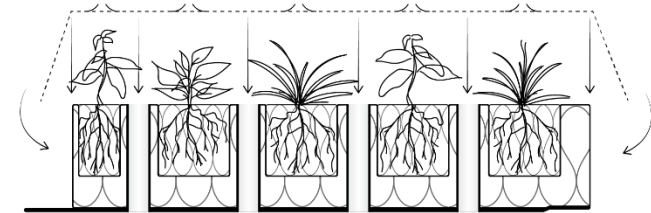
Step 5 Wrap with geotextile

Wrap the module with an acoustically transparent geotextile layer. Cut cross-like openings at the plant positions
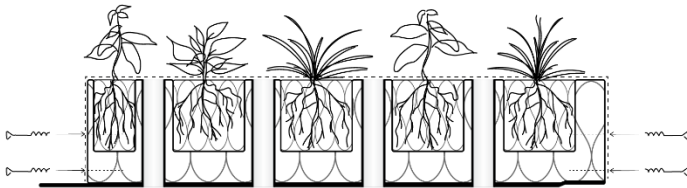
Step 6 Fasten with spiral anchors

Turn the spiral anchors into the substrate layer, to fasten the geotexile layer to the rock wool
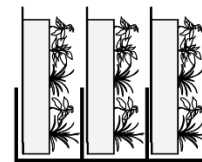
Step 7 Transport modules to site

Stack the modules in a rack to transport them to the site by truck

Step 1 Prepare profiles →

Cut soft thermal insulation strips to size, and insert it into the omega profiles. Also, insert stainless steel bolts from the back, so that they protrude at the front.
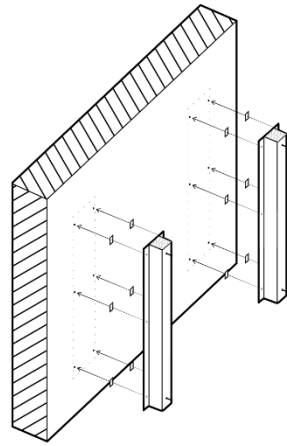
Step 2 Attach profiles →

Drill holes in the facade, and attach the vertical profiles with anchors. Apply plastic thermal breaks at all connection points.
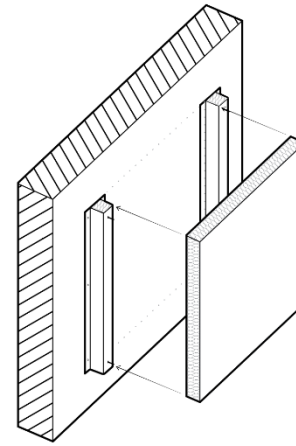
Step 3 Add cavity fill

Place a layer of glass wool in between the vertical profiles. It will stay in place because it is supported at the bottom, by the glass wool panel below.
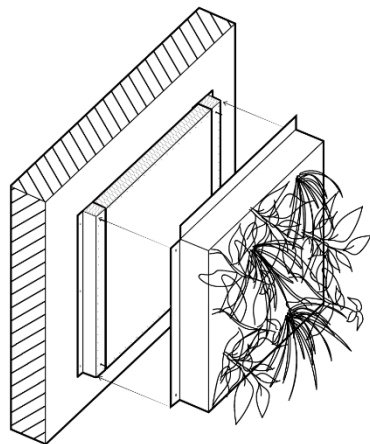
Step 4 Place LWS module →

Attach the LWS module to the protruding bolts on the profiles. The modules overlap in vertical and horizontal directions.
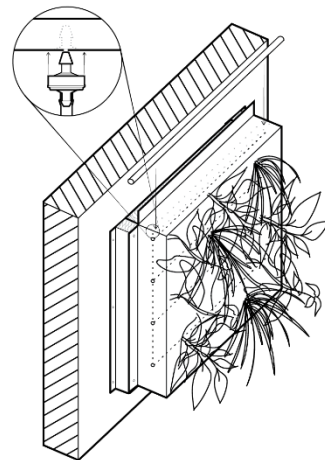
Step 5 Connect supply line →

The lateral irrigation lines connect to the main supply line by means of a pressure-compensated valve
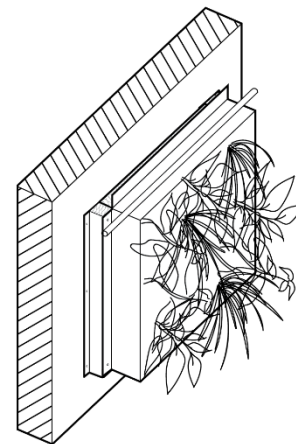
Step 6 Repeat

Repeat step1-5 in horizontal and vertical directions to cover the facade.
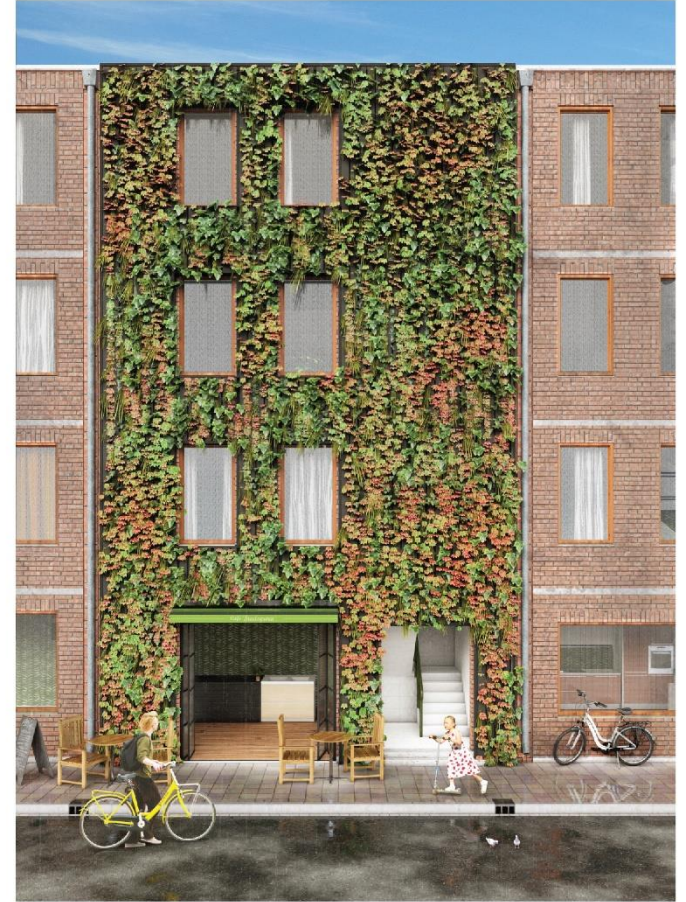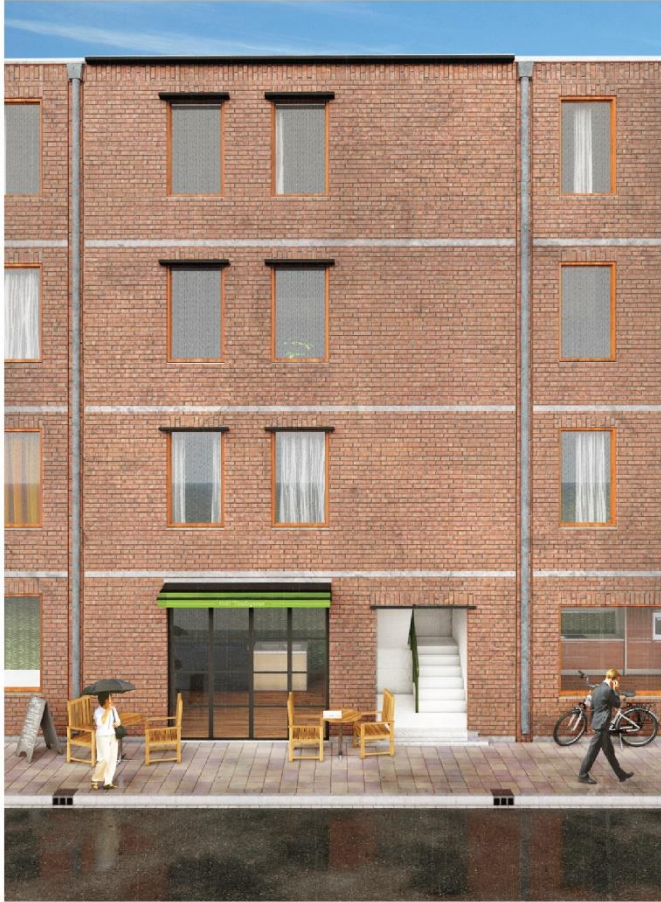
Step 1 Before facade transition ⟶

The facade is part of an urban street canyon, and the road has a high traffic flow. The facade is acoustically reflective, and is strong enough to attach a living wall system to.

Step 2 Applying vertical greenery ⟶

The facade is cleaned, and vertical profiles are attached with center-to-center spacing of 600 mm. Thermal and moisture boundaries are applied.

Step 3 Installed living wall system

The prepared LWS modules are installed from bottom to top, from right to left. In between the modules, irrigation lines are applied. A fresh new facade cladding.

Title
Living wall system module
Visualization

Project
Graduation studio
Optimization of VGS acoustics
Delft University of Technology - MSc4 2020-2021

| Date	Scale	Phase
5-5-2021	-	DEF

Size	Drawn	Drawing no.
A3L	JB	DEF-009

7.2. Dimensions

The LWS module dimensions are based on ISO 2848:1984 (ISO, 1984), which specifies modular coordination by standardizing dimensioning of components. The norm specifies dimensions of 300 mm and 600 mm and multiples thereof. These numbers are convenient, since any of those multiples can be divided evenly into 1, 2, 3, 4, 5, 6, 10, 12, 15, etc. It is for this reason that most buildings have a structural grid size of multiples of 600 mm, and that many facade cladding products follow this standardized dimensioning as well. Therefore, the LWS module will have a width of 600 mm. Additionally, the Dutch Building Decree 2012 (art. 4.28) (Rijksoverheid, 2012), requires an unobstructed height of at least 2,6 m for indoor spaces which are meant to be inhibited for more than four hours consecutively (verblijfsruimten). This generally leads to total floor height of 3000 mm (incl. floor thickness). This dimension can similarly be divided by 5 to yield the ISO 2848 standard of 600 mm. For this reason, the LWS module height will also be 600 mm.

Most LWS types have a cavity space of about 50-100 mm. The cavity is a result of the suspension of the LWS system to vertical profiles. The cavity space can either be ventilated or unventilated:

1. Ventilated: a hygric barrier between LWS and facade, so that the LWS moisture will not enter the facade
2. Unventilated: the still air contained in the unventilated cavity acts as an additional thermal boundary

For the redesign, the primary quality will be acoustical absorption. Hence, the cavity space will be used to accommodate the low-frequency sound absorption system.

7.3. Weight

To ensure a practical transportation and installment, the LWS modules should be able to be lifted by a single person. If too heavy, more workers or more tools are needed to transport and apply the modules. The Dutch Working Conditions Decree (ARBO-besluit, art. 5.2) specifies a maximum weight of 23 kg to be carried by one person, depending on the frequency of the act (Rijksoverheid, 2021). For that reason, it is important to reduce the module weight as much as possible. An important factor in LWS weight is to reduce the embodied moisture, since the porous substrate can absorb a substantial volume of water. Therefore, full irrigation is postponed until after the modules are fixed to the facade.

7.4. Materials and production

A matrix for material options is made (Table 16). Several material options are compared. The criteria include an environmental classification based of NIBE (2021), as well as the material lifespan, recycling potential, and shadow costs (costs to compensate for the embodied energy and carbon footprint in the lifecycle). Also, a weight and price estimation are given, using the CES EduPack database (Granta Design, 2019). Based on Table 16, final choices have been made, which are justified in Table 17.

Part	Option	Material	Amount	Unit	NIBE class.	Weight [kg]	Lifespan [yrs]	Recycl. Pot. [%]	Costs [€]	Shadow costs /unit [€]
	1	Omega profile 2 mm galvanized steel	1.2	m¹	1c	1.9	50	87	0.95	0.45
Profiles	2	Omega profile 2 mm aluminium (coated)	1.2	m¹	2b	0.6	40	63	0.63	5.58
	3	Acetylated pine wood 50x50 mm	1.2	m¹	5c	1.5	50	4.1	20.40	6.94
	1	Thermal glass wool plates 50 mm	0.36	m²	3b	0.2	75	10	1.10	4.11
Cavity fill	2	Thermal rock wool plates 50 mm	0.36	m²	4c	0.7	75	10	1.07	8.61
	3	Thermal sheep wool 50 mm	0.36	m²	7c	0.4	75	0	3.04	42.72
Helmholtz plate	1	Recycled HDPE (High density polyethylene)	0.36	m²	2a	1.4	75	33	2.03	0.71
	2	Recycled PVC (Polyvinyl chloride)	0.36	m²	3a	1.9	30	100	2.31	9.19
Substrate	1	Hydroponic rock wool	0.36	m²	-	1.6	75	0	8.85	-
Geotextile	1	Geotextile layer Aqua Breath	0.5	m²	-	0	10	0	0.50	-

Table 16 - Material options

Part	Material choice	Explanation
Profiles	Galvanized steel	Aluminium omega profiles are commonly used in VGS designs. However, this increases the costs. Pine wood could be used as an alternative. However, the pine wood should be treated by acetylation to make it moisture resistant. This treatment process increases the footprint. Galvanized steel is strong and cheap, and has the best environmental classification.
Cavity fill	Thermal glass wool	Sheep wool is a fibrous absorber that could be applied; however, this material is not sustainable due to its high embodied energy. The shadow costs are too high. Rock wool has a better environmental classification, but it is relatively dense and has a high flow resistivity. Glass wool has a good thermal resistance, has a relatively low flow resistivity, and is light-weight.
Helmholtz plate	Recycled HDPE	Rigid PVC is commonly used in the built environment. However, its durability can suffer when exposed to UV. Also, its manufacturing process is acceptable for injection molding, but is mostly extruded. HDPE is also commonly used, e.g. in LWS planter boxes. This material can easily be recycled to a high degree, which reduces the shadow costs. HDPE is excellent for injection molding.
Substrate	Hydroponic rock wool	Mineral wool LWS always use hydroponic rock wool. This material is common and popular in horticulture. This material is especially used in the green house industry, and is locally produced.
Geotextile	Geotextile	This layer is open for moisture and air, but is water-resistant. The application of this layer prevents the substrate layer of receiving water in case of driving rain.

Table 17 - Material choices

7.5. Thermal insulation

Besides the acoustic performance, the LWS redesign has also a quality of thermal insulation. A calculation is performed (according to NEN 1068:2012) to predict the increase of heat resistance (Rc) for a retrofitting project (full calculation in Appendix I). For the reference facade, a common insulated and ventilated cavity brick wall of 100-140-40-100 mm was used. (R_c = 3.7 m²K/W) (Harbers, 2015). The calculation shows that adding the LWS can increase the heat resistance almost by a factor of 2 (+98%).

7.6. Plant species

To recommend plant species for the LWS redesign, plant species were rated based on how dense the canopies appeared on photos. This rating is only an assumption, as these plant species were not tested. The species that were rated were the most commonly applied plant species in VGS, based on BBC (2019); Mir (2011); Skinner (2019); The Royal Horticulture Society (2021). This list can be found in appendix III. Table 18 shows an excerpt of the most notable well sound absorbing species.

Well sound-absorbing sciohytes

| Bergenia cardifolia | Begonia | Primula | Hosta Sieboldiana |

Well sound-absorbing heliophytes

| Hedera helix | Salvia argentea | Impatiens walleriana | Penagonium |

Table 18 - Excerpt of well sound-absorbing species (full list in Appendix III)

7.7. Irrigation system

The irrigation system is inspired by the systems commonly found in cultivation industry. The system irrigates locally at the plant roots through one-sided supply. A design is made on drawing DEF-003. It shows a simplified irrigation circuit, zooming in on a single LWS module.

- Supply lines: ZPE tylene pipe ∅16x1.8 mm. ZPE tylene is a material that is commonly used in dripping systems, because of its frost- and UV-resistance.
- Connections: pressure compensated plug-in valve (Rainbird/Kameleon High® or similar types). These are applied at all intersections A-E into a perforation that is made with a punch. The pressure compensated valve ensures an equal water distribution to all branches, within the operating pressure of 1-3.5 bar. The valves automatically close when the irrigation system is flushed, for example with decongestant agents (biological degradants and nitric acids).
- Laterals: CNL dripper lines ∅4 mm. Vertically along the side of the LWS module, the line branches into several laterals. The line has perforations at specific distances, supplying the plants.

7.8. Analytical validation: Matlab script

A Matlab script was developed to determine the acoustic absorption of the concept design. The full script can be found in appendix I. The script was continuously developed throughout the design process. Appendix II shows how the scripts were used for validation of the concept designs.

Regarding the final script, the most important Helmholtz parameter values: neck lengths 103 mm, cavity widths 137.5 mm, cavity heights 150 mm, cavity depths 50 mm, and a total of 16 resonators per module:

	Helmholtz type 1	Helmholtz type 2	Helmholtz type 3	Helmholtz type 4
Orifice radius [mm]	10	11	12	13
Number of res [-]	4	4	4	4

Table 19 - Helmholtz parameter values

Regarding the used flow resistivities:

- the substrate layer: 100 mm hydroponic rock wool (porosity 0.98, flow resistivity 15000 Nsm^{-4}, estimations based on Dauchez et al. (2020) and Berardi and Ramakrishnan (2016)
- the cavity fill layer: 50 mm thermal glass wool (porosity 0.98, flow resistivity 5000 MKS rayls/m, estimations based on Berardi and Ramakrishnan (2016), or 5.88 kPa s m^{-2} (Tarnow, 2002)
- 25 resonators, with resonator cavity dimensions 120x120x50 mm, neck orifice radius between 10-16 mm, and a neck length of 100 mm.

Additionally, the effects of moisture in the rockwool insert cubes is considered. The percentage of saturated substrate is assumed to be 30% of the surface area. This medium is estimated to have a porosity of 10% and a flow resistivity of 100.000 rayls/m. These values were assumed, based on the impedance tube measurement results. The absorption coefficient was approximately in the same order of magnitude as the saturated soil (Sr=74%) in Figure 35.

The final script gave an overview of absorption coefficients, which is illustrated in Figure 38 (next page).
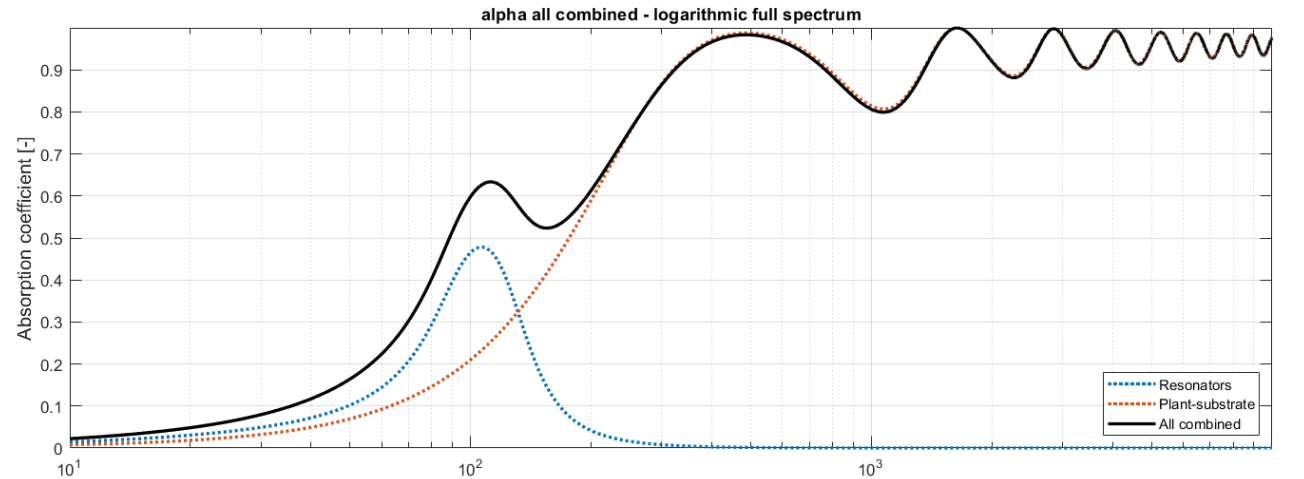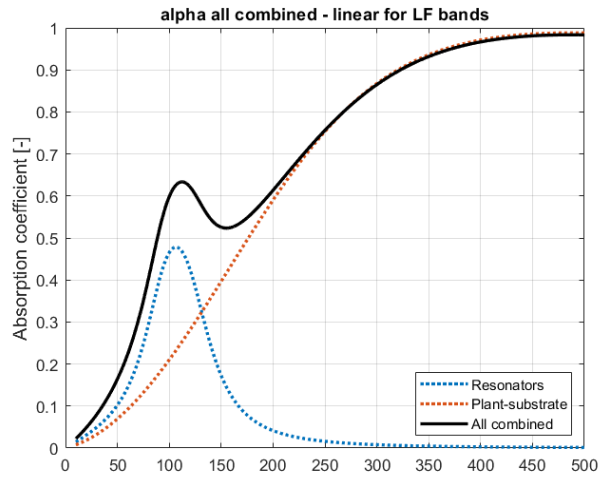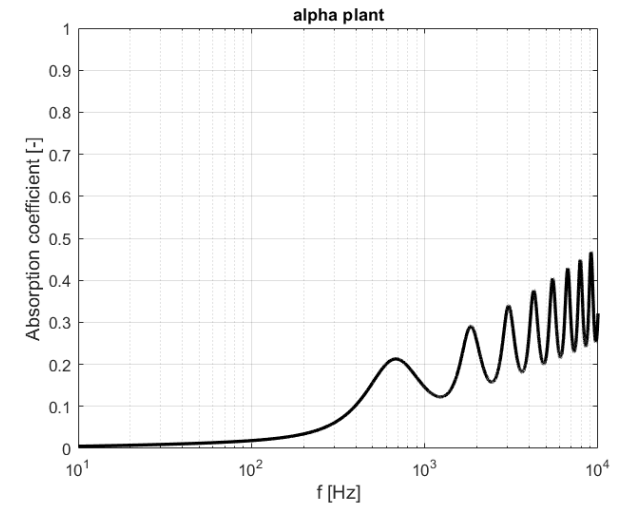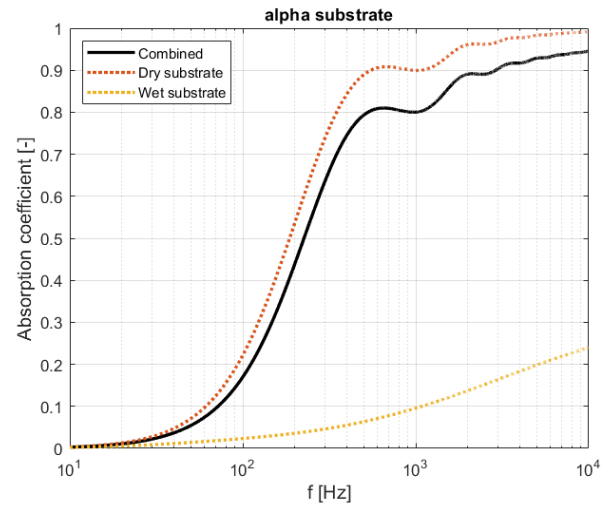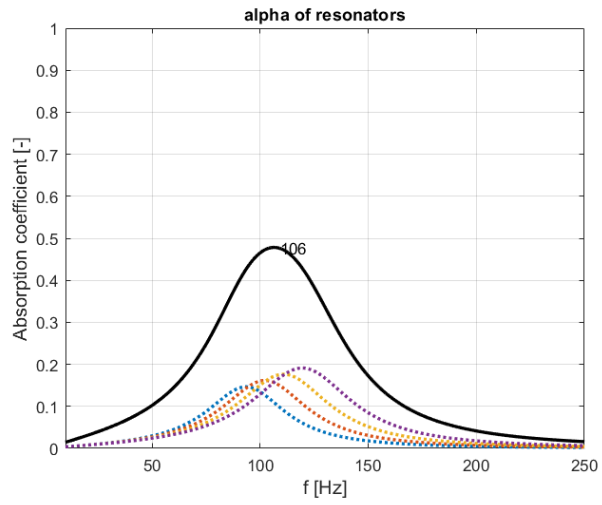
Figure 38 - Final design absorption coefficient results from Matlab

7.7. Experimental validation: Reverberation room experiment

Reverberation room experiments were performed on 7 and 10 may 2021. The method is discussed in chapter 1. The following scenarios were tested:

- Scenario 0: Control test (no sample)
- Scenario 1: Place all modules
- Scenario 2: Cover all resonator necks with painter's tape
- Scenario 3: Remove painter's tape, and remove cavity fill
- Scenario 4: Add cavity fill back in, and offset the boundaries slightly
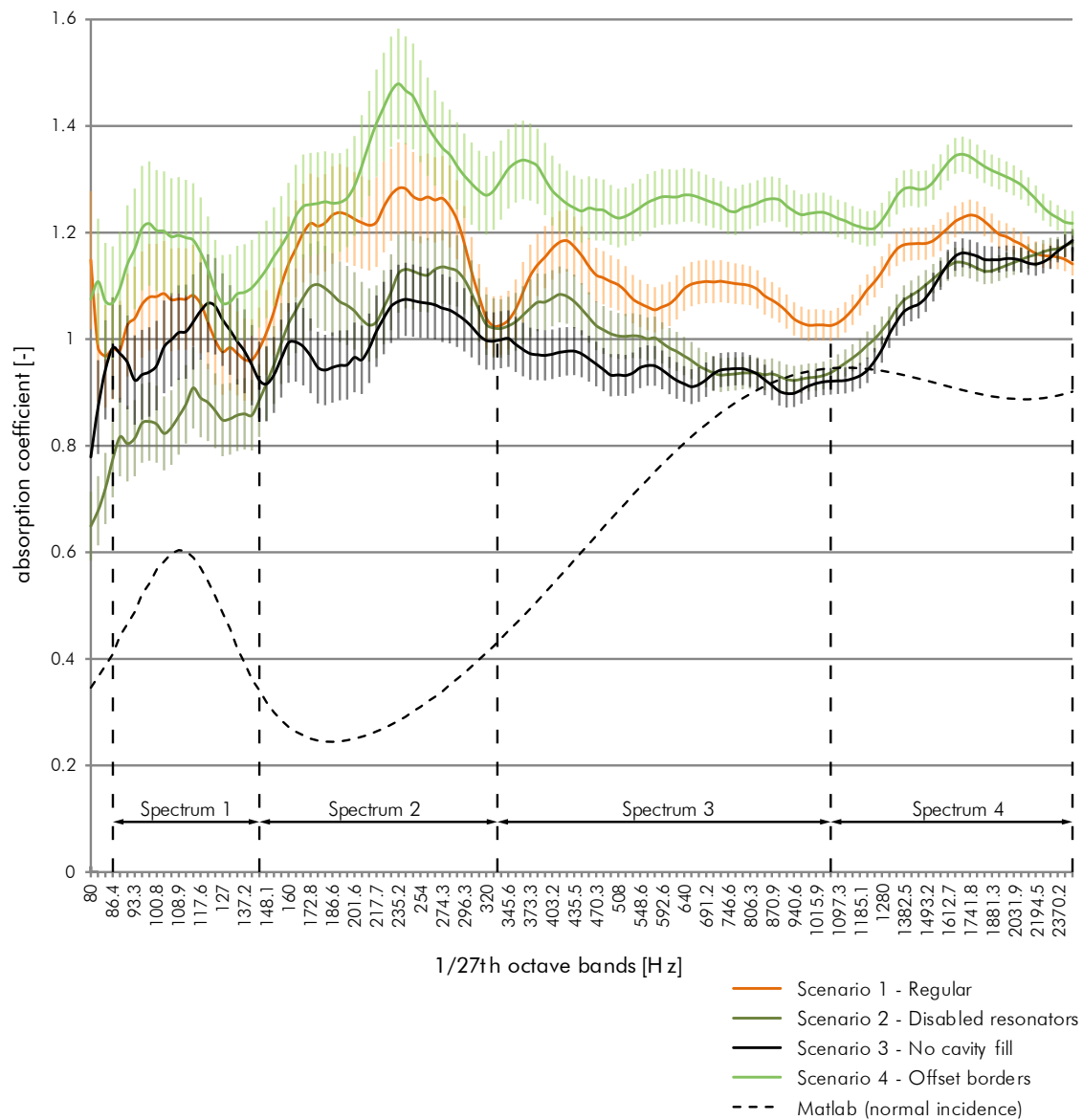
Figure 39 - Reverberation room measurement results

Figure 39 shows the absorption coefficient graphs of all measured scenarios. Additionally, the absorption coefficient was predicted using a Matlab script.

- The measurement graphs mostly have a similar shape.

- The graph from scenario 4 is overall the highest.
- The results can be broadly grouped into four spectra. All graphs, except for the graph of scenario 2, show a peak in spectrum 1 (~85-140 Hz), which is the spectrum in which the Helmholtz resonating action was predicted.
- All graphs show absorption peaks in spectrum 2 (~140-340 Hz), and contain overall the highest absorption coefficients.
- All scenarios show an overall small decrease in spectrum 3 (~340-1080 Hz).
- In spectrum 4 (~1080-2400 Hz), all graphs increase to a peak around 1700 Hz.

The results are interpreted in chapter 8.4. Here, the validity and reliability of the method is also discussed.

7.8. Case study

Acoustic simulations were performed conform the method as described in chapter 1.5. The cross-comparison entails that simulations were performed, both excluding and including the application of acoustic LWSs to the facade walls. All SPL results can be found in Appendix I.

7.8.1. Model A

The model in which the sound propagation from the street canyon toward the adjacent courtyard canyon is simulated, is labeled as model A. The SPL differences at two representative receivers is included in Table 20. Receiver 1 is located close to the facade in the courtyard canyon, and receiver 2 is located further away from the facade.

							SPL comparison [dB] per 1/3 octave band [Hz]												
REC	25.1	31.6	39.8	50.1	63.1	79.4	100.0	125.9	158.5	199.5	251.2	316.2	398.1	501.2	631.0	794.3	1000.0	1258.9	Average
1	-3.5	-9.4	-8.1	-9.2	-3.2	-4.2	-0.4	0.7	-1.9	-6.7	-6.3	0.7	-8.4	-10.7	-12.2	-7.8	-1.4	-11.1	-6.5
2	-0.3	5.5	1.5	2.8	-2.1	-1.6	-6.7	-7.6	-4.3	0.0	-4.1	-13.9	-13.3	-11.9	-9.0	-8.1	-11.8	-6.8	-5.1

Table 20 - Comparative SPL results from model A

Green cells show a reduction in SPL after application of the LWS, and red cells show an increase. The results generally show a substantial reduction in SPL, with the highest reduction being -13.9 dB at receiver 2 (316.2 Hz). An anomaly is the predicted increase of +5.5 dB at receiver 2 (31.6 Hz). This may be caused by simulation inaccuracies. The results suggest that the decrease in SPLs for the receiver placed closer to facade are higher compared to the receiver placed further away. This may be caused by larger diffraction effects at receiver 2.

7.8.2. Model B

The model that only the street canyon is included is labeled as model B. The difference in SPLs at the receivers is included in Table 21. This table shows only the results that were obtained by processing the impulse response algorithm.

		Source 0										Source 1							
Receivers		SPL comparison [dB] per 1/1 octave band [Hz]								Receivers		SPL comparison [dB] per 1/1 octave band [Hz]							
Group	REC	125	250	500	1000	2000	4000	8000	16000	Group	REC	125	250	500	1000	2000	4000	8000	16000
A	1	-0.11	-0.84	-1.42	-0.09	-0.41	-0.44	-0.47	-0.43	B	1	-0.33	-0.79	-1.74	-3.16	-0.98	-1.46	-1.51	-2.34
A	2	-0.23	0.06	0.04	-0.02	-0.22	-0.02	-0.08	-0.05	B	2	-0.42	-0.28	-1.46	-2.19	-1.31	-1.14	-0.96	-0.89
A	3	-0.59	-0.51	-0.01	-0.15	-0.41	-0.36	-0.31	-0.19	A	3	-0.12	-0.04	-0.05	-0.02	-0.20	-0.14	-0.01	0.14
B	4	0.04	-0.28	-1.44	-1.64	-1.10	-1.05	-0.79	-0.60	A	4	0.25	0.05	-0.06	-0.06	-0.09	-0.10	-0.06	-0.02
B	5	-0.16	-0.63	-2.77	-3.76	-1.32	-1.84	-1.95	-3.01	A	5	-0.11	-0.70	-2.14	-0.43	-0.62	-0.64	-0.78	-0.82
C	6	-1.64	-0.01	-1.38	-0.03	-0.92	-0.49	-0.43	-0.54	C	6	-0.60	-0.46	-1.41	-1.94	-0.95	-1.63	-1.50	-2.52
C	7	-0.86	-1.32	-2.16	-2.49	-1.72	-1.95	-1.49	-3.19	C	7	-1.14	0.45	-0.10	-1.91	0.00	-0.32	-0.65	-1.38
C	8	-0.40	-0.60	-1.31	-0.20	-0.48	-0.61	-0.51	-0.82	C	8	-0.48	-0.37	-1.64	-1.95	-1.19	-2.04	-1.44	-3.20
C	9	-0.57	-0.79	-1.25	-2.44	-1.39	-1.51	-0.99	-2.66	C	9	-1.45	0.57	0.38	-0.58	0.20	-0.04	-0.57	-0.83

Table 21 - Comparative SPL results from model B

The results generally show a reduction in SPL, with the highest reduction being -3.76 dB at S0xR5(1000 Hz) and the highest increase being +0.57 dB at S1xR9(250 Hz). The results suggest that the decrease in SPLs for receivers placed closer to the sources are lower compared to receivers further away. A possible explanation is that receivers near the source primarily receive direct sound, which is not affected by reflection. Receivers further away receiver relatively large amounts of reflected sound. Therefore, the 9 receivers were grouped into 3 receiver groups, based on their position relative to the sources. This is illustrated in Figure 40.
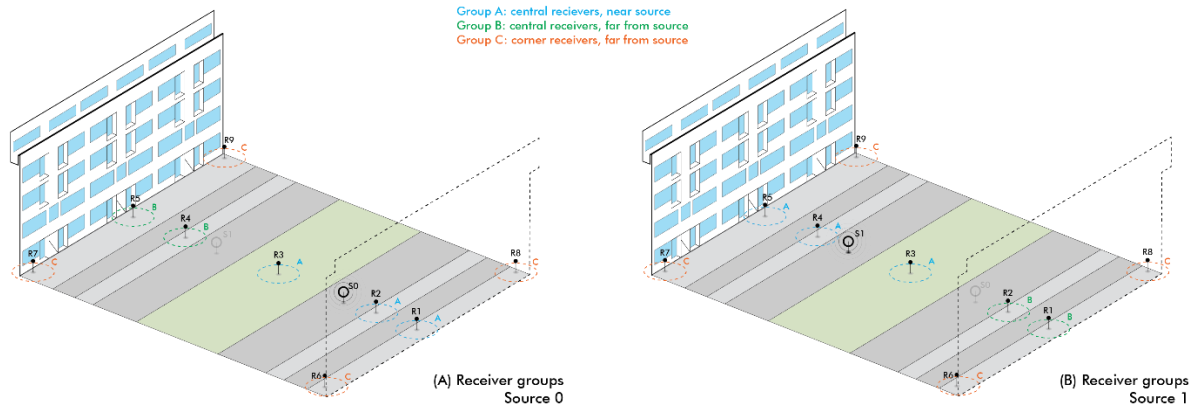
Figure 40 - Receiver groups per souce

The SPL results per receiver group are averaged and included in Table 22.

	SPL comparison [dB] per 1/1 octave band [Hz]								
REC group	125	250	500	1000	2000	4000	8000	16000	Average
A	-0.12	-0.29	-0.77	-0.18	-0.30	-0.27	-0.25	-0.22	-0.30
B	-0.24	-0.46	-1.70	-2.62	-1.17	-1.33	-1.25	-1.65	-1.30
C	-0.71	-0.32	-0.95	-1.04	-0.75	-0.91	-0.91	-1.83	-0.93

Table 22 - Average SPL results per receiver group (Model B)

Based on these averaged results, the following observations were made:
- Receiver group A: For the central receivers that were near the source (avg. 7.3 m), a small reduction in average SPL of -0.30 dB was predicted. In the 125 Hz octave band, the SPL difference was -0.12 dB.
- Receiver group B: For the central receivers further from the source (avg. 24.1 m), a more substantial average SPL reduction of -1.30 dB was predicted. In the 125 Hz octave band, the SPL difference was -0.24 dB.

- Receiver group C: For the corner receivers (avg. 25.15 m distance from source), a reduction in average SPL of -0.93 dB was predicted. In the 125 Hz octave band, the SPL difference was -0.71 dB.
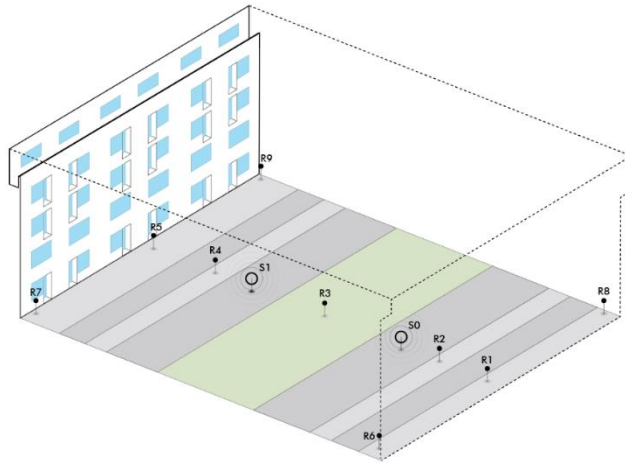
Figure 41 - Model C

7.8.3. Model C

In this model, the window-to-wall ratio (WWR) was changed to research the effect of the application of a higher acoustic LWS surface area (Figure 41). Compared to model B, the total surface area of facade openings was reduced from 296.1 m² to 152.5 m². The model with the smaller windows is illustrated in Figure 41. This reduces the WWR of 50.7% to 28.7%. The difference in SPL at the receivers is included in Table 23

Source 0

Receivers		SPL comparison [dB] per 1/1 octave band [Hz]							
Group	REC	125	250	500	1000	2000	4000	8000	16000
A	1	-0.48	-2.23	-4.68	-1.81	-1.59	-1.84	-1.74	-1.81
A	2	-0.29	-1.08	1.04	-1.04	-1.04	-0.34	0.06	-0.08
A	3	-0.04	-0.89	-0.70	-0.70	-0.69	-0.35	-0.32	0.10
B	4	-0.64	-1.04	-2.86	-2.33	-1.74	-2.80	-1.38	-1.23
B	5	-1.53	-2.79	-3.69	-5.44	-2.57	-3.78	-4.29	-4.86
C	6	-1.30	-0.66	-1.47	-0.92	-1.06	-1.17	-1.11	-2.23
C	7	-0.75	-1.96	-3.07	-3.59	-2.17	-2.39	-2.22	-4.76
C	8	-0.82	-0.73	-1.69	-0.93	-0.82	-1.05	-1.07	-1.06
C	9	-0.99	-1.86	-2.44	-3.02	-2.09	-2.01	-1.73	-4.53

Source 1

Receivers		SPL comparison [dB] per 1/1 octave band [Hz]							
Group	REC	125	250	500	1000	2000	4000	8000	16000
B	1	-2.14	-2.25	-3.63	-5.53	-2.76	-3.96	-4.04	-5.16
B	2	-0.64	-1.23	-3.04	-2.74	-1.83	-2.83	-2.53	-1.68
A	3	-0.11	-0.58	-0.08	-0.18	-0.42	-0.37	-0.16	0.01
A	4	0.42	-0.05	-0.29	-0.19	-0.35	-0.12	-0.11	-0.09
A	5	-1.36	-1.77	-6.54	-1.48	-1.90	-1.91	-1.82	-1.64
C	6	-1.57	-0.94	-2.27	-2.56	-1.13	-2.18	-2.49	-4.39
C	7	-0.50	0.15	-0.66	-2.00	-0.75	-0.16	-0.81	-1.78
C	8	-0.72	0.11	-2.10	-2.03	-2.34	-2.67	-2.90	-4.69
C	9	-0.73	-0.05	-0.69	-0.60	-0.22	-0.35	-0.84	-0.89

Table 23 - Comparative SPL results from model C

Again, green cells show a reduction in SPL after application of the LWS, and red cells show an increase. The results generally show a reduction in SPL, with the highest reduction being -6.54 dB at S1xR5(500 Hz). An anomaly is the predicted increase of +1.04 dB at S0xR2(500 Hz). A comparison between the average SPL results per receiver group of model B and model C is made, to illustrate the effect of increasing the total acoustic LWS surface area (see Table 24 and Table 25, respectively).

REC group	125	250	500	1000	2000	4000	8000	16000	Average
A	-0.12	-0.29	-0.77	-0.18	-0.30	-0.27	-0.25	-0.22	-0.30
B	-0.24	-0.46	-1.70	-2.62	-1.17	-1.33	-1.25	-1.65	-1.30
C	-0.71	-0.32	-0.95	-1.04	-0.75	-0.91	-0.91	-1.83	-0.93

Table 24 - Average SPL results per receiver group (Model B)

125	250	500	1000	2000	4000	8000	16000	
-0.32	-1.05	-1.91	-0.77	-0.91	-0.84	-0.70	-0.59	-0.88
-1.07	-1.70	-3.43	-3.93	-2.31	-3.25	-2.98	-3.11	-2.72
-0.83	-0.47	-0.97	-1.09	-0.89	-0.96	-1.04	-2.08	-1.04

Table 25 - Average SPL results per receiver group (Model C)

Based on these averaged results, the following observations were made:

- Receiver group A: For the central receivers that were near the source (avg. 7.3 m), a reduction in average SPL of -0.88 dB was predicted. The difference with model B was 0.58 dB

- Receiver group B: For the central receivers further from the source (avg. 24.1 m), a substantial average SPL reduction of -2.27 dB was predicted. The difference with model B was 1.42 dB

- Receiver group C: For the corner receivers (avg. 25.15 m distance from source), a reduction in average SPL of -1.04 dB was predicted. The difference with model B was 0.11 dB

- Hence, there is a correlation between the total surface area of the acoustic LWS and the decrease in SPL in the street canyon. Applying more acoustic LWS to a façade allows for a larger decrease in SPL in the street canyon. In the case of model C (5 story building with a WWR of 28.7%), the decrease in SPL is notable by humans.

Discussion & Conclusion

8. Discussion

8.1. Analytical validation

To predict the visco-thermal absorption coefficient of the plant layer, a numerical model proposed by Horoshenkov et al. (2013) was applied. This equivalent fluid model used the equivalent flow resistivity, derived from impedance tube measurements, see chapter 4. However, in a later study, Prisutova and Horoshenkov (2014) argue that measuring plants in an impedance tube (ISO 10543-2) yields inaccurate results, due to too small sample sizes and the relatively small frequency spectrum. Also, the validity of the model has not been extensively justified. Several problems are presented:

- The method only works under the conditions of normal incidence, as the angle of the incident sound wave must be known.
- The method does not take into account the fact that plants can actively reorient their leaves, depending on the direction and intensity of insolation. The tortuosity should be variable.
- The method does not take into consideration plant leaf vibration and scattering effects.
- The method considers a homogenous porosity, flow resistivity, and layer thickness across the entire sample. In reality, these values may vary considerably across a sample.

For the graduation project, the method was reproduced using a set of five different house plants: Begonia Rex, Primula, Chlorophytum, Ficus Pumila, Pilea peperomioides (Appendix III). The method seemed to yield realistic results. Plants with a large LAD, such as the Begonia Rex, yielded a relatively high absorption coefficient. The opposite was true for plants with a low LAD, such as the pancake plant and the spider plant. Nonetheless, the leaf angle is the parameter that has the largest influence on the absorption coefficient. Since determining the leaf angle is complex, the reliability of the method is disputed.

Another factor that influences the reliability of the method, is the fact that the developed Matlab script does not take into account membrane resonances. These modes can occur as a result of plate deformations.

8.2. Reverberation room measurement

8.2.1. Validity of the method

The prototype that was used for the experimental measurements approximates the layered structure of the final design. However, to keep the manufacturing of the prototype executable, the prototype did not fully resemble the final design. The differences are as follows:

- A 9 mm MDF plate represented the 3 mm HDPE Helmholtz plate, since injection molding the plastic would be too expensive for the prototype.
- ¾"x59 mm PVC tubes represented the 2 mm HDPE Helmholtz necks, for the same reason.
- A layer of 50 mm thermal rock wool represented a 100 mm thick layer of hydroponic rock wool. This was done because splitting thermal rock wool was logistically and financially the most viable option to use for the prototype.
- No geotextile cover was used for the prototype.

- No plants were used for the prototype, as this would substantially complicate the logistics, while not providing any substantial increase of the acoustic absorption.
- 50 mm cardboard cross-like spacers were used to support the MDF plates at their four corners. However, the final design uses steel omega profiles (linear supports).
- The prototype modules were not mechanically connected at their boundaries, but were just touching. Also, a 12 mm plywood boundary was applied around the outer perimeter of the prototype set-up, while in the final design this would be aluminium flashing.

This means that the prototype deviates from the final design. Therefore, the experimental results do not fully represent the acoustic behavior of the final design. However, the experiment was primarily performed to research to what extent the Helmholtz resonators would acoustically absorb, in combination with the rock wool and the glass wool. Furthermore, a comparative measurement is performed. By including and consequently excluding the resonant action of the integrated Helmholtz resonators, the difference became visible.

8.2.2. Reliability of the method

The experimental results diverge from the analytical prediction. A combination of several factors may have caused the discrepancies:

- The flow resistivity of the rock wool and the glass wool were assumed based on Berardi and Ramakrishnan (2016) and Dauchez et al. (2020). However, the flow resistivities were not measured.
- The thickness of the rock wool was assumed to be uniform. However, the surface was irregular. The layer thickness may have varied with tolerances 50 ± 15 mm. Since the prototypes were hand-made, all parts may have had small assembling errors.
- The analytical script predicted the absorption coefficient for normal incidence. However, in a reverberation room, a diffuse field with random incidence is applied.
- The analytical script did not account for any other resonant phenomena other than the Helmholtz resonators. However, the MDF panels may have acted as membrane resonators. A quick analytical prediction showed that the panels have a resonant peak in the range of 100-250 Hz.
- Experimental measurements tend to yield higher resonant action than analytically predicted.
- The surface area of the sample might not have been enough to yield accurate measurement results.
- The measurements started at 80 Hz 1/27th octave bands. However, the reverberation room method can usually not accurately measure for such low frequencies, depending on the room volume. Therefore, measurements are generally performed above 125 Hz. Hence, results <125 Hz may not be accurate.
- The measurement results were reprocessed (.wav and .rsm files), which can cause a certain data loss due to compression. This may have caused small inaccuracies.
- Parts of the glass wool (cavity fill) may have acted as visco-thermal absorbers, due to small fissures between, and around, the prototype modules.
- Taping the Helmholtz necks with painter's tape may have still caused some resonances, as the material could flex slightly.

8.2.3. Reliability of a small sample size

The method did not accord to ISO 354:2003, as only 5.4 m² of sample surface area was used, while 10-12 m² is required by the norm. For most researches on porous media, the requirement for 10-12 m² of sample is hardly ever met due to logistic and financial constraints. Similarly, in-situ measurements have to conform to CEN/TS 1793-5 (2003), which requires a sample of >4x4 m to overcome the influence of ground reflections. Various experimental studies proposed alternative methods to use smaller VGS samples:

- Lacasta et al. (2016) have used a two-microphone setup in an in-situ setup of a VGS. Reflected receiver signal differences were deconvoluted in the time-domain. This method gave accurate absorption coefficient results for 250 - 4000 Hz.

- Prisutova and Horoshenkov (2014) built a large impedance tube with dimensions of 30 x 30 x 4150 cm with a bandwidth of 50 – 1800 Hz. Above 572 Hz (½λ), the modal reflections became too complex for accurate predictions of absorption coefficient.

- Romanova et al. (2019) measured a VGS in-situ by using highly a parametric transducer, which could project sound energy centrally (90% within ±10-12° in the hor. plane). The reflection was measured by directional sound intensity probes, consequently ruling out the influence of ambient noise, edge scattering, and ground reflection. Accurate results were yielded for 400 - 1250 Hz.

Hence, it is not uncommon to use alternative methods in experimental research of VGS acoustics. Carvalho and Sousa (2016) argue that adding >5 m² of sample only marginally increases the accuracy of reverberation room measurements. They have researched the effect of applying different sample sizes in reverberation rooms, by using an increment of 1m² samples of 8 mm thick porous layer. In total, 12 configurations were tested, using 1-12 m² of sample, respectively. The results per octave band are shown in Figure 42. Here, it can be seen that for all octave bands, any increase of sample surface area >5 m² only a marginal effect on the absorption coefficient. The comparison between the 5 m² and 12 m² measurements is shown in Figure 42. Here, it is shown that the measurements agree well enough. Hence, it can be argued that the sample size described in this report (5.4 m²) yields reliable results.
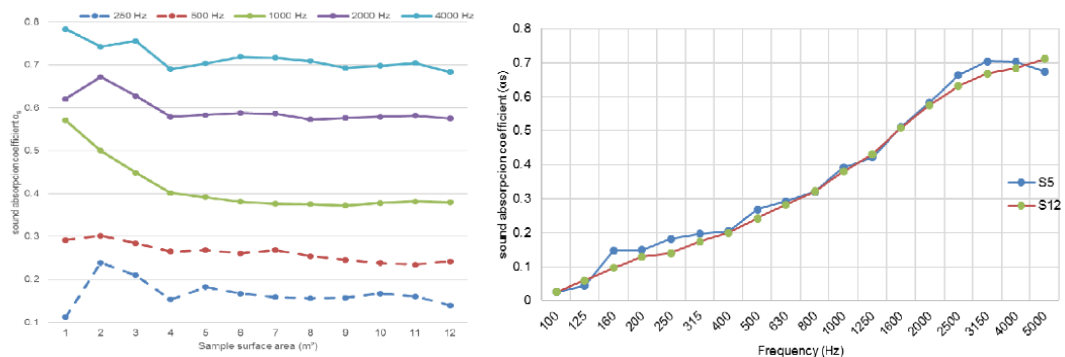
Figure 42 - Measurement results showing (A) the absorption coefficient per frequency band for increasing sample surface area, (B) comparison between the 5m² and 12m² measurements (From Carvalho & Sousa, 2016)

8.3. Limitations of impedance tube measurements

The 3D-printed resonator lids had a thickness of 2 mm. The measurement results show that several resonant modes occur. This is probably due to vibrational modes in the resonator lids. In reality, the sheet would be thicker, and so these vibrations can be ignored. It is assumed that the first resonant peak is the result of the actual Helmholtz action. Secondly, some resonant peaks did not accord to what was predicted using an analytical approach. This happened probably for several reasons:

- The prediction was done using a developed Matlab script that did not use the correct equations.
- The connection bolts might not have been tightened enough to secure an airtight connection. Possibly, some air leaked out through the seal, consequently influencing the resonant frequency.
- The resonators were slightly smaller than the inner diameter of the impedance tube, hence, some sound could reach the back of the tube. This may have caused some absorption peaks.

The lateral orifice configurations yielded far higher measurement result than expected, and thus it cannot be assumed that these peaks are due to regular Helmholtz mass-spring oscillations. Instead, the resonant modes are probably caused by a complex vibration in the thin lids, and the connection bolt and nuts. Even when adding the lateral insert between the two perforated plates, it is unclear whether the resonant peaks were caused by regular Helmholtz behavior.

The effect of adding a geotextile layer to the rock wool is measured. The conclusion was that it has a marginal effect on the absorption coefficient. However, the frequency spectrum was limited to 50-1600 Hz. Therefore, it is not measured what the behavior of the geotextile is for higher frequencies.

8.4. Limitations of acoustic simulations

The simulation results show that there is a correlation between the window-to-wall ratio (WWR) and the decrease in SPL in the street canyon. This is because more wall surface allows for application of more acoustic LWSs. The results show that Model C (WWR=28.7%) yields greater SPL decreases, in comparison to model B (WWR=50.7%). The street canyon that is formed around the Stadhoudersweg in Rotterdam is an example of an urban street canyon that has a relatively high traffic flow, and is therefore subject to high noise levels by traffic (Atlas Leefomgeving, 2021). However, the buildings that form the canyon are built with above-average window-to-wall ratios. For most of the building stock, it may be assumed that this ratio is lower (~25-40%). The results from the Stadhoudersweg canyon (model B) are therefore not necessarily representative for all urban street canyons in the Netherlands. Instead, it can be assumed that the modified facades of the canyon in model C more accurately represent the majority of urban street canyons in the Netherlands.

Regarding the reliability, the used source characteristics might not fully represent the reality. Two point sources with omni-spherical directivity were used, while in reality the sources would be linear. The power levels were based on the research of Can et al. (2010), but may not be identical in the Stadhoudersweg street canyon. Also, any diffraction effects that were more complex than first order diffraction were not

accounted for in the simulation, because CATT-A cannot efficiently handle it. CATT-A applies cone tracing and predicts echograms and impulse responses. The weakness of such image-source models is the computational inefficiency for diffraction and higher-order reflections (Siltanen et al., 2010). Wave-based methods are also computationally demanding, but compute diffraction more efficiently.

8.5. Follow-up research

- The scope of this research was primarily focused on vehicular noise generated by cars with internal combustion engines. However, it can be argued that the increasing number of electric vehicles reduces the propulsion noise (Campello-Vicente et al., 2017; IEA, 2020). Follow-up research can be performed to determine how the noise generated by electric vehicles propagates in urban street canyons.

- The product developed in this research can be applied in the vicinity of airports. Airplanes produce a large amount of LF-noise, known as ground noise (Van der Eerden et al., 2007). Hence, it can be argued that the acoustically optimized LWS can absorb the noise of other sources as well. Follow-up research can be performed to determine how the LWS product can absorb other noise sources as well.

- The scope of this research was for the application of the product on the exterior of a building. However, large inside spaces can also be equipped with sound absorbing solutions, such as the designed product. Follow-up research must be performed to determine what the role of the product could be in room acoustics.

- Regarding the reverberation room measurements, future research could apply a larger sample surface, closer the 10-12m^2 as recommended by ISO 354:2003.

- Regarding the analytical prediction, future research could focus on including random incidence, to improve the model fit with experimental results which use a diffuse sound field.

9. Conclusion

In this research, the following research question was asked:

> " How can the acoustic absorption of vertical greening systems in urban street
> canyons be improved, especially for low-frequency noise?

To answer this question, a combination of qualitative and quantitative research was performed. First, a literature research was carried out. It was found that a well-absorbing VGS is a system that is well-designed (correct plant species for climate and solar orientation) and well-maintained (supply of essential nutrients, etc.). Normal VGSs acoustically absorb well for f>250 Hz, primarily by visco-thermal absorption of the substrate. To increase the absorption, the layer should be thick and the pores should be interconnected and tortuous. To better control this, inert substrates can be used, e.g. hydroponic rock wool. Additionally, plants can attenuate sound to a lesser extent, by sound-drive oscillations of leaves, by scattering, and by visco-thermal absorption. This can be predicted using an equivalent fluid model, where morphological plant parameters are related to acoustical parameters. Additionally, to increase the low-frequency (LF) absorption of VGSs, i.e., <250 Hz, a parallel array of Helmholtz resonators can be integrated in the VGS structure. This is a resonator type where a plug of air vibrates (mass) against a volume of air (spring). The Helmholtz cavity volumes do not necessarily have to be physically subdivided, but should be filled with a locally reactive material with a low flow resistivity, such as glass wool. This enforces propagation normal to the surface.

Four concept designs were consecutively developed. The final design is a living wall system (LWS) based on hydroponic rock wool, with a parallel array of Helmholtz resonators integrated in its structure. To determine its acoustic performance, analytical, experimental, and numerical validation was performed. A Matlab script was developed that applied Delany-Bazley-Miki equations in an equivalent fluid model, and a transfer-function approach for the multi-layer complex impedance. The design yields a near-unity absorption for f>500 Hz. The incorporated resonators have extended the LF-absorption (α>0.5) down to 80 Hz. Impedance tube and reverberation room measurements proved that piercing the porous substrate layer with the Helmholtz resonator necks can yield a combined acoustic absorption. Finally, acoustic simulations showed that applying the proposed LWS to the facades in a reference urban street canyon in Rotterdam can substantially decrease sound levels, both inside the street canyon, as well as in the adjacent courtyard canyon. However, the window-to-wall ratio of the facade largely determines to what extent sound levels can be decreased, since vertical greenery cannot be applied in front of windows.

10. References

1. Asdrubali, F., D'Alessandro, F., Mencarelli, N., Horoshenkov, K., 2014. Sound Absorption Properties of Tropical Plants for Indoor Applications. 21st Int. Congr. Sound Vib.

2. Atlas Leefomgeving, 2021. Geluid wegverkeer alle wegen (Lden) [WWW Document]. URL https://www.atlasleefomgeving.nl/kaarten?config=3ef8 97de-127f-471a-959b-93b7597de188&gm-b=1544180834512%2Ctrue%2C1%3B15532444672 80%2Ctrue%2C0.8%3B&gm-x=150000&gm-y=455000&gm-z=3

3. Aylor, D., 1972. Sound Transmission through Vegetation in Relation to Leaf Area Density, Leaf Width, and Breadth of Canopy. J. Acoust. Soc. Am. 51, 411–414. https://doi.org/10.1121/1.1912852

4. Azkorra, Z., Pérez, G., Coma, J., Cabeza, L.F., Bures, S., Álvaro, J.E., Erkoreka, A., Urrestarazu, M., 2015. Evaluation of green walls as a passive acoustic insulation system for buildings. Appl. Acoust. 89, 46–56. https://doi.org/10.1016/j.apacoust.2014.09.010

5. Basirjafari, S., 2020. Innovative solution to enhance the Helmholtz resonator sound absorber in low-frequency noise by nature inspiration. J. Environ. Heal. Sci. Eng. 18, 873–882. https://doi.org/10.1007/s40201-020-00512-w

6. BBC, 2019. Plants for a living wall [WWW Document]. BBC Gard. World Mag. URL https://www.gardenersworld.com/plants/plants-for-a-living-wall/ (accessed 4.30.21).

7. Berardi, U., 2013. The increase of the sound absorption through rectangular slot perforations. Proc. Meet. Acoust. 19. https://doi.org/10.1121/1.4800911

8. Berardi, U., Ramakrishnan, R., 2016. Materials for Noise Control : Paper ICA2016-490 Comparison of the acoustic behaviour of porous materials in compressed and uncompressed conditions Comparison of the acoustic behaviour of porous materials in compressed and uncompressed conditions.

9. Blumrich, R., Wiedemann, J., 2015. Design of Automotive Aeroacoustic Wind Tunnels 02107, 1–6.

10. Bucur, V., 2006. Urban Forest Acoustics. Springer Heidelberg, Heidelberg.

11. Buikema, E., Vercammen, M., 2010. Gebulder op de grond. Geluid 2, 15–20.

12. Bullen, R., Fricke, F., 1982. Sound Propagation through Vegetation. J. Sound Vib. 80, 11–23.

13. Buratti, C., Moretti, E., 2010. Traffic Noise Pollution : Spectra Characteristics and Windows Sound Insulation in Laboratory and Field Measurements. J. Environ. Sci. Eng. 4, 28–36.

14. Cai, X., Guo, Q., Hu, G., Yang, J., 2014. Ultrathin low-frequency sound absorbing panels based on coplanar spiral tubes or coplanar Helmholtz resonators. Appl. Phys. Lett. 105, 1–5. https://doi.org/10.1063/1.4895617

15. Campello-Vicente, H., Peral-Orts, R., Campillo-Davo, N., Velasco-Sanchez, E., 2017. The effect of electric vehicles on urban noise maps. Appl. Acoust. 116. https://doi.org/10.1016/j.apacoust.2016.09.018

16. Can, A., Leclercq, L., Lelong, J., Botteldooren, D., 2010. Traffic noise spectrum analysis: Dynamic modeling vs. experimental observations. Appl. Acoust. 71. https://doi.org/10.1016/j.apacoust.2010.04.002

17. Carvalho, A.P.O., Sousa, M.R.M., 2016. Effect of sample area in reverberant chamber measurements of sound absorption coefficients. Proc. 22nd Int. Congr. Acoust. 2, 1–10.

18. Chamovitz, D., 2017. What a Plant Knows: A Field Guide to the Senses. Scientific American.

19. Chen, C., Du, Z., Hu, G., Yang, J., 2017. A low-frequency sound absorbing material with subwavelength thickness. Appl. Phys. Lett. 110. https://doi.org/10.1063/1.4984095

20. Costa, S., 2016. Thin Low-Frequency Sound Absorbing Panel By Additive Manufacturing.

21. Cox, T., D'Antonio, P., 2016. Acoustic Absorbers and Diffusers. CRC Press, Third edition. | Boca Raton : Taylor & Francis, 2017. https://doi.org/10.1201/9781315369211

22. Czyzewski, A., Ejsmont, J., 2008. VALIDATION OF HARMONOISE / IMAGINE TRAFFIC NOISE PREDICTION MODEL BY LONG TERM NOISE AND TRAFFIC MONITORING Andrzej Czyzewski Gdansk University of Technology Poland Gdansk University of Technology 17–19.

23. D'Alessandro, F., Asdrubali, F., Mencarelli, N., 2015. Experimental evaluation and modelling of the sound absorption properties of plants for indoor acoustic applications. Build. Environ. 94, 913–923. https://doi.org/10.1016/j.buildenv.2015.06.004

24. Dannemann, M., Kucher, M., Kunze, E., Modler, N., Knobloch, K., Enghardt, L., Sarradj, E., Höschler, K., 2018. Experimental study of advanced helmholtz resonator liners with increased acoustic performance by utilising material damping effects. Appl. Sci. 8, 1–18. https://doi.org/10.3390/app8101923

25. Dauchez, N., Etchessahar, M., Sahraoui, S., 2020. On measurement of mechanical properties of sound absorbing materials. Poromechanics II 627–631. https://doi.org/10.1201/9781003078807-99

26. Davis, M., Pérez, M., Tenpierik, M., Ramírez, F., 2016. More than just a Green Facade: Vertical gardens for sound absorption and architectural acoustics. Interact. between Theory Pract. Civ. Eng. Constr.

27. Davis, M., Tenpierik, M.J., Ramírez, F.R., Pérez, M.E., 2017. More than just a Green Facade: The sound absorption properties of a vertical garden with and without plants. Build. Environ. 116, 64–72. https://doi.org/10.1016/j.buildenv.2017.01.010

28. Delany, M., Bazley, E., 1970. Acoustical Properties of Fibrous Absorbernt Materials. Appl. Acoust. 3, 105–117.

29. Den Boer, E., Schroten, A., 2007. Traffic Noise reduction in Europe. CE Delft.

30. Ding, L., Van Renterghem, T., Botteldooren, D., Horoshenkov, K., Khan, A., 2013. Sound absorption of porous substrates covered by foliage: Experimental results and numerical predictions. J. Acoust. Soc. Am. 134, 4599–4609. https://doi.org/10.1121/1.4824830

31. EEA, 2014. EEA Report No 10/2014 - Noise in Europe 2014, Publications Office of the European Union.

32. Esau, K., 1953. Plant Anatomy. New York: John Wiley & Sons, Inc.; London: Chapman & Hall, Ltd.

33. Escouflaire, M., 2014. Theoretical and Numerical Investigation of Time-Domain Impedance Models for Computational AeroAcoustics.

34. EU CORDIS, 2013. HOSANNA – Holistic and sustainable abatement of noise by optimized combinations of natural and artificial means.

35. Forssén, J., Van Der Aa, B., 2013. Initial results for traffic noise mitigation with Helmholtz resonators in the ground surface beside a road. 42nd Int. Congr. Expo. Noise Control Eng. 2013, INTER-NOISE 2013 Noise Control Qual. Life 3, 2345–2352.

36. Fuchs, H. V., 2013. Applied Acoustics: Concepts, Absorbers, and Silencers for Acoustical Comfort and Noise Control. Springer Berlin Heidelberg, Berlin, Heidelberg. https://doi.org/10.1007/978-3-642-29367-2

37. Godbold, O., 2008. Investigating Broadband Acoustic Absorption Using Rapid Manufacturing.

38. Goia, F., 2016. Search for the optimal window-to-wall ratio in office buildings in different European climates and the implications on total energy saving potential. Sol. Energy 132, 467–492. https://doi.org/10.1016/j.solener.2016.03.031

39. Gommer, B., 2016. Resistance in Helmholtz resonators.

40. Granta Design, 2019. CES 2019 version 19.2.0.

41. Guillaume, G., Gauvreau, B., L'Hermite, P., 2015. Numerical study of the impact of vegetation coverings on sound levels and time decays in a canyon street model. Sci. Total Environ. 502, 22–30. https://doi.org/10.1016/j.scitotenv.2014.08.111

42. Gunawardena, K., Steemers, K., 2020. Urban living walls: reporting on maintenance challenges from a review of European installations. Archit. Sci. Rev. 63, 526–535. https://doi.org/10.1080/00038628.2020.1738209

43. Halperin, D., 2014. Environmental noise and sleep disturbances: A threat to health? Sleep Sci. 7, 209–212. https://doi.org/10.1016/j.slsci.2014.11.003

44. Harbers, M., 2015. College behaaglijkheid en warmte [WWW Document]. Hogesch. van Arnhem en Nijmegen.

45. Haupt, A., 1953. Plant Morphology. McGraw-Hill Publications in the Botanical Sciences, New York, Toronto.

46. Horoshenkov, K., Benkreira, H., Rohr, R., 2011a. The effect of moisture and soil type on the acoustical properties of green noise control elements. Forum Acusticum 2011.

47. Horoshenkov, K., Benkreira, H., Rohr, R., 2011b. Acoustic characterization of porous substratum used in green noise control elements. Inter-noise 2011.

48. Horoshenkov, K., Khan, A., Benkreira, H., 2013. Acoustic properties of low growing plants. J. Acoust. Soc. Am. 133, 2554–2565. https://doi.org/10.1121/1.4798671

49. Horoshenkov, K., Khan, A., Benkreira, H., Mandon, A., Rohr, R., 2014. Acoustic performance of vegetation and soil substratum in an urban context - Chapter 3. CRC Press.

50. Hygge, S., 2003. Classroom experiments on the effects of different noise sources and sound levels on long-term recall and recognition in children. Appl. Cogn. Psychol. 17. https://doi.org/10.1002/acp.926

51. IEA, 2020. Global EV Outlook 2020. Paris.

52. ISO, 2003. ISO 354:2003 Acoustics - Measurement of sound absorption in a reverberation room.

53. ISO, 1984. ISO 2848:1984 Building construction - Modular coordination - Principles and rules.

54. Kenney, W.A., 2000. Leaf Area Density as an urban forestry planning and management tool. For. Chron. 76, 235–239. https://doi.org/10.5558/tfc76235-2

55. Killengreen, T., Olafsen, S., 2007. the Spectrum Shape of Outdoor 2007.

56. Kinsler, L., Frey, A., Coppens, A., Sanders, J., 1982. Fundamentals of Acoustics, 4th editio. ed. John Wiley & Sons, Inc.

57. Köhler, M., 2008. Green facades - A view Back and some Visions. Urban Ecosyst 11, 423–436.

58. Komatsu, T., 2008. Improvement of the Delany-Bazley and Miki models for fibrous sound-absorbing materials. Acoust. Sci. Technol. 29, 121–129. https://doi.org/10.1250/ast.29.121

59. Krimm, J., 2018. Acoustically Effective Facades Design.

60. Lacasta, A.M., Penaranda, A., Cantalapiedra, I.R., Auguet, C., Bures, S., Urrestarazu, M., 2016. Acoustic evaluation of modular greenery noise barriers. Urban For. Urban Green. 20, 172–179. https://doi.org/10.1016/j.ufug.2016.08.010

61. Leventhall, G., Pelmear, P., Benton, S., 2003. A Review of Published Research on Low Frequency Noise and its Effects. DEFRA Rep. 88.

62. Lin, Y., West, G., 2016. Retrieval of effective leaf area index (LAIe) and leaf area density (LAD) profile at individual tree level using high density multi-return airborne LiDAR. Int. J. Appl. Earth Obs. Geoinf. 50, 150–158. https://doi.org/10.1016/j.jag.2016.03.014

63. Mahn, J., 2011. Road Traffic and Aircraft Noise Spectrums. Univ. Canterbury 3–11.

64. Männel, M., Forssén, J., van der Aa, B., 2013. Improving the acoustic performance of low noise road surfaces using resonators. J. Acoust. Soc. Am. 133, 3323–3323. https://doi.org/10.1121/1.4805559

65. Martens, M., Michelsen, A., 1981. Absorption of acoustic energy by plant leaves. J. Acoust. Soc. Am. 69, 303–307.

66. Martens, M, Severens, P., Van Wissen, H., van der Heijden, L., 1985. Acoustic reflection characteristics of deciduous plant leaves. Environ. Exp. Bot. 25, 285–292. https://doi.org/10.1016/0098-8472(85)90013-9

67. Martens, M., Van der Heijden, L., Walthaus, H., Van Rens, W., 1985. Classification of soils based on acoustic impedance, air flow resistivity, and other physical soil parameters. J. Acoust. Soc. Am. 78, 970–981.

68. Mechel, F., 2008. Formulas of Acoustics, Second edi. ed. Springer-Verlag Berlin.

69. Mechel, F., 1994. Helmholtz Resonators with Added Porous Absorbers. Acustica 80, 268.

70. Miki, Y., 1990. Acoustical properties of porous materials - Modifications of Delany-Bazley models. J. Acoust. Soc. Japan 11, 19–24.

71. Mir, M.A., 2011. Green Facades and Building Structures. Fac. Civ. Eng. MSc, 119.

72. Moya, T.A., van den Dobbelsteen, A., Ottelé, M., Bluyssen, P.M., 2019. A review of green systems within the indoor environment. Indoor Built Environ. 28, 298–309. https://doi.org/10.1177/1420326X18783042

73. NEN, 2012. NEN 1068:2012 Thermische isolatie van gebouwen - Rekenmethoden.

74. NIBE, 2021. NIBE Milieuclassificaties [WWW Document]. URL https://www.nibe.info/nl/members

75. Ottelé, M., 2011. The Green Building Envelope Vertical Greening, Department of Materials and Environment. Delft.

76. Ottelé, M., Perini, K., Fraaij, A.L.A., Haas, E.M., Raiteri, R., 2011. Comparative life cycle analysis for green façades and living wall systems. Energy Build. 43, 3419–3429. https://doi.org/10.1016/j.enbuild.2011.09.010

77. Park, S.H., 2013. Acoustic properties of micro-perforated panel absorbers backed by Helmholtz resonators for the improvement of low-frequency sound absorption. J. Sound Vib. 332, 4895–4911. https://doi.org/10.1016/j.jsv.2013.04.029

78. Peeters, B., Van Blokland, G., 2007. The noise emission model for European road traffic. IMAGINE Deliv. 6–12.

79. Pérez, G., Coma, J., Cabeza, L.F., 2018. Vertical Greening Systems for Acoustic Insulation and Noise Reduction, in: Nature Based Strategies for Urban and Building Sustainability. pp. 157–165. https://doi.org/10.1016/B978-0-12-812150-4.00015-X

80. Perini, K., Ottelé, M., Haas, E.M., Raiteri, R., 2011. Greening the building envelope, facade greening and living wall systems. Open J. Ecol. 01. https://doi.org/10.4236/oje.2011.11001

81. Persson, K., Björkman, M., 1988. Annoyance due to low frequency noise and the use of the dB(A) scale. J. Sound Vib. 127, 491–497. https://doi.org/10.1016/0022-460X(88)90374-4

82. Pommier, A.G., Provendier, D., Gutleben, C., Musy, M., Pommier, G., 2014. Impacts du végétal en ville: Fiche de synthèse du programme de recherche VegDUD - Rôle du végétal dans le développement urbain durable. Plante Cité.

83. Porges, G., 1977. Applied Acoustics. Edward Arnold, London.

84. Prisutova, J., Horoshenkov, K., 2014. The frequency and angular dependence of the absorption coefficient of common types of living plants. Inter-noise 2014.

85. Puczok, D., 2007. Digital modelling of musical sound sources. Univ. Degli Stud. Di Bol.

86. Ramsey, W., Ungerleider, A., 2008. Hybrid Composite Hydroponic Substrate System - Patent Application Publication. Priv. Point Contain. Sm Card 1, 11–14.

87. Randeberg, R.T., 2000. Perforated Panel Absorbers with Viscous Energy Dissipation Enhanced by Orifice Design. Thesis.

88. Remael, S., 2014. Patrick Blanc, the Master of the Vertical Garden. Wall Str. J.

89. Ribeiro, C., Mietlicki, F., Jamard, P., 2020. Health Impact of Noise Transport in the Densely 3339–3346.

90. Rijksoverheid, 2021. Arbeidsomstandighedenbesluit Artikel 5.2 - Voorkomen gevaren. Netherlands.

91. Rijksoverheid, 2012. Bouwbesluit Online 2012 Artikel 4.28 [WWW Document]. URL https://rijksoverheid.bouwbesluit.com/Inhoud/docs/wet/bb2003_nvt/artikelsgewijs/hfd4/afd4-6/par4-6-1/art4-28

92. Romanova, A., Horoshenkov, K. V., Hurrell, A., 2019. An application of a parametric transducer to measure acoustic absorption of a living green wall. Appl. Acoust. 145, 89–97. https://doi.org/10.1016/j.apacoust.2018.09.020

93. Rossing, T., 2007. Springer Handbook of Acoustics. Springer New York, New York, NY. https://doi.org/10.1007/978-0-387-30425-0

94. Salter, C., 1998. Acoustics: Architecture, Engineering & The Environment, 1st ed. William Stout Publishers.

95. Sanchez, M., Van Renterghem, T., Botteldooren, D., 2016. The effect of street canyon design on traffic noise exposure along roads 1–31.

96. Setaki, F., Tenpierik, M., Turrin, M., van Timmeren, A., 2014. Acoustic absorbers by additive manufacturing. Build. Environ. 72, 188–200. https://doi.org/10.1016/j.buildenv.2013.10.010

97. Shield, B., Dockrell, J., 2008. The effects of classroom and environmental noise on children's academic performance. ICBEN 9th Int. Congr. Noise as a Public Heal. Probl. 2008.

98. Siltanen, S., Lokki, T., Savioja, L., 2010. Rays or Waves? Understanding the Strengths and Weaknesses of Computational Room Acoustics Modeling Techniques. Proc. Int. Symp. Room Acoust. ISRA 2010 29–31 1–6.

99. Skinner, D., 2019. Living walls [WWW Document]. Gard. Time UK. URL https://www.gardentimeuk.com/whats-new/2019/1/18/76d03qvjovul0lfdj4cj6e0cjll6mv (accessed 4.30.21).

100. Smyrnova, Y., Kang, J., Cheal, C., Tijs, E., De Bree, H., 2010. Laboratory Test of Sound Absorption of Vegetation. Eur. Acoust. Assoc.

101. Tang, S.H., Ong, P.P., Woon, H.S., 1986. Monte Carlo simulation of sound propagation through leafy foliage using experimentally obtained leaf resonance parameters. J. Acoust. Soc. Am. 80, 1740–1744. https://doi.org/10.1121/1.394287

102. Tarnow, V., 2002. Measured anisotropic air flow resistivity and sound attenuation of glass wool. J. Acoust. Soc. Am. 111, 2735–2739. https://doi.org/10.1121/1.1476686

103. Tenpierik, M., 2015. Mouca II - Muro Orgánico Urbano Aplicado al Confort Acústico, TU Delft.

104. The Royal Horitculture Society, 2021. Green walls [WWW Document]. R. Hortic. Soc. URL https://www.rhs.org.uk/advice/profile?pid=547 (accessed 4.30.21).

105. Thomas, P., Van Renterghem, T., De Boeck, E., Dragonetti, L., Botteldooren, D., 2013. Reverberation-based urban street sound level prediction. J. Acoust. Soc. Am. 133, 3929–3939. https://doi.org/10.1121/1.4802641

106. Thomazelli, R., Caetano, F.D.N., Bertoli, S.R., 2016. Acoustic properties of green walls: Absorption and insulation. p. 015017. https://doi.org/10.1121/2.0000426

107. UNDESA, 2018. World Urbanization Prospects, Demographic Research.

108. Van den Akker, J., Van Kekem, A., 2006. Vooronderzoek absorptie grondgeluid Polderbaan Schiphol, Alterra-rapport 1358.

109. Van der Aa, B., 2010. Ground Buried Resonators - Analytical and numerical modelling of their noise reducing effect for sound propagating outdoors from traffic noise sources. Eindhoven Univ. Technol.

110. Van der Eerden, F., 2000. Noise reduction with coupled prismatic tubes. Univ. Twente.

111. Van der Eerden, F., Salomons, E., Beeks, T., 2007. Mitigation of low-frequency groundnoise from runways. Inter-noise 2007.

112. Van der Linden, A., Erdtsieck, P., Kuipers-van Gaalen, I., Zeegers, A., 2011. Bouwfysica, 7th ed. ThiemeMeulenhoff, Amersfoort.

113. Van Renterghem, T., Botteldooren, D., 2016. View on outdoor vegetation reduces noise annoyance for dwellers near busy roads. Landsc. Urban Plan. 148, 203–215. https://doi.org/10.1016/j.landurbplan.2015.12.018

114. Van Renterghem, T., Botteldooren, D., 2014. Influence of rainfall on the noise shielding by a green roof. Build. Environ. 82, 1–8. https://doi.org/10.1016/j.buildenv.2014.07.025

115. Van Renterghem, T., Botteldooren, D., 2009. Reducing the acoustical façade load from road traffic with green roofs. Build. Environ. 44, 1081–1087. https://doi.org/10.1016/j.buildenv.2008.07.013

116. Van Renterghem, T., Botteldooren, D., Hornikx, M., Jean, P., Defrance, J., Smyrnova, Y., Kang, J., 2012. Road traffic noise reduction by vegetated low noise barriers in urban streets. Proc. - Eur. Conf. Noise Control 944–948.

117. Van Renterghem, T., Forssén, J., Attenborough, K., Jean, P., Defrance, J., Hornikx, M., Kang, J., 2015. Using natural means to reduce surface transport noise during propagation outdoors. Appl. Acoust. 92, 86–101. https://doi.org/10.1016/j.apacoust.2015.01.004

118. Van Renterghem, T., Hornikx, M., Forssen, J., Botteldooren, D., 2013. The potential of building envelope greening to achieve quietness. Build. Environ. 61, 34–44. https://doi.org/10.1016/j.buildenv.2012.12.001

119. Vardoulakis, S., Fisher, B.E.A., Pericleous, K., Gonzalez-Flesca, N., 2003. Modelling air quality in street canyons: A review. Atmos. Environ. 37, 155–182. https://doi.org/10.1016/S1352-2310(02)00857-9

120. Vér, I., Beranek, L., 2006. Noise and Vibration Control Engineering, Second edi. ed. John Wiley & Sons, Hoboken.

121. Vladimir, M., Madalina, C., 2019. Optimizing urban landscapes in regard to noise pollution. Procedia Manuf. 32, 161–166. https://doi.org/10.1016/j.promfg.2019.02.197

122. Wagemans, M., 2016. Modularity of living wall systems 200.

123. Wong, N.H.N.C., Kwang Tan, A.Y., Tan, P.Y., Chiang, K., Wong, N.H.N.C., 2010. Acoustics evaluation of vertical greenery systems for building walls. Build. Environ. 45, 411–420. https://doi.org/10.1016/j.buildenv.2009.06.017

124. World Health Organization, 2011. Burden of disease from environmental noise. WHO Regional office for Europe, Copenhagen.

125. Yang, H.-S., Kang, J., Cheal, C., 2013. Random-Incidence Absorption and Scattering Coefficients of Vegetation. Acta Acust. united with Acust. 99, 379–388. https://doi.org/10.3813/AAA.918619

126. Yovel, Y., Stilz, P., Franz, M.O., Boonman, A., Schnitzler, H.-U., 2009. What a Plant Sounds Like: The Statistics of Vegetation Echoes as Received by Echolocating Bats. PLoS Comput. Biol. 5, e1000429. https://doi.org/10.1371/journal.pcbi.1000429

127. Zhao, X.D., Yu, Y.J., Wu, Y.J., 2016. Improving low-frequency sound absorption of micro-perforated panel absorbers by using mechanical impedance plate combined with Helmholtz resonators. Appl. Acoust. 114, 92–98. https://doi.org/10.1016/j.apacoust.2016.07.013

128. Zwikker, C., Kosten, C., 1949. Sound Absorbing Materials. Elsevier.

Appendix I - Calculations

1. Matlab script

```matlab
% Optimization of Acoustic Absorption of Vertical Greening Systems
% Script for predicting the combined absorption coefficient of a parallel
% array of Helmholtz resonators and
% Jesse Bakker, Delft University of Technology
% 09-05-21

close all; clear all

%%%%%%%%%%%%%%%%% I N P U T S %%%%%%%%%%%%%%%%%%

% Helmholtz resonator array
neck_L = [103]/1000;                    %[mm] Neck length
neck_a = [10 11 12 13]/1000;            %[mm] Orifice radius
cav_w = [137.5 137.5 137.5 137.5]/1000;%[mm] resonator width
cav_h = [150 150 150 150]/1000;         %[mm] resonator height
cav_d = [50]/1000;                      %[mm] Helmholtz cavity depth
res_num = [4 4 4 4];                    %[-] Resonator count
cav_sig = 5000;                         %[rayl m^-1] Flow resistivity of porous layer in cavity

% Vegetation layer
plant_name = 'Begonia';                 %[-] Plant type
plant_R = [100]/1000;                   %[mm] Plant circular footprint diameter
plant_h = [170]/100;                    %[cm] Plant height
plant_a = [43]/10000;                   %[cm^2] Area of single leaf
plant_n = 14;                           %[-] Number of leaves on plant
plant_phi = 71;                         %[°] Dominant angle of leaf orientation
plant_eps = 0.95;                       %[-] Porosity
plant_d = [100]/1000;                   %[mm] Layer thickness

% Substrate layer (dry)
sub_d = [100]/1000;                     %[mm] Soil layer thickness
sub_eps = 0.96;                         %[-] Porosity of soil
sub_tor = 1;                            %[-] Tortuosity of soil
sub_sig = 15000;                         %[rayl m^-1] Flow resistivity of soil

% Substrate layer (wet)
sub_wet = 0.3;                          %[-] Percentage of substrate that is saturated
sub_wet_eps = 0.1;                      %[-] Estimated porosity of saturated soil
sub_wet_sig = 100000;                   %[rayl m^-1] Estimated flow resistivity of saturated soil


%%%%%%%%%%%%%%%%% C A L C U L A T I O N %%%%%%%%%%%%%%%%%

% Plant parameters which are calculated
plant_S = pi*(plant_d/2).^2;        %[cm] Plant footprint
plant_V = plant_h*plant_S;          %[cm^3] Equivalent volume occupied by plant
plant_Av = (plant_a*plant_n)/plant_V; %[cm^-1] Leaf area density
plant_DAL = plant_phi*(pi./180);    %[rad] Dominat angle of leaf orientation in radians
plant_tor = cos(plant_DAL/2)+2*sin(plant_DAL/2); % [-] Tortuosity

% Vegetation flow resistivity according to Horoshenkov et al. (2013)
if plant_phi <= 40;
    plant_sig = 10^((0.0067.*plant_Av)+0.746);
elseif plant_phi >= 70;
    plant_sig = 10^((0.0083.*plant_Av)+1.413);
else
    plant_sig = 10; %To enter manual sigma, set plant_phi = 50
end

% Resonator porosity determination
res_S = cav_w.*cav_h; %[m^2] Individual resonator area
res_SA = res_S.*res_num; %[m^2] Combined resonator area, per type
res_ST = sum(res_SA,2); %[m^2] Sum of resonator areas = total sample area
res_eps = res_SA./res_ST; %[-] Ratio of resonator type area : total sample area

or_S = pi.*(neck_a.^2); %[m^2] Orifice area
or_eps = (res_num.*or_S)./res_SA; %[-] Porosity per resonator type = or_S./res_S;

or_epsT = (res_num.*or_S)./res_ST; %total resonator porosity
or_epsTS = sum(or_epsT,2); %total resonator porosity

%optional porous material in neck
%dn = [0]/1000;
%sigma2 = 0;
%Ri = (sigma2.*dn)./epsA;
```

```matlab
% Sample / panel
pan_h = [550]/1000; %Total sample height
pan_w = [550]/1000; %Total sample widht
pan_S = pan_h*pan_w; %Total sample area
pan_perc = (res_ST/pan_S)*100; %Percentage of inhibiting area by resonators

% Additional inputs
A_c0 = 342.34; %[m/s] Speed of sound
A_rho0 = 1.21; %[kg/m3] Density of air
A_Z0 = A_c0.*A_rho0; %[] Specific acoustic impedance

% Calculation resonator
A_f = [10:1:10000]; %[Hz] Frequency spectrum
A_k0 = 2.*pi.*A_f./A_c0; % Normal wave number
A_w = 2.*pi.*A_f; %Angular frequency
A_j = sqrt(-1); %Imaginary number

for x = 1:length(A_f);
    for y = 1:length(neck_a);

%Delany & Bazley equations for cavity filled porous layer:
res_X(x) = (A_rho0.*A_f(x))./cav_sig;
res_Zp(x) = A_Z0.*((1+0.0571.*res_X(x).^-0.754)-(A_j.*0.087.*res_X(x).^-0.732)); %Impedance of
porous layer
res_kp(x) = (A_w(x)./A_c0).*(((1+0.0978.*res_X(x)).^-0.7)-(A_j.*0.189.*res_X(x).^-0.595));
%Complex wavenumber

res_delta(y) = 0.85.*(1-1.125.*sqrt(or_eps(y))); %Neck length correction

res_Z1(x,y) = -A_j.*res_Zp(x).*cot(res_kp(x).*cav_d); %Cox & D'Antonio equation for cavity
completely filled with porous layer:
res_Z2(x,y) =
(1./or_eps(y)).*(2.*res_delta(y).*neck_a(y)+neck_L).*A_j.*A_w(x).*A_rho0+res_Z1(x,y);%impedanc
e when considering 1 specific resonator type

res_Z3(x,y)=res_Z2(x,y)./res_eps(y);

%impedance of individual resonant absorbers
res_ind_R(x,y) = (res_Z3(x,y)-A_Z0)./(res_Z3(x,y)+A_Z0); %reflection factor
res_ind_res(x,y) = 1-abs(res_ind_R(x,y)).^2; %absorption coefficient
    end
end

res_Z = (sum((res_Z3).^-1,2)).^-1; %Combined resonator impedance
res_R = (res_Z-A_Z0)./(res_Z+A_Z0); %reflection factor of total array
res_a = 1-abs(res_R).^2; %absorption coefficient of total array
res_ZX = res_Z.';

%---------------- plant layer  ----------------

plant_Z1=(sqrt(plant_tor)./plant_eps).*(1+0.070.*(A_f./plant_sig).^(-0.632));
plant_Z2=(sqrt(plant_tor)./plant_eps).*(0.107.*(A_f./plant_sig).^(-0.632));

plant_k1=((A_w.*sqrt(plant_tor))./A_c0).*(0.160.*(A_f./plant_sig).^(-0.618));
plant_k2=((A_w.*sqrt(plant_tor))./A_c0).*(1+0.109.*(A_f./plant_sig).^(-0.618));

plant_Z=A_Z0.*(plant_Z1+(A_j.*plant_Z2));
plant_k=plant_k2+(A_j.*plant_k1);

plant_Z2=plant_Z.*coth(-A_j.*plant_d.*plant_k); %1x1000
plant_R=(plant_Z2-A_Z0)./(plant_Z2+A_Z0);
plant_a=1-sqrt(real(plant_R).^2+imag(plant_R).^2).^2;



%---------------- substrate layer (dry) ----------------
sub_Z1 = (sqrt(sub_tor)./sub_eps).*(1+0.070.*(A_f./sub_sig).^(-0.632));
sub_Z2 = (sqrt(sub_tor)./sub_eps).*(0.107.*(A_f./sub_sig).^(-0.632));

sub_k1 = ((A_w.*sqrt(sub_tor))./A_c0).*(0.160.*(A_f./sub_sig).^(-0.618));
sub_k2 = ((A_w.*sqrt(sub_tor))./A_c0).*(1+0.109.*(A_f./sub_sig).^(-0.618));

sub_Z = A_Z0.*(sub_Z1+(1i.*sub_Z2));
sub_k = sub_k2+(1i.*sub_k1);

sub_Z2 = sub_Z.*coth(-A_j.*sub_d.*sub_k);
sub_R = (sub_Z2-A_Z0)./(sub_Z2+A_Z0);
sub_a = 1-sqrt(real(sub_R).^2+imag(sub_R).^2).^2;
sub_epsT = 1-or_epsTS;
```

```matlab
%---------------- substrate layer (wet) -----------------
sub_wet_Z1 = (sqrt(sub_tor)./sub_wet_eps).*(1+0.070.*(A_f./sub_wet_sig).^(-0.632));
sub_wet_Z2 = (sqrt(sub_tor)./sub_wet_eps).*(0.107.*(A_f./sub_wet_sig).^(-0.632));

sub_wet_k1 = ((A_w.*sqrt(sub_tor))./A_c0).*(0.160.*(A_f./sub_wet_sig).^(-0.618));
sub_wet_k2 = ((A_w.*sqrt(sub_tor))./A_c0).*(1+0.109.*(A_f./sub_wet_sig).^(-0.618));

sub_wet_Z = A_Z0.*(sub_wet_Z1+(1i.*sub_wet_Z2));
sub_wet_k = sub_wet_k2+(1i.*sub_wet_k1);

sub_wet_Z2 = sub_wet_Z.*coth(-A_j.*sub_d.*sub_wet_k);
sub_wet_R = (sub_wet_Z2-A_Z0)./(sub_wet_Z2+A_Z0);
sub_wet_a = 1-sqrt(real(sub_wet_R).^2+imag(sub_wet_R).^2).^2;


%---------------- substrate layer (combined dry and wet) -----------------
sub_dry = 1-sub_wet;
sub_com_Z1 = (1./(sub_Z2./sub_dry))+(1./(sub_wet_Z2./sub_wet));
sub_com_Z2 = 1./sub_com_Z1;
sub_com_R = (sub_com_Z2-A_Z0)./(sub_com_Z2+A_Z0);
sub_com_a = 1-sqrt(real(sub_com_R).^2+imag(sub_com_R).^2).^2;



%----------------total combined impedance -----------------
% With resonator piercing
sub_cor_Z1 = (1./(sub_com_Z2./sub_epsT))+(1./(res_ZX));
sub_cor_Z2 = 1./sub_cor_Z1;

ps_Z = plant_Z.*((sub_cor_Z2-plant_Z.*tanh(1j.*plant_k.*plant_d))./(plant_Z-
sub_cor_Z2.*tanh(A_j.*plant_k.*plant_d))); %transfer matrix approach
ps_a = 1-abs((ps_Z-A_Z0)./(ps_Z+A_Z0)).^2;

% Without resonator piercing (just plant-soil)
ps_Z2 = plant_Z.*((sub_com_Z2-plant_Z.*tanh(1j.*plant_k.*plant_d))./(plant_Z-
sub_com_Z2.*tanh(A_j.*plant_k.*plant_d)));
ps_a2 = 1-abs((ps_Z2-A_Z0)./(ps_Z2+A_Z0)).^2;



%----------------plot-----------------

%resonators plot
subplot(2,3,1);
plot(A_f,res_ind_res,':',A_f,res_a,'k','Linewidth',2);
xlabel('f [Hz]','FontName','arial','FontSize',12);
ylabel('Absorption coefficient [-]','FontSize',12);
[res_pks,res_locs] = findpeaks(res_a,A_f);
text(res_locs+1,res_pks,num2str(res_locs'));
axis([10,250,0,1]);
grid on
title("alpha of resonators")

%substrate plot
subplot(2,3,2);
semilogx(A_f,sub_com_a,'k','Linewidth',2);
hold on
semilogx(A_f,sub_a,':','Linewidth',2);
semilogx(A_f,sub_wet_a,':','Linewidth',2);
hold off
xlabel('f [Hz]','FontName','arial','FontSize',12);
ylabel('Absorption coefficient [-]','FontSize',12);
grid on
legend('Combined','Dry substrate','Wet substrate','Location','northwest');
title("alpha substrate")
axis([10,10000,0,1]);

%plant plot
subplot(2,3,3);
semilogx(A_f,plant_a,'k','Linewidth',2);
xlabel('f [Hz]','FontName','arial','FontSize',12);
ylabel('Absorption coefficient [-]','FontSize',12);
grid on
title("alpha plant")
axis([10,10000,0,1]);

%total plot linear
```

```matlab
subplot(2,3,4);
plot(A_f,res_a,':','Linewidth',2);
hold on
semilogx(A_f,ps_a2,':','Linewidth',2);
semilogx(A_f,ps_a,'k','Linewidth',2);
hold off
xlabel('f [Hz]','FontName','arial','FontSize',12);
ylabel('Absorption coefficient [-]','FontSize',12);
%[a_pks,a_locs] = findpeaks(ps_a,A_f);
%text(a_locs+1,a_pks,num2str(a_locs'));
grid on
legend('Resonators','Plant-substrate','All combined','Location','southeast');
title("alpha all combined - linear for LF bands")
axis([0,500,0,1]);

%total plot logx
subplot(2,3,[5,6]);
semilogx(A_f,res_a,':','Linewidth',2);
%plot(A_f,ps_a,'k','Linewidth',2);
hold on
semilogx(A_f,ps_a2,':','Linewidth',2);
semilogx(A_f,ps_a,'k','Linewidth',2);
hold off
xlabel('f [Hz]','FontName','arial','FontSize',12);
ylabel('Absorption coefficient [-]','FontSize',12);
%[a_pks,a_locs] = findpeaks(ps_a,A_f);
%text(a_locs+1,a_pks,num2str(a_locs'));
grid on
legend('Resonators','Plant-substrate','All combined','Location','southeast');
title("alpha all combined - logarithmic full spectrum")
axis([10,10000,0,1]);

%---- Workspace devisions ---
A_01 = ("---STANDARD---");
cav_00 = (''); cav_01 = ("---RESONATOR CAVITY---");
com_00 = (''); com_01 = ("---LAYER COMBINATION---");
neck_00 = (''); neck_01 = ("---RESONATOR NECKS---");
or_00 = (''); or_01 = ("---RESONATOR ORIFICES---");
pan_00 = (''); pan_01 = ("---SAMPLE / PANEL---");
plant_00 = (''); plant_01 = ("---PLANT LAYER---");
ps_00 = (''); ps_01 = ("---PLANT-SUBSTRATE LAYER COMBINATION---");
res_00 = (''); res_01 = ("---RESONATOR CALCULATION---");
sub_00 = (''); sub_01 = ("---SUBSTRATE LAYER---");
```

2. Calculation of thermal insulation

The increase of the R_c-value is calculated below.

Reference wall (no LWS)

Reference wall with LWS
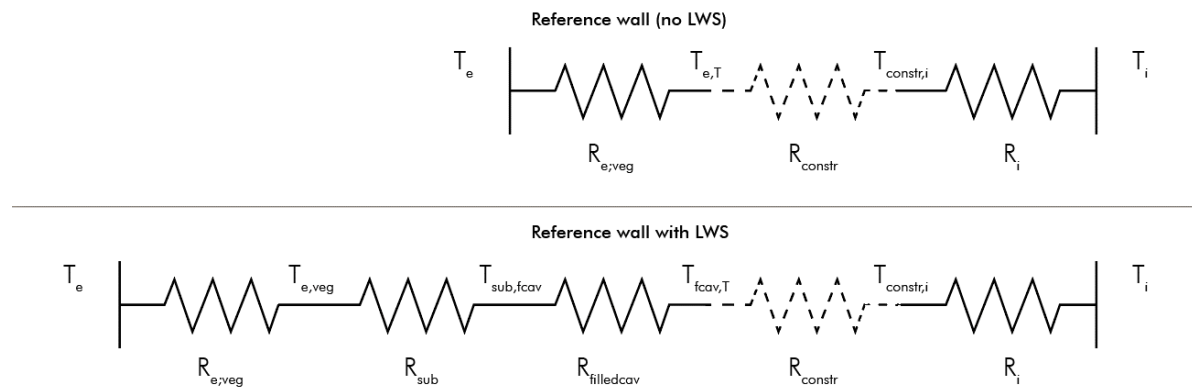
	$R_{e;veg}$	R_{sub}[2]	$R_{filledcav}$[3]	R_{constr}	R_i
R_d (m²K/W)	0.13 [1]	$\frac{0.1}{0.035} = 2.86$	$\frac{0.050}{0.035} = 1.43$	3.7 [4]	0.13
R_T (m²K/W)	7.99	Total thermal resistance			
ΔU_a (W/m²K)	0.00	Correction factor for convection			
ΔUf_a (W/m²K)	0.002	Correction factor for structural connection (plastic thermal break) $0.8 \cdot \frac{n \cdot \lambda \cdot A_{fa}}{d} \cdot \left(\frac{R_1}{R_T}\right)^2 = 0.8 \cdot \frac{4 \cdot 0.17 \cdot 0.001}{0.075} \cdot \left(\frac{2.14}{8.7}\right)^2 = 0.002$			
ΔU_W (W/m²K)	0.006	Correction factor for building quality $0.05 \cdot \frac{1}{R_T} = 0.05 \cdot \frac{1}{8.7} = 0.006$			
ΔU (W/m²K)	0.008	Total correction factor ($\Delta U_a + \Delta Uf_a + \Delta U_W$)			
β	0.06	$R_T \cdot \Delta U = 7.99 \cdot 0.008 = 0.07$			
R_c (m²K/W)	7.87	Total heat resistance $\frac{R_T}{1+\beta} - R_i - R_e = \frac{8.70}{1+0.07} - 0.26 = 7.28$			
Improvement	97%	In comparison with the with the existing facade			

(1) $R_e = R_i$ may be assumed due to the turbulent airflow along vegetation (Ottelé, 2011).

(2) Substrate layer of 100 mm rock wool, $\lambda = 0.035$ W/m²K

(3) Cavity fill of 50 mm glass wool, $\lambda = 0.035$ W/m²K

(4) Considering a standard insulated and ventilated cavity masonry wall (Harbers, 2015).

3. Simulation results (model A)

F [Hz]	Without LWS REC 1 dB(A)	REC 2 dB(A)	With LWS REC 1 dB(A)	REC 2 dB(A)	Comparison dB	dB
25.1	17.0	15.4	13.5	15.0	-3.5	-0.3
31.6	23.1	14.9	13.7	20.5	-9.4	5.5
39.8	24.8	20.8	16.7	22.3	-8.1	1.5
50.1	20.9	15.6	11.8	18.4	-9.2	2.8
63.1	16.0	15.8	12.8	13.7	-3.2	-2.1
79.4	13.2	12.0	8.9	10.4	-4.2	-1.6
100.0	4.5	8.1	4.1	1.5	-0.4	-6.7
125.9	4.6	9.0	5.3	1.4	0.7	-7.6
158.5	6.0	7.5	4.1	3.2	-1.9	-4.3
199.5	8.9	5.1	2.2	5.1	-6.7	0.0
251.2	4.8	4.1	-1.4	0.0	-6.3	-4.1
316.2	-6.8	-0.4	-6.1	-14.2	0.7	-13.9
398.1	-4.0	-1.0	-12.4	-14.3	-8.4	-13.3
501.2	-0.7	0.1	-11.4	-11.8	-10.7	-11.9
631.0	-1.4	-1.8	-13.6	-10.8	-12.2	-9.0
794.3	-3.7	-3.8	-11.5	-11.9	-7.8	-8.1
1000.0	-11.1	-5.1	-12.5	-16.8	-1.4	-11.8
1258.9	-12.9	-11.7	-23.9	-18.6	-11.1	-6.8
1584.9	-11.0	-9.8				
1995.3	-13.6	-14.1				
2511.9	-18.1	-30.4				
3162.3	-33.0					

Total	-6.5	-5.1	dB

102

5. Simulation results (model B)

Lower SPL **Higher SPL** **Further** **Closer**

Simulation B1	Simulation B2	B2-B1	Distances
Single canyon - Original facade (masonry brick surfaces)	Single canyon - With acoustic LWS modules	Comparison	REC-SRC REC-wall

Source 0

SPL [dB(A)] per 1/1 octave band [Hz] | SPL [dB(A)] per 1/1 octave band [Hz] | SPL comparison [dB] per 1/1 octave band [Hz] | Distance [m]   Group

R		125	250	500	1000	2000	4000	8000	16000	125	250	500	1000	2000	4000	8000	16000	125	250	500	1000	2000	4000	8000	16000	REC-SRC	REC-wall	Grp
1	h	41.67	43.49	45.74	52.27	51.88	42.77	42.09	39.75	41.56	42.65	44.32	52.18	51.47	42.33	41.62	39.32	-0.11	-0.84	-1.42	-0.09	-0.41	-0.44	-0.47	-0.43	9.50	1.50	A
	E	41.72	43.32	45.90	52.49	51.81	42.76	42.04	39.79	41.61	42.79	44.10	52.10	51.42	42.27	41.60	39.28	-0.11	-0.53	-1.80	-0.39	-0.39	-0.49	-0.44	-0.51			
2	h	45.22	47.8	54.03	58.58	57.10	49.12	48.56	47.55	44.99	47.86	54.07	58.56	56.88	49.10	48.48	47.50	-0.23	0.06	0.04	-0.02	-0.22	-0.02	-0.08	-0.05	4.30	6.70	A
	E	45.04	47.75	54.03	58.66	57.02	49.10	48.56	47.52	44.99	47.66	53.94	58.57	56.92	49.03	48.50	47.49	-0.05	-0.09	-0.09	-0.09	-0.10	-0.07	-0.06	-0.03			
3	h	41.99	41.42	47.45	50.26	50.01	41.89	40.88	38.96	41.4	40.91	47.44	50.11	49.60	41.53	40.57	38.77	-0.59	-0.51	-0.01	-0.15	-0.41	-0.36	-0.31	-0.19	8.05	19.05	A
	E	41.71	41.2	47.57	50.40	49.81	41.79	40.73	38.86	41.63	40.95	47.38	50.11	49.53	41.56	40.57	38.78	-0.08	-0.25	-0.19	-0.29	-0.28	-0.23	-0.16	-0.08	7.28		
4	h	35.41	38.81	38.79	42.44	43.60	34.59	32.40	27.74	35.45	38.53	37.35	40.80	42.50	33.54	31.61	27.14	0.04	-0.28	-1.44	-1.64	-1.10	-1.05	-0.79	-0.60	20.66	6.70	B
	E	35.50	38.67	38.63	42.44	43.60	34.48	32.34	27.65	35.29	38.41	37.44	40.73	42.45	33.53	31.58	27.12	-0.21	-0.26	-1.19	-1.71	-1.15	-0.95	-0.76	-0.53			
5	h	33.45	37.18	40.16	39.76	42.05	32.47	30.14	26.13	33.29	36.55	37.39	36.00	40.73	30.63	28.19	23.12	-0.16	-0.63	-2.77	-3.76	-1.32	-1.84	-1.95	-3.01	27.50	1.50	B
	E	33.39	37.13	39.27	39.59	41.98	32.29	29.93	26.05	33.08	36.52	37.27	36.24	40.69	30.59	28.15	23.12	-0.31	-0.61	-2.00	-3.35	-1.29	-1.70	-1.78	-2.93	24.08		
6	h	37.82	41.67	42.95	47.62	49.74	39.98	37.97	34.75	36.18	41.66	41.57	47.59	48.82	39.49	37.54	34.21	-1.64	-0.01	-1.38	-0.03	-0.92	-0.49	-0.43	-0.54	18.35	1.00	C
	E	37.45	42.61	44.58	47.63	48.14	39.94	37.87	33.99	37.00	42.31	43.60	47.51	47.67	39.57	37.41	33.24	-0.45	-0.30	-0.98	-0.12	-0.47	-0.37	-0.46	-0.75			
7	h	33.82	38.27	40.59	42.49	42.67	34.56	32.22	26.34	32.96	36.95	38.43	40.00	40.95	32.61	30.73	23.15	-0.86	-1.32	-2.16	-2.49	-1.72	-1.95	-1.49	-3.19	31.95	1.00	C
	E	34.11	38.49	41.22	43.31	43.09	34.01	31.24	25.86	33.53	37.58	39.99	41.99	41.88	32.70	29.87	23.02	-0.58	-0.91	-1.23	-1.32	-1.21	-1.31	-1.37	-2.84			
8	h	36.47	42.46	43.22	47.84	49.30	40.08	38.00	34.73	36.07	41.86	41.91	47.64	48.82	39.47	37.49	33.91	-0.40	-0.60	-1.31	-0.20	-0.48	-0.61	-0.51	-0.82	18.35	1.00	C
	E	37.48	42.6	44.59	47.59	48.15	39.93	37.84	33.95	36.99	42.3	43.56	47.49	47.65	39.54	37.37	33.16	-0.49	-0.30	-1.03	-0.10	-0.50	-0.39	-0.47	-0.79			
9	h	33.38	37.88	39.84	41.84	42.37	34.24	32.01	25.69	32.81	37.09	38.59	39.40	40.98	32.73	31.02	23.03	-0.57	-0.79	-1.25	-2.44	-1.39	-1.51	-0.99	-2.66	31.95	1.00	C
	E	34.00	38.38	41.02	43.13	42.93	33.83	31.05	25.30	33.45	37.54	39.97	41.94	41.86	32.69	29.83	22.85	-0.55	-0.84	-1.05	-1.19	-1.07	-1.14	-1.22	-2.45	25.15		

h = impulse response algorithm data, E = echogram algorithm data

Group A	-0.19	-0.36	-0.58	-0.17	-0.30	-0.27	-0.25	-0.21	-0.29	dB
Group B	-0.16	-0.45	-1.85	-2.62	-1.22	-1.39	-1.32	-1.77	-1.34	dB
Group C	-0.69	-0.63	-1.30	-0.99	-0.97	-0.97	-0.87	-1.76	-1.02	dB

Source 1

SPL [dB(A)] per 1/1 octave band [Hz] | SPL [dB(A)] per 1/1 octave band [Hz] | SPL comparison [dB] per 1/1 octave band [Hz] | Distance [m]   Group

R		125	250	500	1000	2000	4000	8000	16000	125	250	500	1000	2000	4000	8000	16000	125	250	500	1000	2000	4000	8000	16000	REC-SRC	REC-wall	Grp
1	h	33.85	37.79	39.23	39.88	42.37	32.47	30.40	26.48	33.52	37	37.49	36.72	41.39	31.01	28.89	24.14	-0.33	-0.79	-1.74	-3.16	-0.98	-1.46	-1.51	-2.34	26.10	1.50	B
	E	33.75	37.36	39.23	39.76	42.32	32.42	30.25	26.18	33.49	36.88	37.41	36.60	41.28	30.91	28.86	24.04	-0.26	-0.48	-1.82	-3.16	-1.04	-1.51	-1.39	-2.14			
2	h	35.69	38.63	38.98	42.78	43.77	34.46	32.41	27.90	35.27	38.35	37.52	40.59	42.46	33.32	31.45	27.01	-0.42	-0.28	-1.46	-2.19	-1.31	-1.14	-0.96	-0.89	20.90	6.70	B
	E	35.44	38.65	38.61	42.49	43.61	34.30	32.28	27.80	35.2	38.33	37.45	40.48	42.43	33.32	31.44	27.01	-0.24	-0.32	-1.16	-2.01	-1.18	-0.98	-0.84	-0.79			
3	h	42.01	41.21	48.57	50.64	49.97	41.93	41.33	39.22	41.89	41.17	48.52	50.62	49.77	41.79	41.32	39.36	-0.12	-0.04	-0.05	-0.02	-0.20	-0.14	-0.01	0.14	8.55	19.05	A
	E	41.95	41.09	48.38	50.76	49.91	41.99	41.22	39.24	41.94	41.06	48.37	50.60	49.75	41.88	41.21	39.30	-0.01	-0.03	-0.01	-0.16	-0.16	-0.11	-0.01	0.06			
4	h	45.04	48.75	53.99	58.83	57.53	49.30	48.96	47.96	45.29	48.8	53.93	58.77	57.44	49.20	48.90	47.94	0.25	0.05	-0.06	-0.06	-0.09	-0.10	-0.06	-0.02	4.06	6.70	A
	E	45.13	48.75	53.98	58.82	57.51	49.27	48.94	47.96	45.07	48.68	53.89	58.74	57.42	49.21	48.89	47.93	-0.06	-0.07	-0.09	-0.08	-0.09	-0.06	-0.05	-0.03			

103

| 5 | h | 40.85 | 43.15 | 42.48 | 52.55 | 49.63 | 41.69 | 41.10 | 38.45 | | 40.74 | 42.45 | 40.34 | 52.12 | 49.01 | 41.05 | 40.32 | 37.63 |
| | E | 40.82 | 43.08 | 43.42 | 52.45 | 49.61 | 41.66 | 40.91 | 38.31 | | 40.64 | 42.54 | 40.04 | 52.08 | 48.99 | 41.07 | 40.36 | 37.65 |

| -0.11 | -0.70 | -2.14 | -0.43 | -0.62 | -0.64 | -0.78 | -0.82 | | 10.90 | 1.50 | A |
| -0.18 | -0.54 | -3.38 | -0.37 | -0.62 | -0.59 | -0.55 | -0.66 |

| 6 | h | 33.89 | 37.93 | 40.58 | 42.19 | 42.41 | 34.05 | 31.94 | 26.72 | | 33.29 | 37.47 | 39.17 | 40.25 | 41.46 | 32.42 | 30.44 | 24.20 |
| | E | 33.92 | 38.13 | 40.88 | 42.88 | 43.10 | 34.08 | 31.40 | 25.89 | | 33.57 | 37.76 | 40.13 | 42.05 | 42.29 | 33.04 | 30.26 | 23.69 |

| -0.60 | -0.46 | -1.41 | -1.94 | -0.95 | -1.63 | -1.50 | -2.52 | | 29.95 | 1.00 | C |
| -0.35 | -0.37 | -0.75 | -0.83 | -0.81 | -1.04 | -1.14 | -2.20 |

| 7 | h | 36.45 | 41.17 | 42.25 | 47.39 | 47.98 | 39.39 | 37.09 | 33.81 | | 35.31 | 41.62 | 42.15 | 45.48 | 47.98 | 39.07 | 36.44 | 32.43 |
| | E | 37.16 | 41.95 | 43.45 | 47.22 | 47.57 | 39.42 | 37.29 | 33.70 | | 36.44 | 42.2 | 43.27 | 46.86 | 47.28 | 39.09 | 36.72 | 32.45 |

| -1.14 | 0.45 | -0.10 | -1.91 | 0.00 | -0.32 | -0.65 | -1.38 | | 16.69 | 1.00 | C |
| -0.72 | 0.25 | -0.18 | -0.36 | -0.29 | -0.33 | -0.57 | -1.25 |

| 8 | h | 33.58 | 37.67 | 40.46 | 42.35 | 42.56 | 34.55 | 31.95 | 26.81 | | 33.10 | 37.3 | 38.82 | 40.40 | 41.37 | 32.51 | 30.51 | 23.61 |
| | E | 34.16 | 38.35 | 41.12 | 43.20 | 43.32 | 34.26 | 31.61 | 26.51 | | 33.69 | 37.86 | 40.21 | 42.11 | 42.31 | 33.06 | 30.26 | 23.53 |

| -0.48 | -0.37 | -1.64 | -1.95 | -1.19 | -2.04 | -1.44 | -3.20 | | 29.95 | 1.00 | C |
| -0.47 | -0.49 | -0.91 | -1.09 | -1.01 | -1.20 | -1.35 | -2.98 |

| 9 | h | 36.70 | 41.29 | 42.00 | 47.98 | 48.83 | 39.75 | 37.73 | 34.00 | | 35.25 | 41.86 | 42.38 | 47.40 | 49.03 | 39.71 | 37.16 | 33.17 |
| | E | 37.24 | 41.97 | 43.58 | 47.25 | 47.58 | 39.46 | 37.29 | 33.50 | | 36.58 | 42.3 | 43.46 | 47.09 | 47.44 | 39.24 | 36.90 | 32.60 |

| -1.45 | 0.57 | 0.38 | -0.58 | 0.20 | -0.04 | -0.57 | -0.83 | | 16.69 | 1.00 | C |
| -0.66 | 0.33 | -0.12 | -0.16 | -0.14 | -0.22 | -0.39 | -0.90 |

Group	A	-0.04	-0.22	-0.96	-0.19	-0.30	-0.27	-0.24	-0.22		-0.30	dB
Group	B	-0.31	-0.47	-1.55	-2.63	-1.13	-1.27	-1.18	-1.54		-1.26	dB
Group	C	-0.73	-0.01	-0.59	-1.10	-0.52	-0.85	-0.95	-1.91		-0.83	dB

Total for simulation B

Group	A	-0.12	-0.29	-0.77	-0.18	-0.30	-0.27	-0.25	-0.22		-0.30	dB
Group	B	-0.24	-0.46	-1.70	-2.62	-1.17	-1.33	-1.25	-1.65		-1.30	dB
Group	C	-0.71	-0.32	-0.95	-1.04	-0.75	-0.91	-0.91	-1.83		-0.93	dB

(A) Top-down view

(B) Side view

Legend: Lower SPL (green) | Higher SPL (red) | Further (blue) | Closer (orange)

Source 0

Simulation C1 — Single canyon - Original facade (masonry brick surfaces)
SPL [dB(A)] per 1/1 octave band [Hz]

R		125	250	500	1000	2000	4000	8000	16000
1	h	42.37	45.05	48.55	54.29	53.05	44.08	43.33	41.03
	E	42.7	45.55	48.09	53.78	52.98	44.13	43.28	40.88
2	h	43.94	47.53	53.68	59.42	57.66	49.11	48.77	47.73
	E	45.29	48.08	54.25	58.87	57.29	49.32	48.75	47.67
3	h	41.83	41.73	47.96	50.77	50.04	42.02	40.92	38.86
	E	41.93	41.77	47.89	50.69	50.10	42.07	40.94	38.89
4	h	36.11	39.63	40.39	43.41	44.34	36.33	32.95	28.36
	E	36.12	39.36	39.91	43.45	44.12	35.55	33.24	28.20
5	h	34.98	39.72	40.93	42.04	43.44	34.37	32.45	27.98
	E	35.16	39.38	41.76	42.96	43.90	34.66	32.14	27.51
6	h	37.03	42.51	42.92	48.74	50.26	40.57	38.77	36.09
	E	37.84	43.14	44.38	48.37	48.53	40.36	38.53	35.31
7	h	33.20	38.52	40.83	42.86	42.70	34.64	32.98	27.51
	E	34.44	38.81	41.35	43.71	43.38	34.35	31.86	27.40
8	h	36.77	42.19	43.09	48.25	49.70	40.43	38.43	35.05
	E	37.65	43.01	44.16	48.01	48.25	40.07	38.10	34.41
9	h	33.46	38.68	40.28	42.32	42.63	34.41	32.52	27.35
	E	34.30	38.71	41.21	43.56	43.27	34.24	31.66	27.13

h = impulse response algorithm data, E = echogram algorithm data

Simulation C2 — Single canyon - With acoustic LWS modules
SPL [dB(A)] per 1/1 octave band [Hz]

R		125	250	500	1000	2000	4000	8000	16000
1	h	41.89	42.82	43.87	52.48	51.46	42.24	41.59	39.22
	E	41.99	43.18	43.95	52.30	51.47	42.22	41.55	39.22
2	h	43.65	46.45	54.72	58.38	56.62	48.77	48.83	47.65
	E	45.19	47.85	54.02	58.66	57.00	49.10	48.58	47.58
3	h	41.79	40.84	47.26	50.07	49.35	41.67	40.60	38.96
	E	41.79	41.19	47.43	50.25	49.60	41.60	40.62	38.83
4	h	35.47	38.59	37.53	41.08	42.60	33.53	31.57	27.13
	E	35.62	38.60	37.47	41.16	42.53	33.52	31.57	27.09
5	h	33.45	36.93	37.24	36.60	40.87	30.59	28.16	23.12
	E	33.87	36.94	37.24	37.52	40.84	30.56	28.11	23.08
6	h	35.73	41.85	41.45	47.82	49.20	39.40	37.66	33.86
	E	37.09	42.32	43.33	47.51	47.56	39.45	37.33	33.14
7	h	32.45	36.56	37.76	39.27	40.53	32.25	30.76	22.75
	E	33.35	37.36	39.62	41.46	41.44	32.26	29.51	22.60
8	h	35.95	41.46	41.40	47.32	48.88	39.38	37.36	33.99
	E	37.01	42.29	43.34	47.38	47.53	39.45	37.33	33.15
9	h	32.47	36.82	37.84	39.30	40.54	32.40	30.79	22.82
	E	33.41	37.42	39.65	41.63	41.51	32.29	29.58	22.89

C2-C1 Comparison
SPL comparison [dB] per 1/1 octave band [Hz]

R		125	250	500	1000	2000	4000	8000	16000
1	h	-0.48	-2.23	-4.68	-1.81	-1.59	-1.84	-1.74	-1.81
	E	-0.71	-2.37	-4.14	-1.48	-1.51	-1.91	-1.73	-1.66
2	h	-0.29	-1.08	1.04	-1.04	-1.04	-0.34	0.06	-0.08
	E	-0.10	-0.23	-0.23	-0.21	-0.29	-0.22	-0.17	-0.09
3	h	-0.04	-0.89	-0.70	-0.70	-0.69	-0.35	-0.32	0.10
	E	-0.14	-0.58	-0.46	-0.44	-0.50	-0.47	-0.32	-0.06
4	h	-0.64	-1.04	-2.86	-2.33	-1.74	-2.80	-1.38	-1.23
	E	-0.50	-0.76	-2.44	-2.29	-1.59	-2.03	-1.67	-1.11
5	h	-1.53	-2.79	-3.69	-5.44	-2.57	-3.78	-4.29	-4.86
	E	-1.29	-2.44	-4.52	-5.44	-3.06	-4.10	-4.03	-4.43
6	h	-1.30	-0.66	-1.47	-0.92	-1.06	-1.17	-1.11	-2.23
	E	-0.75	-0.82	-1.05	-0.86	-0.97	-0.91	-1.20	-2.17
7	h	-0.75	-1.96	-3.07	-3.59	-2.17	-2.39	-2.22	-4.76
	E	-1.09	-1.45	-1.73	-2.25	-1.94	-2.09	-2.35	-4.80
8	h	-0.82	-0.73	-1.69	-0.93	-0.82	-1.05	-1.07	-1.06
	E	-0.64	-0.72	-0.82	-0.63	-0.72	-0.62	-0.77	-1.26
9	h	-0.99	-1.86	-2.44	-3.02	-2.09	-2.01	-1.73	-4.53
	E	-0.89	-1.29	-1.56	-1.93	-1.76	-1.95	-2.08	-4.24

	125	250	500	1000	2000	4000	8000	16000		
Group A	-0.29	-1.23	-1.53	-0.95	-0.94	-0.85	-0.70	-0.60	-0.89	dB
Group B	-0.99	-1.76	-3.38	-3.88	-2.24	-3.18	-2.84	-2.91	-2.65	dB
Group C	-0.90	-1.19	-1.73	-1.77	-1.44	-1.52	-1.57	-3.13	-1.66	dB

Distances

R	REC-SRC	REC-wall	Distance [m] (extra)	Group
1	9.50	1.50		A
2	4.30	6.70		A
3	8.05	19.05	7.28	A
4	20.66	6.70		B
5	27.50	1.50	24.08	B
6	18.35	1.00		C
7	31.95	1.00		C
8	18.35	1.00		C
9	31.95	1.00	25.15	C

Source 1

Simulation C1 — Single canyon - Original facade (masonry brick surfaces)
SPL [dB(A)] per 1/1 octave band [Hz]

R		125	250	500	1000	2000	4000	8000	16000
1	h	35.63	39.26	41.08	42.77	44.25	34.86	32.90	29.17
	E	35.48	39.58	41.90	43.19	44.40	35.01	32.82	28.87
2	h	35.84	39.64	40.66	43.41	44.44	36.13	33.95	28.66
	E	36.08	39.38	40.19	43.51	44.46	35.67	33.31	28.45
3	h	41.92	41.66	48.70	50.98	50.27	42.37	41.31	39.36
	E	42.13	41.62	48.60	50.98	50.17	42.27	41.41	39.26
4	h	45.19	48.88	54.16	58.91	57.75	49.44	49.07	48.02
	E	45.33	48.93	54.13	58.94	57.65	49.44	49.06	48.02

Simulation C2 — Single canyon - With acoustic LWS modules
SPL [dB(A)] per 1/1 octave band [Hz]

R		125	250	500	1000	2000	4000	8000	16000
1	h	33.49	37.01	37.45	37.24	41.49	30.90	28.86	24.01
	E	34.22	37.31	37.38	38.13	41.43	30.88	28.83	23.96
2	h	35.2	38.41	37.62	40.67	42.61	33.30	31.42	26.98
	E	35.55	38.53	37.45	40.93	42.50	33.29	31.40	26.96
3	h	41.81	41.08	48.62	50.80	49.85	42.00	41.15	39.37
	E	42.03	41.18	48.35	50.65	49.76	41.86	41.19	39.28
4	h	45.61	48.83	53.87	58.72	57.40	49.32	48.96	47.93
	E	45.2	48.76	53.91	58.78	57.44	49.23	48.92	47.95

C2-C1 Comparison
SPL comparison [dB] per 1/1 octave band [Hz]

R		125	250	500	1000	2000	4000	8000	16000
1	h	-2.14	-2.25	-3.63	-5.53	-2.76	-3.96	-4.04	-5.16
	E	-1.26	-2.27	-4.52	-5.06	-2.97	-4.13	-3.99	-4.91
2	h	-0.64	-1.23	-3.04	-2.74	-1.83	-2.83	-2.53	-1.68
	E	-0.53	-0.85	-2.74	-2.58	-1.96	-2.38	-1.91	-1.49
3	h	-0.11	-0.58	-0.08	-0.18	-0.42	-0.37	-0.16	0.01
	E	-0.10	-0.44	-0.25	-0.33	-0.41	-0.41	-0.22	0.02
4	h	0.42	-0.05	-0.29	-0.19	-0.35	-0.12	-0.11	-0.09
	E	-0.13	-0.17	-0.22	-0.16	-0.21	-0.21	-0.14	-0.07

Distances (Source 1)

R	REC-SRC	REC-wall	Group
1	26.10	1.50	B
2	20.90	6.70	B
3	8.55	19.05	A
4	4.06	6.70	A

5	h	41.94	44.46	46.61	53.84	50.93	43.00	42.17	39.29		40.58	42.69	40.07	52.36	49.03	41.09	40.35	37.65
	E	41.78	45.08	46.22	53.43	51.11	42.98	42.10	39.34		41.04	42.89	39.91	52.24	49.08	41.06	40.35	37.63
6	h	34.59	38.23	40.66	42.96	42.62	34.26	32.45	27.54		33.02	37.29	38.39	40.40	41.49	32.08	29.96	23.15
	E	34.11	38.40	41.01	43.20	43.29	34.33	31.81	27.10		33.55	37.72	40.01	41.93	42.17	32.90	30.12	23.34
7	h	36.31	41.42	42.48	47.32	48.65	39.23	37.36	34.14		35.81	41.57	41.82	45.32	47.90	39.07	36.55	32.36
	E	37.17	41.93	43.37	47.18	47.54	39.42	37.31	33.80		36.44	42.14	43.06	46.70	47.14	38.98	36.68	32.46
8	h	33.35	37.31	40.44	41.88	43.29	34.69	33.15	28.45		32.63	37.42	38.34	39.85	40.95	32.02	30.25	23.76
	E	34.39	38.63	41.30	43.65	43.58	34.62	32.21	27.78		33.74	37.87	40.12	42.12	42.23	32.94	30.14	23.29
9	h	36.44	41.49	42.35	47.44	48.69	39.81	37.76	34.00		35.71	41.44	41.66	46.84	48.47	39.46	36.92	33.11
	E	37.27	41.97	43.46	47.24	47.60	39.52	37.33	33.58		36.51	42.21	43.24	46.83	47.27	39.12	36.82	32.55

-1.36	-1.77	-6.54	-1.48	-1.90	-1.91	-1.82	-1.64	10.90	1.50	A
-0.74	-2.19	-6.31	-1.19	-2.03	-1.92	-1.75	-1.71			
-1.57	-0.94	-2.27	-2.56	-1.13	-2.18	-2.49	-4.39	29.95	1.00	C
-0.56	-0.68	-1.00	-1.27	-1.12	-1.43	-1.69	-3.76			
-0.50	0.15	-0.66	-2.00	-0.75	-0.16	-0.81	-1.78	16.69	1.00	C
-0.73	0.21	-0.31	-0.48	-0.40	-0.44	-0.63	-1.34			
-0.72	0.11	-2.10	-2.03	-2.34	-2.67	-2.90	-4.69	29.95	1.00	C
-0.65	-0.76	-1.18	-1.53	-1.35	-1.68	-2.07	-4.49			
-0.73	-0.05	-0.69	-0.60	-0.22	-0.35	-0.84	-0.89	16.69	1.00	C
-0.76	0.24	-0.22	-0.41	-0.33	-0.40	-0.51	-1.03			

Group	A	-0.34	-0.87	-2.28	-0.59	-0.89	-0.82	-0.70	-0.58	-0.88 dB
Group	B	-1.14	-1.65	-3.48	-3.98	-2.38	-3.33	-3.12	-3.31	-2.80 dB
Group	C	-0.78	-0.22	-1.05	-1.36	-0.95	-1.16	-1.49	-2.80	-1.23 dB

Total for simulation C

Group	A	-0.32	-1.05	-1.91	-0.77	-0.91	-0.84	-0.70	-0.59	-0.88 dB
Group	B	-1.07	-1.70	-3.43	-3.93	-2.31	-3.25	-2.98	-3.11	-2.72 dB
Group	C	-0.84	-0.70	-1.39	-1.56	-1.20	-1.34	-1.53	-2.96	-1.44 dB

(A) Top-down view

(B) Side view

Appendix II - Concept designs
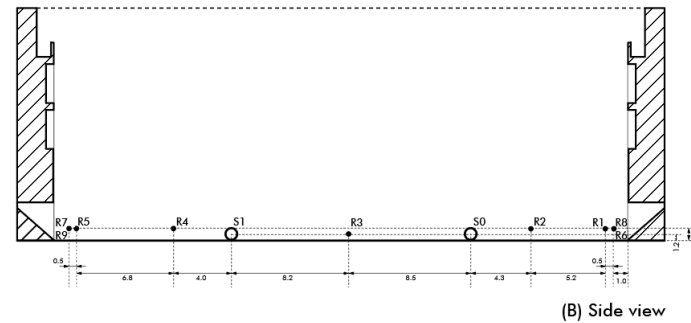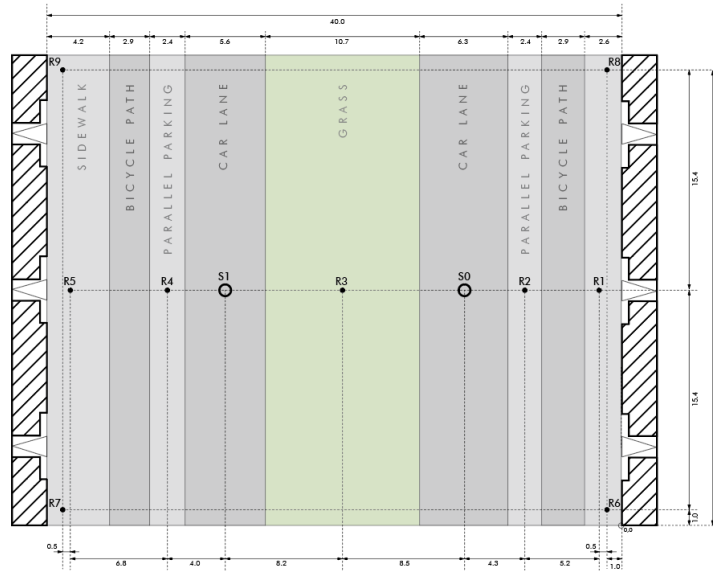
Concept design 1

Design hypothesis

The first concept design was made in anticipation of the P2 presentation. It is possible to utilize the cavity space behind LWS modules for the accommodation of a LF-absorbing system. A parallel array of uniquely tuned quarter-wavelength tubes should be able to elegantly attenuate in the LF-spectrum. The mineral wool as used in the hydroponic LWS is able to absorb in the MF- to HF-spectrum, as well as the vegetation species.

Design of quarter-wavelength tube array

The next step was to design a parallel array of QW-tubes to yield a broadband absorption coefficient. First it was determined what dimensions the tubes should have, and how many tubes were needed. A reference area of 1 m² was considered. The number of tubes and the area could be proportionally scaled up or down afterwards. To analytically determine the absorption curve, a Matlab script was used based on the low-reduced frequency model (Zwikker and Kosten, 1949), developed for the graduation project of Costa (2016). The optimal combination of tubes was found by trial and error.

Effect of adding porous material in the orifice

Figure A II-1 and A II-2 show the absorption coefficients of a parallel array of QW-tubes with a frequency interval of 20 Hz. However, Figure A II-1 and A II-2 show the effect of adding a porous material to the tube. It broadens the absorption bandwidth due to increased flow resistivity, thus increasing the inflection point between two spikes. However, this has the side effect that the absorption peaks decrease significantly.
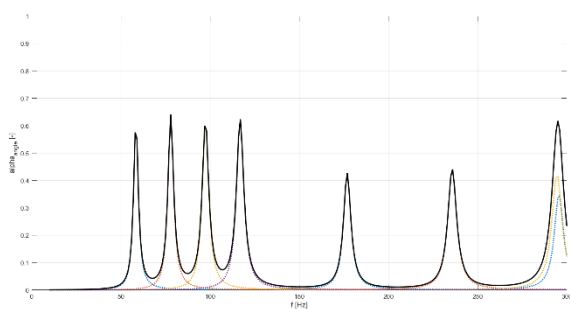
Fig. A II-1 – 20 Hz interval
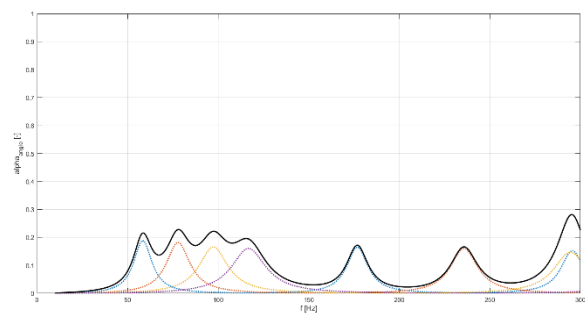
Fig. A II-2 – 20 Hz interval with extra resistance

The effect of decreasing the resonant frequency interval

Figure A II-3 and A II-4 show similar arrangements of a parallel array of QW-tubes with resonant frequency intervals of 20 Hz and 10 Hz, respectively. The differences show that applying a smaller frequency interval, increases the absorption coefficient of the combination.
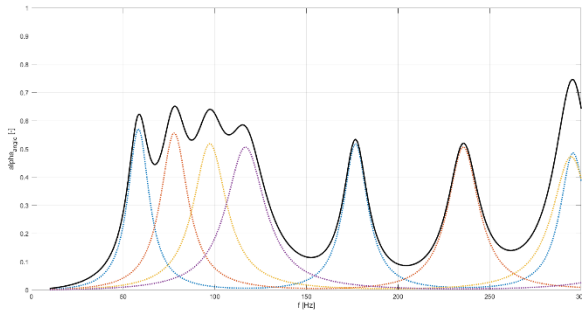
Fig A II-3 – 20 Hz interval
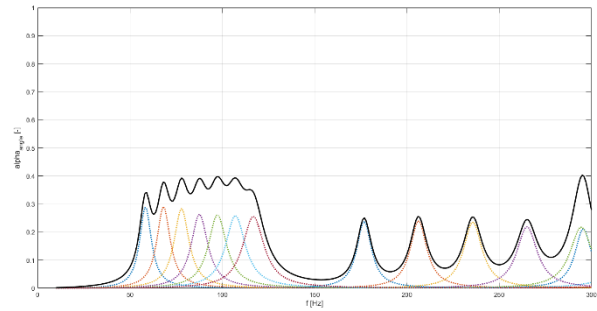
Fig A II-4 – 10 Hz interval

Optimal tube dimensions

For every QW- tube, the length, end correction, and optimal diameter was calculated. This was done by using the Matlab script from Costa (2016). The script returned a 3D plot in which the effective resonant frequency was plotted against the absorption coefficient and the tube diameter. An example of such a result is shown in fig. A II-4: the optimal tube radius for a quarter-wavelength tube resonating at 70 Hz is the apex of the graph.
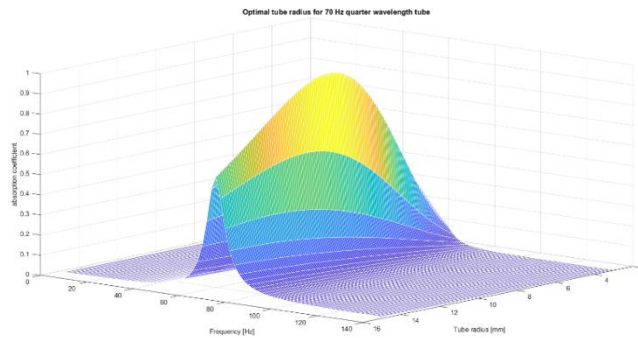
Fig A II-4 – Optimal tube radii

From this trial-and-error study, the following could be concluded (table A II-1):

Strategy	Advantages	Disadvantages
Large resonant frequency intervals	Easier production by the overall less complex design	More tubes are needed for broadband absorption
Small resonant frequency intervals	The absorption peaks merge without the need of a porous material: less tubes are needed to yield broadband absorption	Many tubes with different dimensions are needed, complicating the production

The concept design

For elaboration of the concept design, the strategy using small frequency intervals was used. Because the frequency interval was decreased, no porous material needed to be added. A frequency interval of 2 to 3 Hz was used. A division of 2.5 Hz is prevented to prevent decimal numbers. Using this strategy, the absorption coefficients were predicted (figure A II-5) The design approximately satisfies the list of requirements.
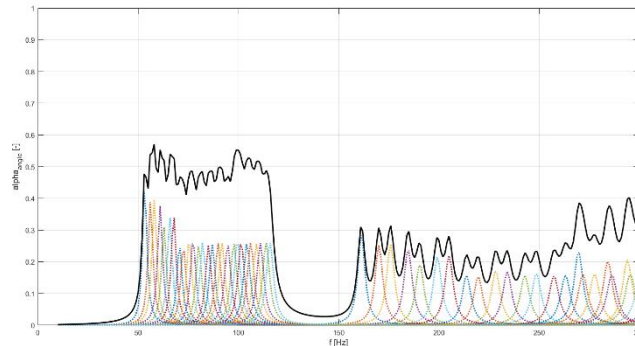
Fig A II-5 – Absorption coefficient results

The reference area was based on the the Flexipanel by SemperGreen, a LWS based on mineral wool. The panel dimensions were 620 x 500 x 100 mm (w x h x d), for an area was 0.3 m². The panel system was to be mounted on two vertical profiles, here assumed to be profiles 50x100 mm wood. This presented a cavity space behind the panel of 570 x 500 x 100 mm (w x h x d). To check whether the volume of the tubes would fit in this space, the sum of the tube volumes was compared to the volume of the cavity. The result was that the tubes, if placed 100% efficient, would inhibit 100% of the cavity volume. This means that, by utilizing 100% of the cavity space for quarter wavelength tubes, the absorption curve can approximately satisfy the absorption objective. Hence, it would theoretically be possible to add a quarter wavelength tube array to a living wall system element which could absorb low frequency sound.

In an attempt to model this, a Rhino 3D-model was made using Grasshopper. In the cavity space, a cloud of points was generated, which could be consequently used as anchors to manually wrap polylines around. The polylines were then used as the axial guidelines from which pipes were extruded. Thus, the quarter wavelength tubes were manually formed and placed as efficiently as the design skills allowed.

Figure A II-6 shows how the concept design is built up. Here, it is shown in (1) and (2) that the space in between the two vertical profiles is fully used to accommodate all different QW-tubes. (3) and (4) show how the tubes pierce the mineral wool panel, to receive the incident sound wave.
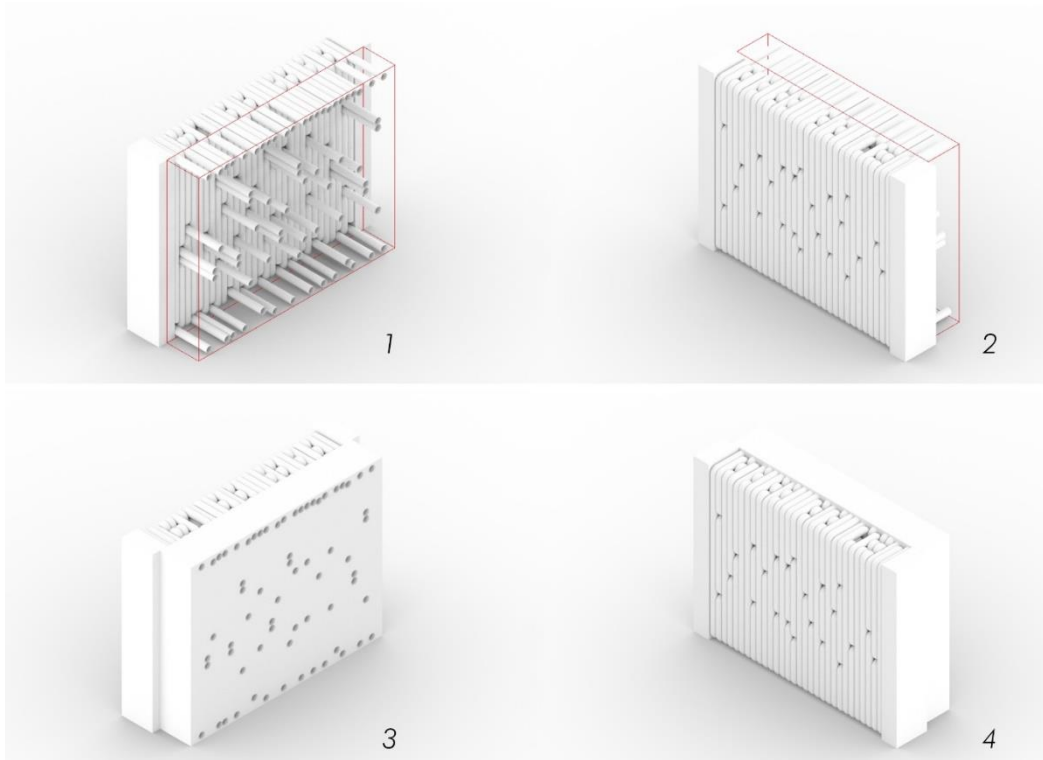
Fig A II-6 – 3D views of concept design geometry.
(1)   shows the front axonometry, with the VGS artificial wool panel wireframed in red
(2)   shows the back axonometry, with the VGS artificial wool panel wireframed in red
(3)   shows the front axonometry, with the tubes sticking through the VGS artificial wool panel
(4)   shows the back axonometry, with the tubes sticking through the VGS artificial wool panel
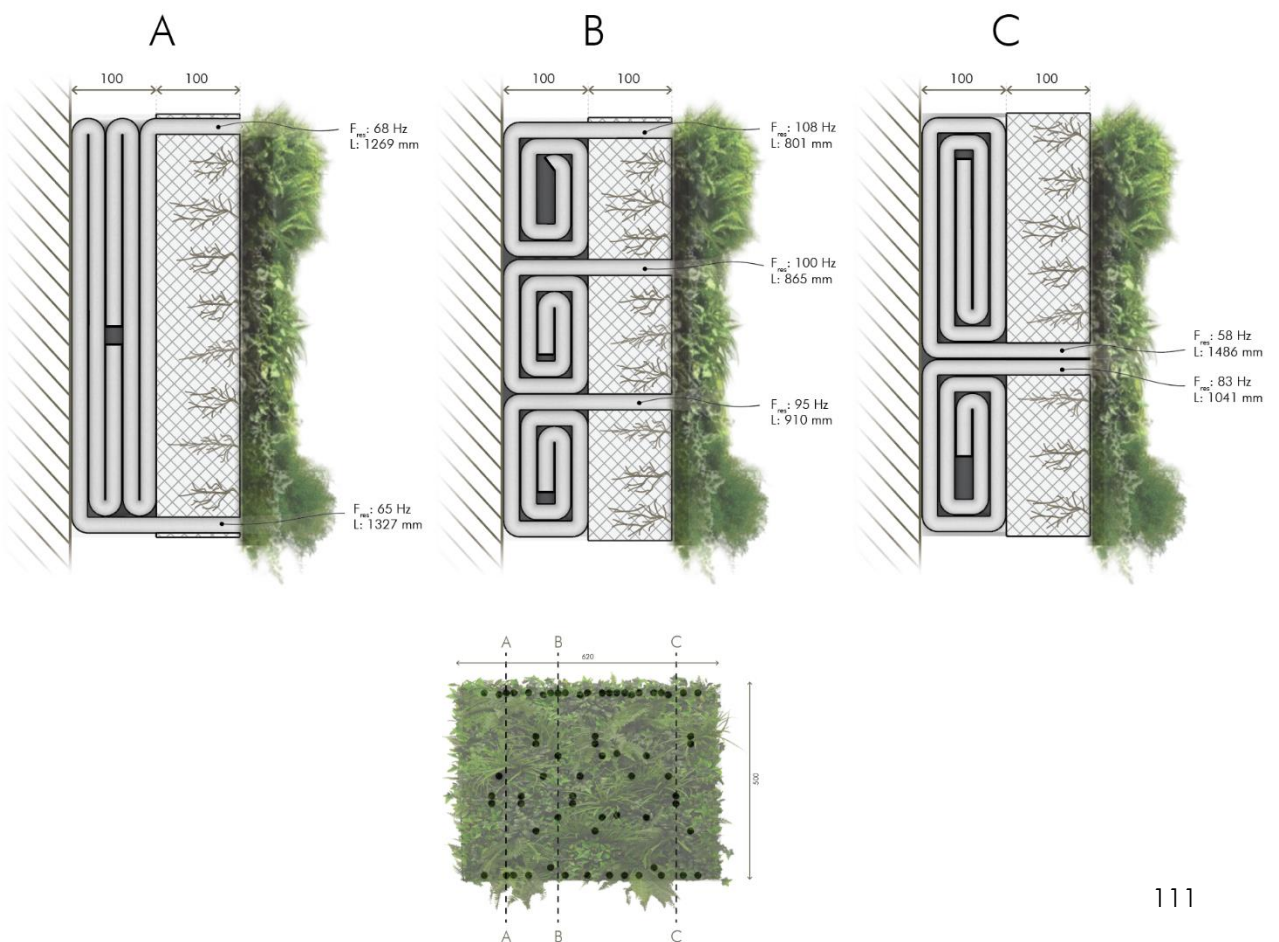
Fig A II-7 - Sections

Figure A II-7 shows three vertical sections A-A, B-B, and C-C. Not all the tubes could be placed. The cavity was filled without accommodating all the tubes needed to yield the absorption as displayed in figure A II-8. It was found that the placed tubes used only 71% of the available cavity volume.
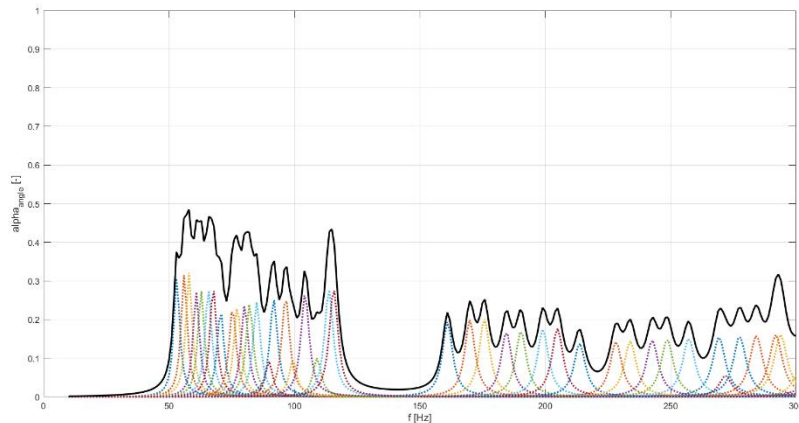
Fig A II-8 – Final result

Design evaluation

The first concept design regards the integration of a parallel array of QW-tubes in the cavity space of a mineral wool LWS. QW-tubes were manually placed in the cavity space. Ultimately, the entire cavity space was utilized, but not all tubes could be placed. In the design process it was discovered that combining tubes of different lengths is quite complicated. The geometry is more complicated than was initially assumed. Additionally, it was found that the placed tubes used only 71% of the available cavity volume. This is because the tubes have a circular cross-section, and therefore always have voids in between them. The result is a fairly inefficient design, which has an insufficient absorption performance, as shown in figure A II-8.

Therefore, the conclusion must be drawn that the implementation of QW-tubes does not work sufficiently enough. The tubes are too bulky, and the design is too complicated for mass production.

Concept design 2

Design hypothesis

The first concept design did not satisfy the list of requirements. Therefore, a different LF-absorber system is selected for the second concept design: the Helmholtz resonator. Hence, it is possible to apply a parallel array of Helmholtz resonators inside the cavity area of a mineral wool LWS. Similar to concept design 1, the necks of the resonators will pierce the substrate layer.

Design process

To elaborate on this concept idea, a workflow was developed using Rhino, Grasshopper, GhPython, and Matlab. This report will not go into too much detail of the actual script. Instead, a global explanation on its operation is given.

Input

First, the script requires a domain in which the LF broadband absorption should take place. For example, the domain of 50-204 Hz can be set with frequency intervals of 4 Hz. This means that Helmholtz resonators will be generated using the input of 50 Hz, 54 Hz, 58 Hz, etc.

Resonator dimension optimization

The idea was to design a number of individual Helmholtz resonators with rectangular cavities of different sizes. The reason for this size variation, is so that the resonators could be tuned to resonate at different frequencies. Together, these resonators could yield a broadband absorption. Resonators can be tuned by altering the resonator dimensions of the cavity and/or the neck. First, constraints were set on the dimensions of the resonator cavities, to create a modular system that fits together efficiently. Inspiration was taken from the LEGO® system. Hence, the resonator cavity dimensions are multiples of a fundamental size of 25x25 mm. This ensured that the different resonators could be packed efficiently. The cavity depth is the same for all types, here 150 mm is assumed.

Resonator type	A	B	C	D
Cavity depth [mm]	150	150	150	150
Cavity width [mm]	25	50	50	75
Cavity height [mm]	25	25	50	50

Table A II-2
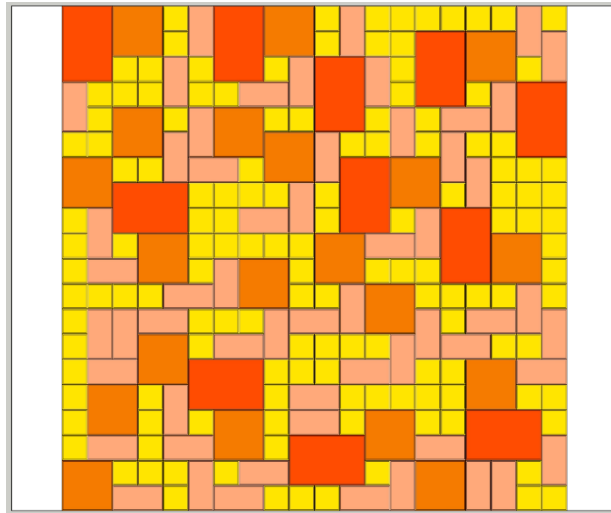
Fig A II-8 – Resonator types in module

Only four different resonator cavity dimensions were assumed. Now, the next parameter was considered: the neck size. As the resonator neck had a fixed length of 100 mm, tuning to a specific resonant frequency can be done by altering the orifice radius. Here, too, constraints had to be set, such as the minimum and maximum orifice radius and manufacturing tolerances have to be assumed. For example, for the script, a minimum orifice radius of 4 mm was assumed. Any smaller than that could lead to blockages. The maximum orifice radius was set to 8 mm. Also, the minimum radius increase was set to 0.1 mm.

Now, the boundaries in which the resonators can operate are set. The boundary is the range in which the resonator can resonate, based on its cavity dimensions and its maximum and minimum orifice radius. Consequently, an optimization can be performed. To utilize the space in the LWS cavity as efficiently as possible, it was aspired to select a Helmholtz cavity that was as small as possible. The optimization procedure is depicted in figure A II-9. Ultimately, the smallest suitable resonator cavity is selected. The input frequency is compared to the lower and upper limits of the resonator cavities (see table A II-3 and figure A II-9). Certain values were assumed, such as a depth of 150 mm, minimum orifice radius of 4 mm, maximum orifice radius of 8 mm, and neck length of 100 mm.

Fig A II-9 – Helmholtz cavity optimization

Resonator type	A (25x25 mm)	B (50x25 mm)	C (50x50 mm)	D (75x50 mm)
F_{res} lower limit [Hz]	135	93	64	52
F_{res} upper limit [Hz]	265	184	127	103

Table A II-3

To illustrate the optimalization, suppose we want to generate a Helmholtz resonator that resonates at 100 Hz. Hence, the input is 100 Hz. The script looks at table A II-3, and finds the resonator types which can resonate at 100 Hz. Resonator cavities D, C, and B are all suitable to resonate at this frequency, using different orifice radii. Yet, resonator B is selected, since this has the smallest resonator cavity footprint.

Orifice placement optimization

Based on the previous steps, a list will be generated with optimized resonators (see figure A II-10). Then, by using the GenePool (the purple slider array in figure A II-10), the number of each resonator could be adjusted. This in turn created a list which has a branch per resonator type, indicated by the curly brackets {}. In these branches, every individual resonator is given a unique number. For instance, resonator 203.7-4 is the fourth Helmholtz resonator, resonating at 203.7 Hz, and has cavity dimensions of 25x25x150 mm with an orifice radius of 5.9 mm.
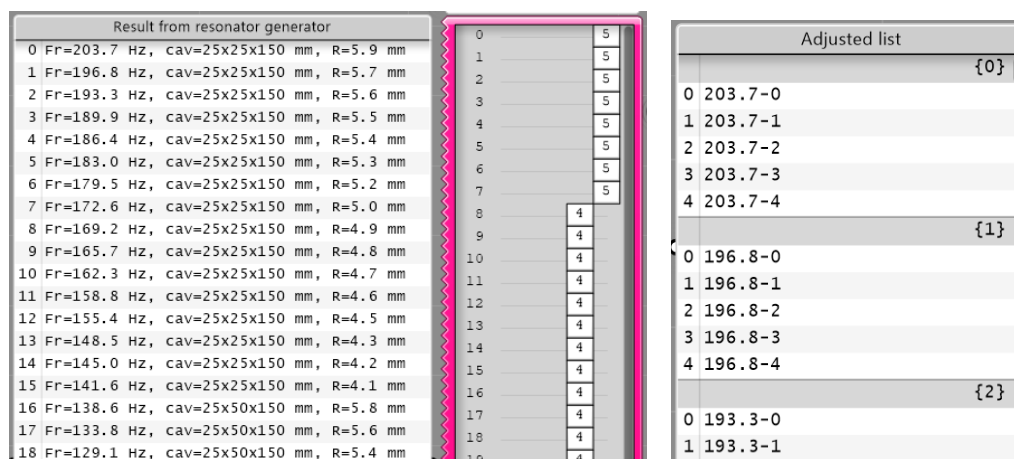
Fig A II-10 – Grasshopper lists

Now that the complete input list was generated, all resonators could be placed inside the LWS cavity area. To achieve this, a packing algorithm is designed. Ultimately, the packing algorithm is a loop that attempts to place the 2D resonator cavity geometry on a grid. The size of the grid is the size of the LWS cavity, which is subdivided in squares of 25x25 mm. At every iteration, the script checks whether the space it has randomly selected is available for resonator placement. If not, it attempts up to 20 times in different locations. The largest resonators (50x75 mm) are placed first, and the smallest (25x25 mm) are placed last, because these can fill up any remaining space.
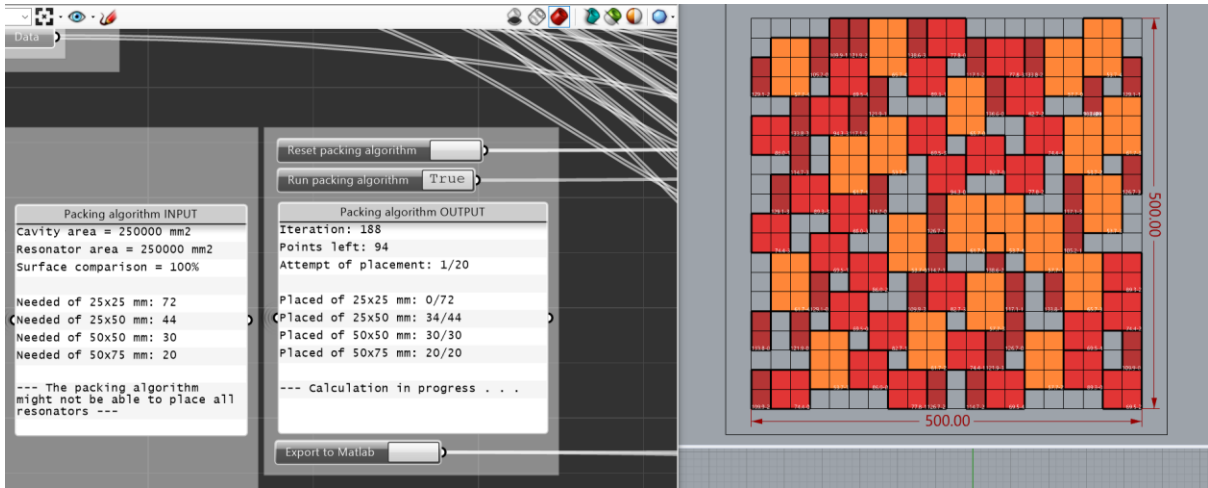
Fig A II-11 – Grasshopper algorithm

This algorithm thus generates the parallel array of resonators, provided the total resonator area does not exceed the grid area.
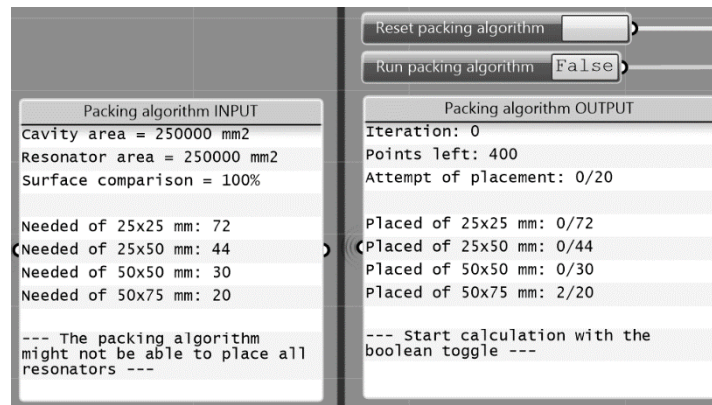
Fig A II-12 – Grasshopper algorithm information

Next, orifices with optimized radii were placed at the centre points of the placed Helmholtz resonators. These circles would mark the spot where the mineral wool substrate layer of the LWS would be perforated. The problem that arose was that the perforations were evenly distributed, leaving little space for the planter inserts to be placed. The issue is illustrated in figure A II-13 A & B. To resolve the problem, the orifices of the type A resonators (25x25 mm) were assigned a certain 'gravity' that attracted the orifices of the bigger resonators. This altered the placement of the orifices.
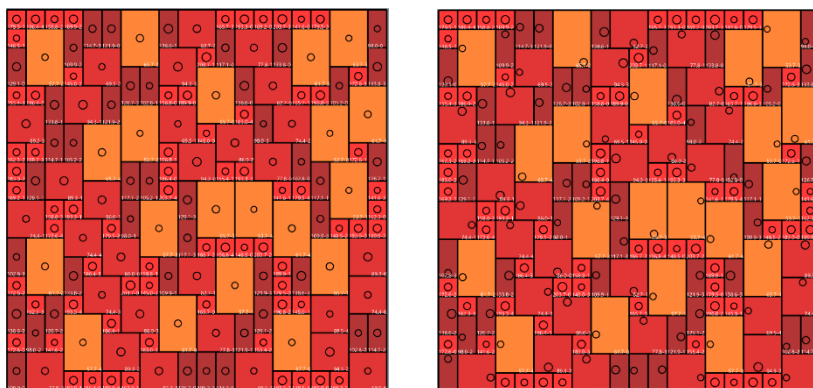
Fig A II-13 A & B – Orifice placement

Figure A II-14 shows how bringing together the resonator orifices opens up more free space. This allows the planter inserts (cylinders of R=35 mm) to be placed more evenly. Figure A II-14 shows the generated planter placement before and after the orifice placement optimization.
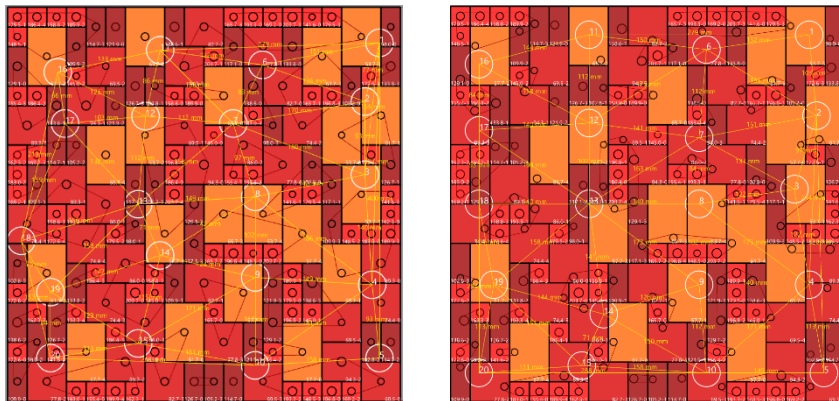
Fig A II-14 A & B – Planter insert view

Figure A II-15 A & B show the structure behind the placement optimization. In the optimized view, a lot more placement options (red points) for the planter inserts can be seen. The white points are the available points that are closest to an even grid of 4x4 planter inserts.
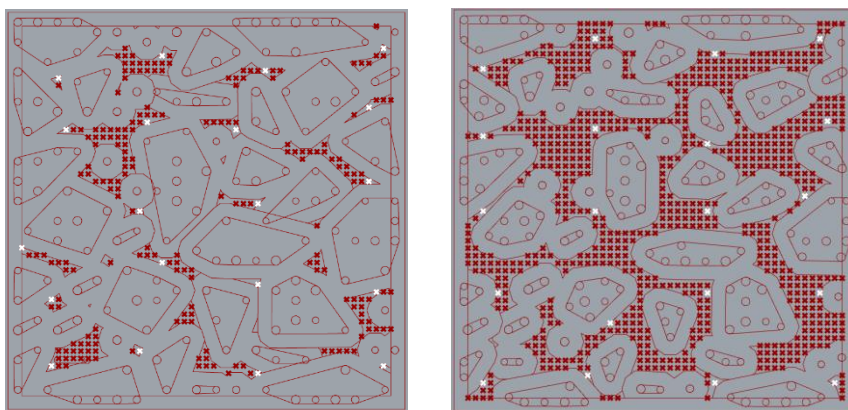
Fig A II-15 A & B – Structure behind the planter insert placement

Analytical prediction of absorption coefficient

Finally, the geometry could be baked to Rhino. The total Grasshopper definition will not be included in the appendix, but is available on request. To analytically validate the absorption coefficient, a link was made from the Grasshopper script to Matlab. In Grasshopper, relevant data such as the Helmholtz resonator dimensions and numbers were entwined into a branched dataset. This was exported into a .csv-file using a custom C#-definition. In Matlab a script was written that could calculate the combined acoustic impedance and absorption coefficient of an array of Helmholtz resonators. The data stream was imported and were set as the equivalent parameter values. The Matlab script then gave figure A II-16 as output. The absorption coefficient seemed promising.
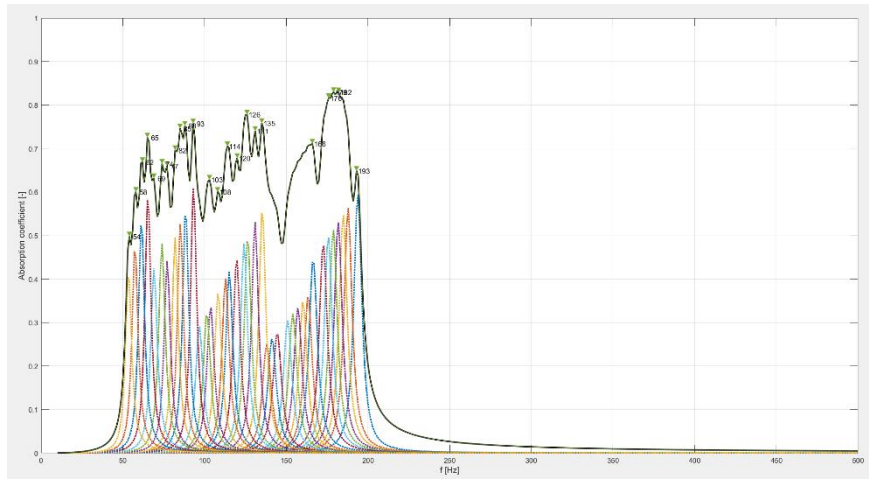
Fig A II-16 – Final absorption coefficient results

The final design is displayed in figure A II-17.
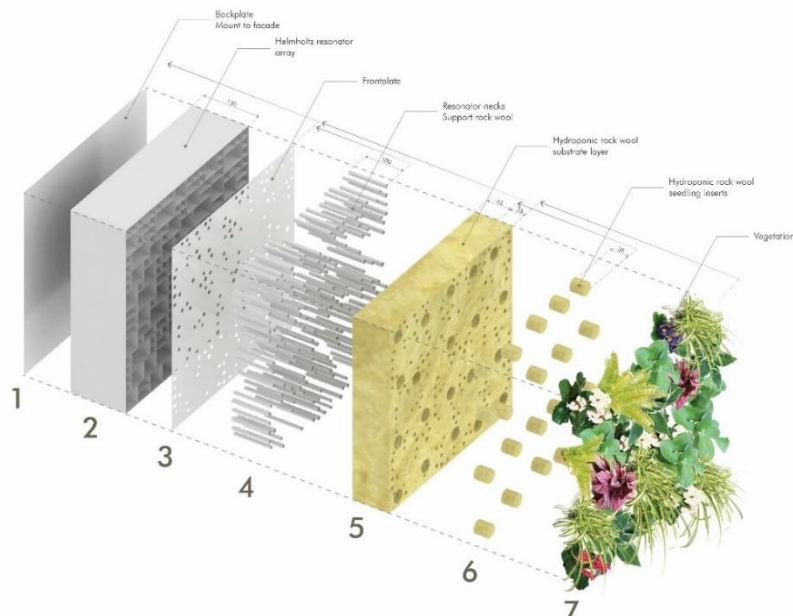
Fig A II-17 – Exploded design view

Design evaluation

The workflow for the second concept design has resulted in an automated script that could generate the design. The design yielded a fairly satisfactory absorption coefficient in the LF spectrum. However, regarding design simplicity and manufacturability, the design is quite complicated. Even considering the production of a prototype was complicated. The crux is in the fact that the resonators are all individual enclosed volumes. This uses a relatively high amount of material, meaning the product would be heavy, and complication for transportation and installation. Additionally, using this much material would mean a higher embodied energy. Ultimately, the design would work in theory, but not in practice.

Concept design 3

Design hypothesis

Concept design 2 was too complicated. Therefore, the aim of concept design 3 was to simplify the LWS design. Hence, it is possible to produce a broadband compact absorber (BCA) by backing the substrate layer with a perforated plate. This perforated plate is a parallel array of Helmholtz resonators with a continuous cavity. To increase the mass in the neck, lateral orifices can be made. In this scenario, the plant layer can attenuate the high frequencies, the substrate layer can attenuate the middle to high frequencies, and the resonator can attenuate the low frequencies.
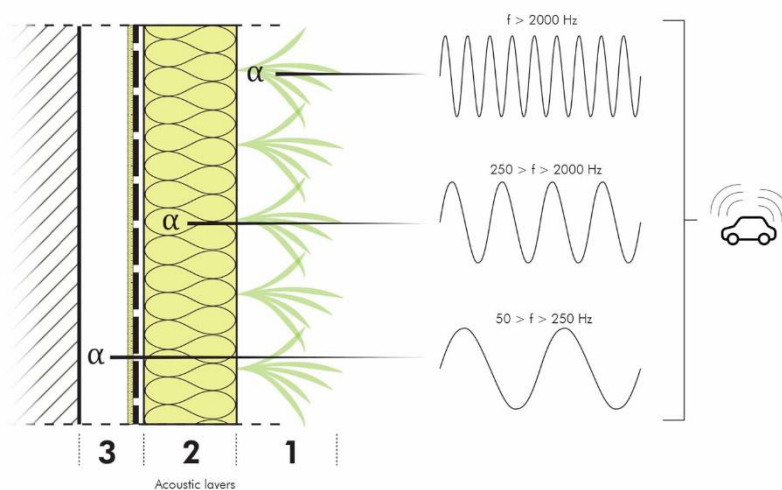
Fig A II-18 – Concept 3

Discovery of alternative Helmholtz arrays

Both concept designs 1 and 2 were too complicated because of the large number of geometries. At the time of the development of the third concept design, the literature on perforated sheets was reviewed. The perforated sheet (not micro-perforated) is a parallel array of Helmholtz resonators that is relatively easy to produce. It essentially is a sheet with large perforations, backed by an air cavity. The primary advantage is that the resonator cavity walls are omitted. Instead, the resonator cavity dimensions are determined by the orifice spacing. A build-up of pressure at the invisible cavity boundaries makes the particle velocity locally equal to zero.

Here, the resonator was combined with a porous absorbent, to create a broadband compact absorber (BCA). As explained before, a BCA combines the resonant LF-absorption peaks of a resonator with the high MF- and HF-absorption of a porous absorber. In case of the LWS, the mineral wool substrate layer can be used as the porous absorber, and this can be backed by a resonator tuned for LF-absorption. The potential advantages of this design were:

- No perforations through the substrate layer
- This in turn allows complete freedom to place more planter inserts

- The resonator is much simpler to be manufactured, and uses a minimum amount of material

- It makes the LWS module a more light-weight product

- The total LWS thickness is reduced

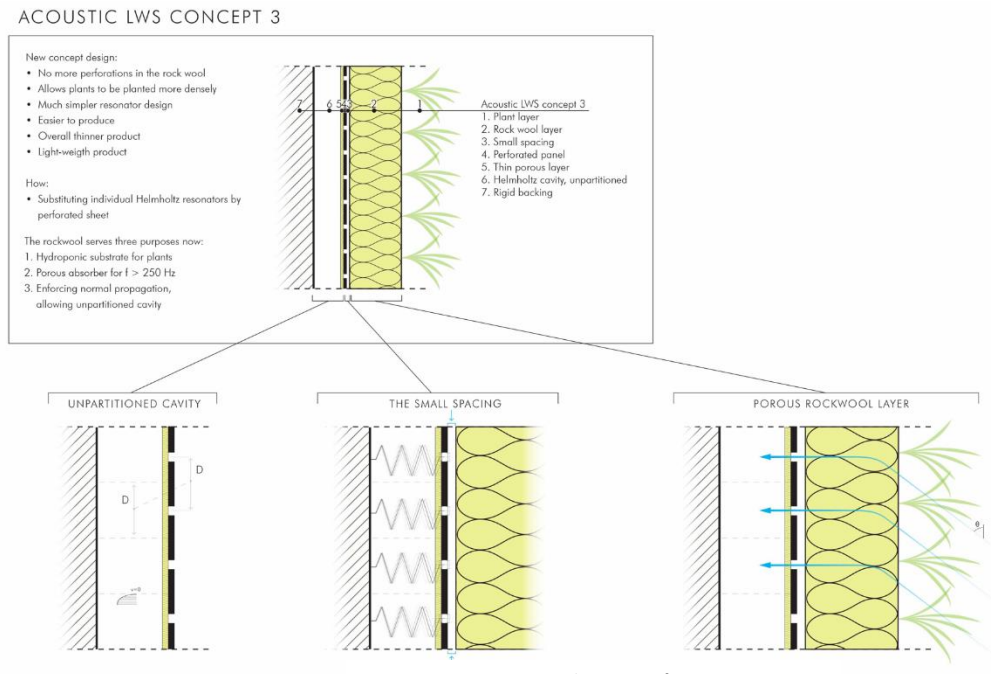The design proposal was visualized, see figure A II-19

Fig A II-19 – Explanation of concept 3

The unpartitioned cavity is only possible if the propagation direction is normal to the surface. For random incidence, lateral propagation will occur inside the continuous cavity, affecting the absorption coefficient. This problem can be solved by application of non-locally reacting media, such as a porous material. The substrate layer, made of hydroponic rock wool, can enforce normal propagation as a result of internal acoustic refraction.

An additional problem was the resonant frequency of the perforated plate. For mass-spring systems, the mass factor needs to be relatively big to resonate at low frequencies. Two parameters can be altered to increase the mass factor: the neck length and the orifice radius. However, increasing the orifice radius also inversely influences the spring stiffness, ultimately increasing the resonant frequency. Therefore, the only remaining parameter to be changed, was the neck length. How can the length of the necks be increased in case of a perforated plate? Increasing the plate thickness was a solution. However, the plate thickness cannot be increased to sufficient extents, as the weight would be too high. An alternative solution was proposed, named the lateral orifice (figure A II-21). The idea was to introduce a second perforated plate, which was placed in front of the first perforated plate. The second plate was offset in the Y-direction. In theory, a sound wave that interacts with the lateral orifice has to propagate laterally to enter the resonator. This increases the effective neck length, without increasing the thickness of the system.
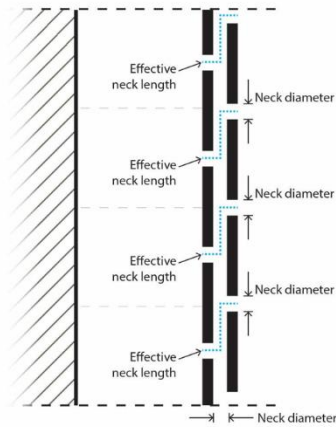
120

Fig A II-20 – Lateral orifice

Would this design actually work? The available theory was not sufficient to strongly confirm whether the made assumptions were correct. As a result, a few questions were asked:

- Can the incident sound wave reach the resonator through the void matrix of the porous layer?
- How does moisture in the porous substrate layer affect this propagation?
- Does the unpartitioned cavity need to be enclosed at its boundaries?
- Does the resonator need to be offset by a small spacing to allow for the Helmholtz mass to overshoot (due to inertia of the oscillation)?
- Can the porous layer enforce normal propagation?
- Can the lateral orifice concept increase the effective neck length?

These questions led to performing the impedance tube measurements, discussed in chapter 6.

Design evaluation

Concept design 3 has applied a parallel Helmholtz array with a continuous cavity in combination with a porous layer. The porous layers served three purposes: absorbing in the MF/ HF-spectrum, enforcing normal propagation to the resonators, and being a substrate in which plants can root. The concept was simple in its design, but extremely complex for acoustic absorption prediction. From the experimental validation, it can be concluded that constructing such a multilayer system does work. However, the design does not yield satisfactory absorption coefficient in most scenarios. The height of the resonating peaks is dependent on the porosity of the porous absorber. Therefore, the LF absorption is insufficient when the substrate contains moisture. Also, the lateral orifices do not work as intended. This would mean that either the perforated plate would need to be very thick (to make mass high), or inward necks must be made. It was found that perforating the substrate layer with a long neck (as in concept design 2) actually yields better results. Therefore, concept design 3 is rejected.

Concept design 4

Design hypothesis

Concept design 3 did not satisfy the Program of demand, because the Helmholtz resonator performance depended on the saturation rate of the substrate. Hence, the resonator necks should pierce the substrate layer. It is still possible to make a continuous cavity, however, the cavity should be filled with a non-reactive medium to prevent lateral propagation in the cavity.

Helmholtz neck piercing through the substrate layer

At the time of the development of this concept design, the Helmholtz equations were scrutinized in detail. It became clear that increasing the resonator orifice area not only influences the mass, but also the spring. It was concluded that the resonator necks should be long and narrow, to yield a low resonating frequency. Concept design 3 does not allow for long necks, because it considered perforated plates. Concept design 4 will piercing the long necks through the substrate layer for the following reasons:

- This allows the application of long resonator necks (for low resonant frequencies)
- This allows the resonators to oscillate without being influenced by moisture in the substrate
- This creates a suspension system, which suspends the substrate layer can structurally

Furthermore, the new concept design needs to implement a non-reactive medium to prevent lateral propagation in the cavity. Concept design 3 used the substrate layer in part for enforcing normal propagation. In the new case, one of two solutions can be applied. Firstly, the necks can be filled with a little bit of porous material. Secondly, the cavity can be filled with a porous layer. To investigate which solution would be best, both solutions were analytically tested.
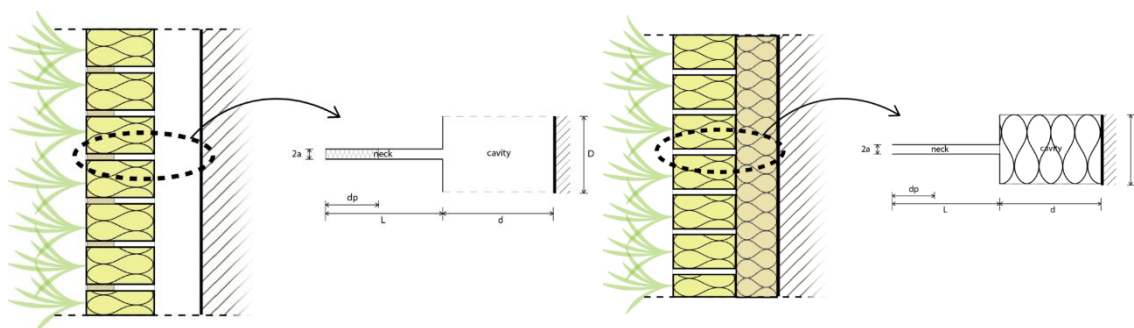

Fig A II-21 A & B – Placement of porous material

Figure A II-21 shows the scenario where the neck is filled with porous material. A Matlab script was developed. Here, R_i was determined using a material thickness of 50 mm and a flow resistivity of 5000. Also, the cavity was filled with air. Figure A II-22 shows the absorption coefficient. The cure is extremely broad and flattened out, to the point that the resonator does not absorb sufficiently. This can be explained by the fact that adding porous material to the neck increases the visco-thermal absorption and dampens the resonator oscillations. Consequently, the curve becomes wider, but its peak is also decreased. This scenario

of adding 50 mm of porous material in the necks (which is approximately needed for enforcing normal propagation), is therefore no suitable solution.
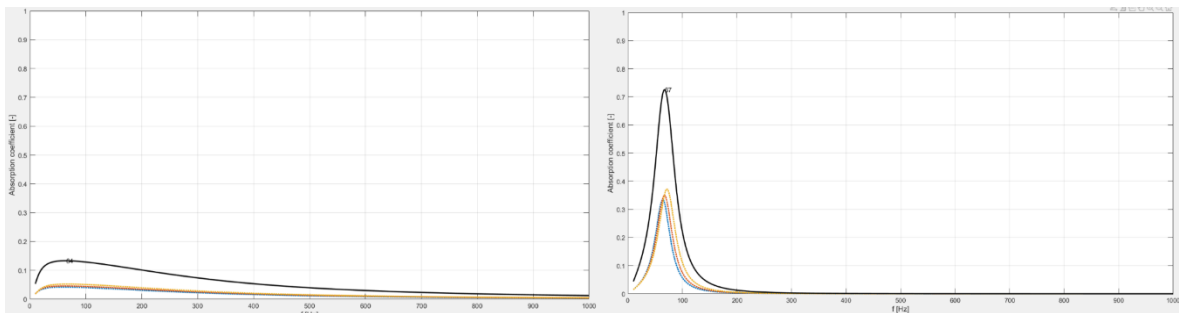

Fig A II-22 A & B – Matlab results

Secondly, the cavity was filled with a porous material, while the necks contained only air. Similarly, a layer thickness (in this case equal to cavity depth) of 50 mm was used, also using a flow resistivity of 5000. This yields an absorption as depicted in figure Fig A II-22 B. The absorbing peak is locally high, around α=0.72 for at 67 Hz. The comparison with the first scenario shows that filling the cavity with a porous material yields high resonant absorption, while still preventing lateral propagation in the LWS cavity.

Resonator size

Next, it is the objective to determine how many resonators are needed. This design does not apply individual Helmholtz cavities, and therefore, the cavity size mainly depends on the distance between orifices. This raises the question: what would be a better design: one large resonator, or many smaller resonators that have an equal resonator area? The answer was not directly obvious, hence, a Matlab live-script was developed. Consider two resonator configurations with equal resonator area of 5625 mm^2:

- Resonator configuration A: 1 Helmholtz resonator with cavity dimensions 75x75x50 mm, orifice radius 6.6 mm. The absorption is depicted in figure A II-23 A

- Resonator configuration B: 9 Helmholtz resonators with cavity dimensions 25x25x50 mm, orifice radius 2.1 mm. The absorption is depicted in figure A II-23 B.
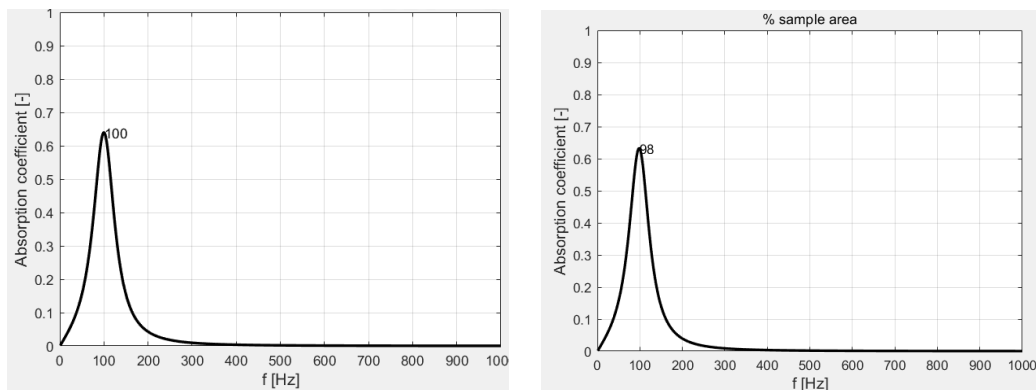

Fig A II-23 A & B – Response of different resonator configurations

Figures A II-23 A & B show similar resonant peaks, of around $\alpha=0.63$ at 100 Hz. Therefore, it does not matter how many resonators are used, as long as the resonator area is equal. This is because the absorption coefficient is calculated over the sample area. Both scenarios yield the same acoustic performance. However, configuration A requires only one Helmholtz neck, while configuration B requires 9 resonator necks. The better design is the simpler design, since this can be produced more easily and is therefore more cost-effective.

Hence, the bigger the resonator, the better. In the limit, the LWS could accommodate a single big resonator of 550x550 mm. However, this would not work, since the orifice would have to be enormous, and the absorption bandwidth is too narrow. The PoD requires the design to absorb in a spectrum roughly between 63-250 Hz. Therefore, subdividing the cavity width of 550 mm and height of 550 mm into 5 equal parts yields 25 resonators per module of dimensions 110x100 mm. Figure A II-24 shows the visualization of this concept.

Cavity filled with porous layer
to ensure normal propagation

Penetrating resonator necks
on rigid plate

Hydroponic rock wool
substrate layer

75

100
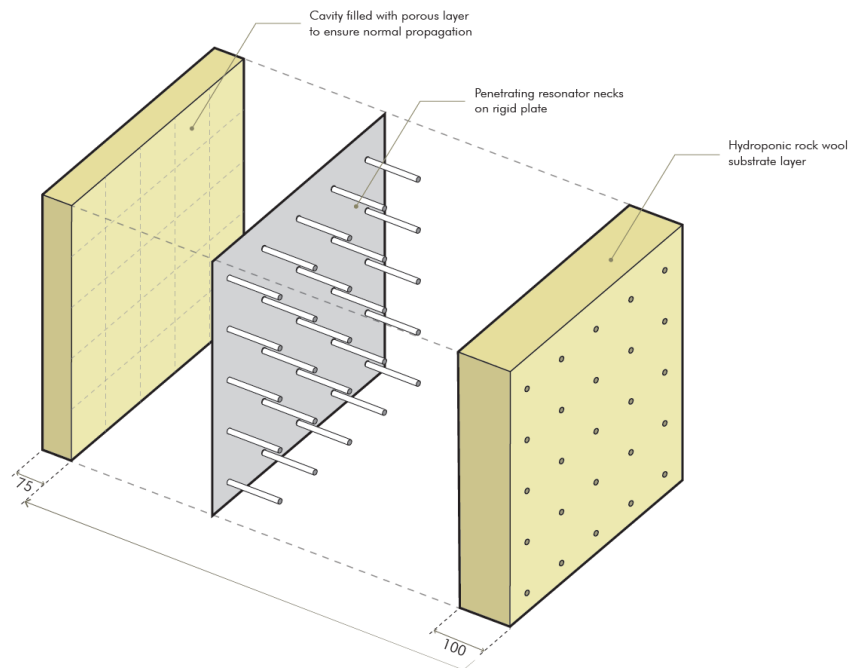
Fig A II-24 – Concept 4

The moisture problem

The next challenge to be solved was the absorption coefficient of the substrate. An increase of moisture inside the porous layer decreases the porosity. Consequently, the absorption coefficient is negatively affected. A quasi-hydroponic mixture can be made by mixing-in perlite, to increase the pore size distribution and drainage capability. However, these solutions cannot be applied to mineral wool, since it is already very porous on its own. It does not compact over time. Hence, the solution is simply to prevent moisture as much as possible.

To find out how moisture propagates in rock wool, an experiment was done. Water was dripped on a specific point on a block of hydrophilic rock wool (figure A II-25 A). The schematized version is depicted in figure A II-25 B.
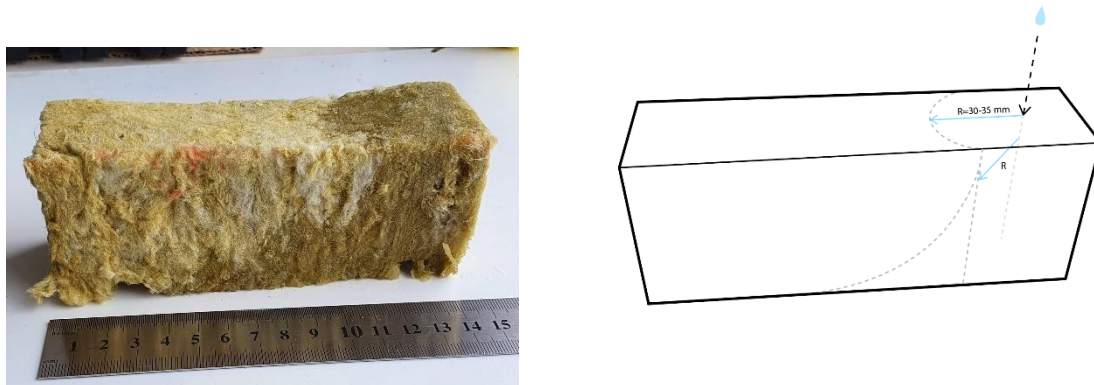

Fig A II-25 A & B – Moisture in rock wool

It was observed that moisture expands in two directions. First, the capillary action of the rock wool determines the radial expansion. This expansion has a limit of 30-35 mm. Additionally, the moisture propagates downwards in the rock wool, due to gravity. However, when the moisture reaches a hard boundary, in this case the table on which the rock wool sample lies, the moisture cannot continue. Hence, the moisture moves laterally. When it moves laterally, in this case to the left, it encounters still dry material. Therefore, the capillary action propagates it upward for a maximum of 30-35 mm. This sequence of phenomena generates a sort of trumpet shape.
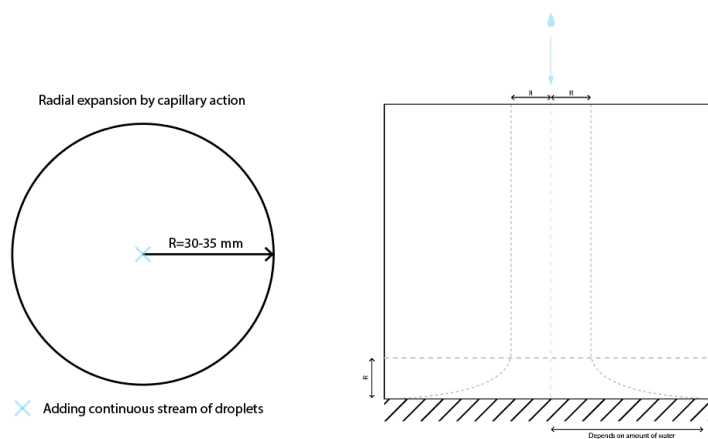
Fig A II-26 – Capillary propagation

From this, the following can be concluded:
- It is possible to locally irrigate, due to a maximum radial expansion of 30-35 mm
- A hard boundary propagates the moisture laterally. Therefore, not too much water must be added.

The amount of water that must be added, is approximated in table A II-4. The saturation rates are assumed. The sample volume was assumed to be a cylinder of 80 mm thickness, and a radius of 35 mm (308 cm^3).

Scenario	Saturation rate	Water volume
Winter	15%	45 ml
Summer	60%	175 ml

Table A II-4

Based on the research, an irrigation system is proposed (figure A II-27. Normally, mineral wool LWS are irrigated from a single hose from the top of the module. This saturates the entire rock wool layer and a substantial amount of water is not absorbed by the plants. Essentially, it is a simple irrigation system, but water is wasted and the mineral wool is saturated in places where it does not need it.
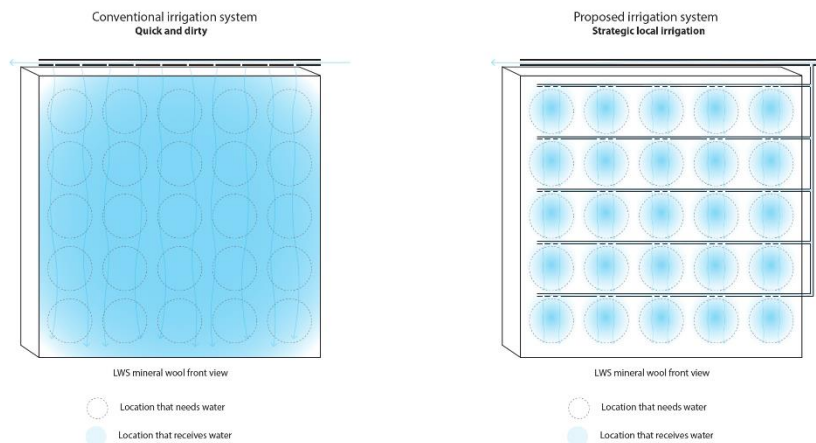
Fig A II-27 – New irrigation system

The proposed system uses a branch of lateral irrigation lines, that irrigate locally at the plant's roots. This ensures that the LWS contains only as much moisture as it needs for the plants to grow. This has several advantages:

- Less water is wasted, saving on the water bill
- Less nutrients are needed, saving in costs, and the piping is subject to less congestion
- The LWS is more light-weight, putting less structural strain on the facade
- The plants on the top and on the bottom of the LWS receive exactly the same amount of water
- Most importantly, the mineral wool is dry on more than 50% of its surface area, which enables high acoustical absorption at all times
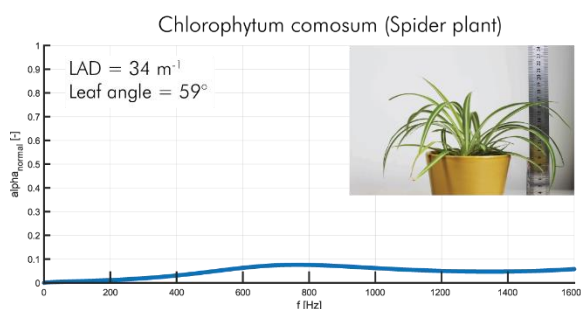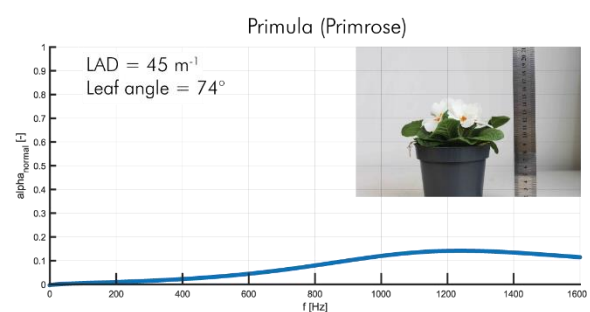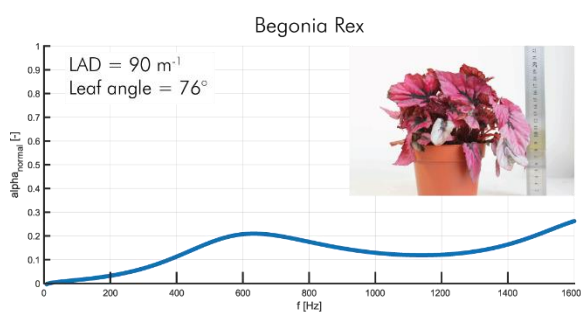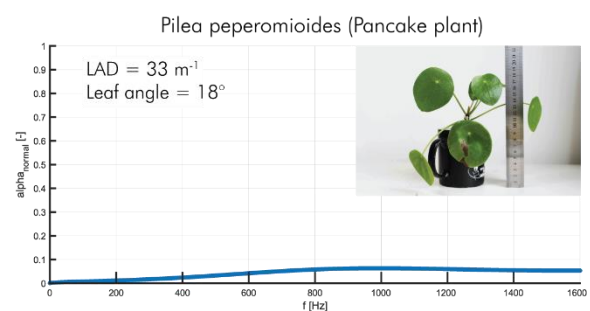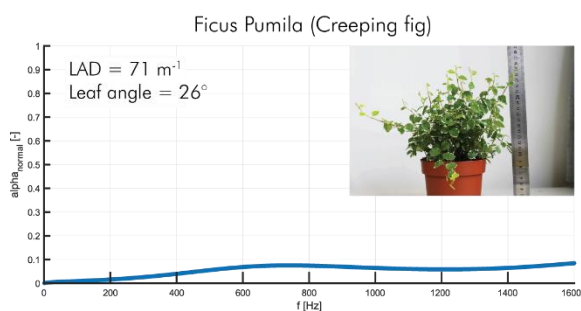
Design evaluation

Concept design 4 is essentially the combination of concept designs 2 and 3. Piercing the substrate layer with the resonator necks allows for a high absorption coefficient in the LF-spectrum. The Helmholtz resonators do not have individual resonator cavities, which is advantageous for many reasons. Instead, the cavity is filled with a porous layer of glass wool. The irrigation system that consists out of a branch of lateral lines has many advantages, including ensuring the supply of just enough water to feed the plants, but also to leave the module overall as dry as possible. Analytically, the concept design seems to be able to yield a substantial broadband absorption. Overall, the concept design has the potential to become the final design. Therefore, the design will be elaborated in the final engineering phase.

Appendix III - Research on plants

Research on plant species

Leaf area was determined by taking high-resolution pictures of flattened out leaves, using a transparent sheet. These photos were imported in Adobe Photoshop, where the histogram was used to count the pixels. Additionally, the pixels in a 1 cm² square were counted. Using 3 leaves per plant, the average leaf area was determined. Next, the number of leaves per plant were manually counted. For the creeping fig, the number leaves on 3 rachides were counted, after which the total number of rachides was counted. Multiplying the average leaf area by the average leaf count yielded the total leaf area per plant. Then, the outer dimensions of the plant canopies were measured (height and footprint), to yield the canopy volume. Dividing the total leaf area by the canopy volume, yielded the leaf area density (LAD). Additionally, the leaf angles were measured (leaf plane orientation compared to tangent plane) to predict the tortuosity, and the porosity of the canopies was assumed between 0.96-0.99. The values were imported into a Matlab script, which yielded the absorption coefficients.

Ficus Pumila (Creeping fig)

LAD = 71 m⁻¹
Leaf angle = 26°

Pilea peperomioides (Pancake plant)

LAD = 33 m⁻¹
Leaf angle = 18°

Begonia Rex

LAD = 90 m⁻¹
Leaf angle = 76°

Primula (Primrose)

LAD = 45 m⁻¹
Leaf angle = 74°

Chlorophytum comosum (Spider plant)

LAD = 34 m⁻¹
Leaf angle = 59°

Selection of shade-loving plants (sciophytes)

Species	Photo	Estimated acoustic potential
Bergenia cardifolia		★★★
Hosta Sieboldiana		★★★
Heuchera		★★★
Primula		★★★
Begonia		★★★
Philodendron scandens		★★★
Viola sororia		★★★
Adiantum pedatum Polystichum Nephrolepis exaltata		★★

Pachysandra terminalis		★★
Hecherella		★★
Tiarella cordifolia		★★
Pieris japonica		★★
Campanula poscharskyana		★
Lysimachia nummularia 'aurea'		★
Lamium maculatum		★
Euphorbia amygdaloides		★

Selection of sun-loving plants (heliophytes)

Species	Photo	Estimated acoustic potential
Campanula lactiflora		★★
Hedera helix		★★
Salvia argentea		★★
Impatiens walleriana		★★
Scabiosa caucasica		★★
Pelargonium zonale		★★
Lobelia x speciosa		★
Nasturtium officinale		★

Soleirolia soleirolii		★
Chlorophytum saundersiae		★
Bergenia cardifolia		★
Euphorbia amygdaloides		★
Festuca glauca		★
Helianthemum		★
Bacopa cordata		★

Appendix IV - Low-frequency noise in urban street canyons

Low-frequency noise in urban street canyons

In urban areas, vehicular traffic is a primary source of noise. The residents and pedestrians that use this urban space are consequently exposed to higher noise levels. This chapter summarizes the relevant factors that determine in how this traffic noise is perceived by humans, both in the urban street canyon, and in adjacent canyons.

Vehicular traffic noise

When regarding vehicular traffic noise, two predominant source representation groups can be distinguished, which are rolling noise and propulsion noise (Czyzewski and Ejsmont, 2008). Rolling noise is the sound generated by friction between the tires and the road surface, and propulsion noise is the sound generated by fuel combustion in internal combustion engines (ICE), transmission, and exhaust. When regarding linear sound levels, the propulsion noise is primarily low-frequency with its peaks between 50-100 Hz (Mahn, 2011), see figure A IV-1. Killengreen and Olafsen (2007) performed over 2100 in-situ traffic noise frequency spectrum measurements, i.e., more than 3,500,000 vehicles cumulatively. They conclude that here is always a peak in the 50 – 100 Hz frequency range.
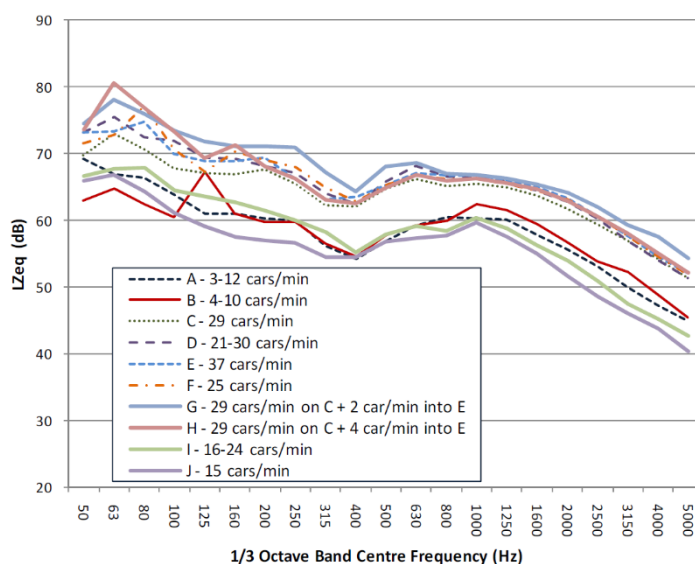

Fig. A IV-1 – Experimental results (LZeq) of in-situ measurements of New-Zealand road traffic at various traffic flows (from Mahn, 2011)

This is exemplified in detail by the study of Can et al. (2010). They have researched the frequency spectrum of road traffic in an urban street canyon. Experimental in-situ measurements were compared to static and dynamic numerical models (63Hz – 8kHz), to find the discrepancies and limits of the numerical models. The urban street canyon was the Cours Lafayette in Lyon, France, which is a three-lane one-way road with 5 intersections with traffic lights (S1– S5). The straddling facades were 5 stories high. The average traffic flow was about 1400 vehicles per hour. First, experimental measurements were taken at multiple positions (P1 – P4) at ear level.
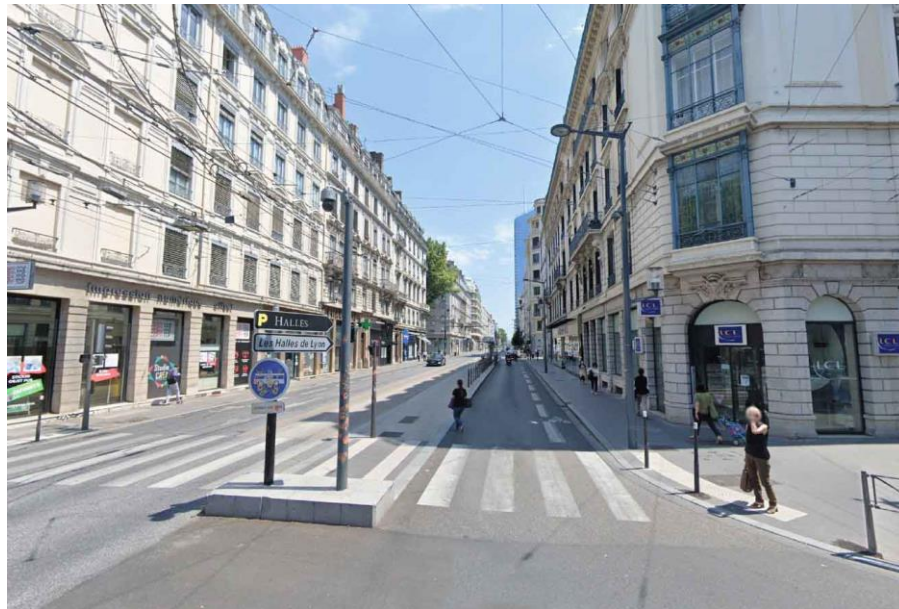

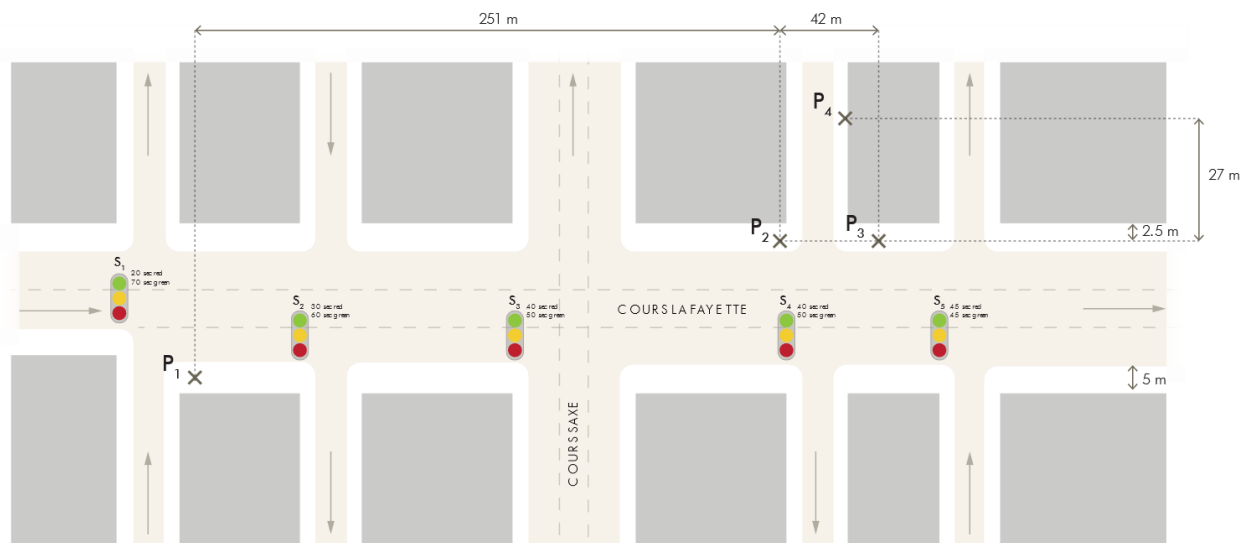Fig. A IV-2 – Cours Lafayette from the crossing with le Cours Saxe (Google Maps)

Fig. A IV-3 – Urban street canyon of Cours Lafayette and the receiver positions of the experimental set-up (from Can et al. 2010)

135

A static model estimates a mean vehicle speed by means of a traffic flow and does not consider the deceleration and stopping of vehicles at stoplights. For this study Harmonoise model (Peeters and Van Blokland, 2007) was used, assuming a mix of light-weight vehicles and buses. A dynamic model takes the effects of deceleration and stopping at traffic lights in consideration, by regarding individual vehicle kinematics as a function of time (e.g. 1 sec intervals). In this study, the SYMUVIA model was used. All results (LZ_{eq} in linear sound pressure levels) are shown in figure A IV-4.
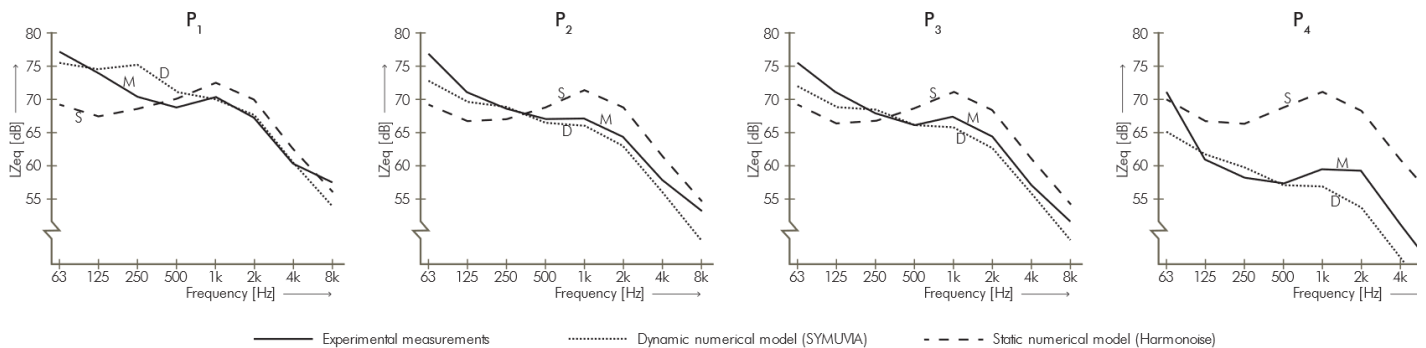

Fig. A IV-4 – Comparison of experimental, dynamic -, and static models of traffic noise (from Can et al. 2010)

Firstly, the sound levels tend to decrease per increasing frequency band for all three methods and for almost all positions. Between 63 Hz and 8 kHz, sound levels decrease at least 20 dB. The frequency spectra of
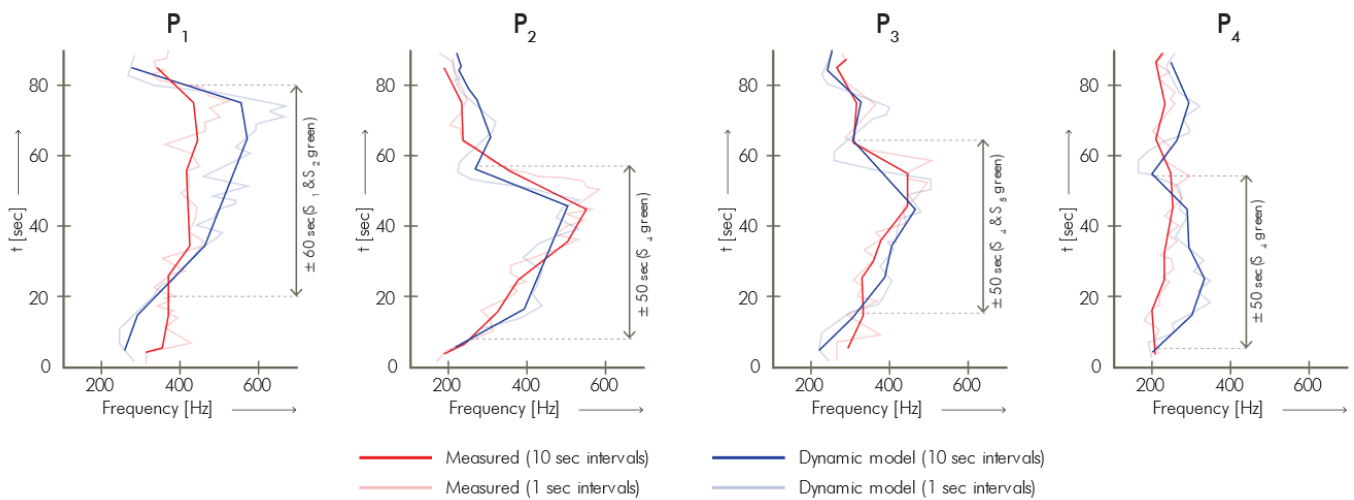
Fig. A IV-5 – Avg. center of frequency spectrum as a function of time (from Can et al. 2010)

position P2 show a less pronounced peak in the 1000 – 1200 Hz region. This can be explained by the fact that there is less rolling noise and more propulsion noise, because vehicle speed is low or even zero due to the near traffic light. The frequency spectra of position P4, located further down a perpendicular street, show that the overall SPL is decreased, but not for low frequencies. This shows that in urban street canyons, the low frequencies propagate further. It also shown that the static model overestimates the LZeq (equivalent sound pressure level without frequency weighting) significantly, most probably due to an overestimation of the actual traffic speeds (since stand-stills and deceleration are not accounted for).

In the diagrams above, the average centre of the frequency spectrum is shown as a function of time. The dark red and blue graphs show the average frequency shift with 10 second time intervals, while the light red and blue graphs show the same, but with 1 sec intervals. It is shown in all graphs that the time the graphs increase to overall higher frequencies correspond approximately to the time the nearby traffic light(s) are on green. This shows that higher vehicle speeds induce sound level peaks on higher frequencies, and vice versa, low to no vehicle speed induce sound level peaks on lower frequencies. Since this dynamic behaviour of vehicles is not accounted for in the static model, it systematically underestimates the low-frequency sound levels. It is demonstrated that the dynamic model follows the experimental measurements much closer. Hence, the dynamic model is more accurate than the static model and therefore outperforms it. Many studies on traffic use a static traffic model, because it is less complex.

Similarly, the study from Buratti and Moretti (2010) performed experimental in-situ measurements of road and rail traffic on several types of Italian road- and railways. They found that urban roads with a continuous traffic flow and a velocity above 50 km/h had a peak around 1000 Hz, which can be correlated to the high proportion of rolling noise in the frequency spectrum. Conversely, on urban roads with overall low vehicle velocities due to traffic lights and roundabouts, the low-frequency range had an increased peak in the sound levels, and a decreased peak in the 1000 Hz region.

The low-frequency problem

Humans do not perceive all sound frequencies equally loudly, but rather react more sensitively to a narrow frequency spectrum associated with human speech (Salter, 1998). This roughly entails that low (<200 Hz) and very high (>5 kHz) frequencies are perceived to be less loud. To illustrate this, suppose a test environment in which many different test sounds of different frequencies and of different loudness are played to a large group of people. Their objective it is to report the sounds that appear to sound equally loud. When these individual sounds with perceived equal loudness are all connected with a line, so-called equal loudness contours (ELC) develop for different sound levels (Porges, 1977).

However, the application of the A-weighting on vehicular traffic noise is disputed. Humans react to sound on a highly subjective manner which cannot be simplified to a numerical measure. For example, the research of Van Renterghem and Botteldooren (2016) studied the effect of outdoor vegetation on urban noise perception. They reported that being surrounded by greenery can lower the chance of being annoyed by noise. Aside from that, many factors influence sound perception, including psychological disturbances, age, recognizability of the sound, intermittence, and the amount of low-frequency sound (Porges, 1977).

This last factor illustrates that noise with a high portion of low-frequency in its spectrum is perceived to be more annoying than overall higher frequency noise (Leventhall et al., 2003). Persson and Björkman (1988) have performed a laboratory experiment to research the annoyance of low-frequency noise, i.e., a signal with a peak in the sound levels below 200 Hz. They experimentally tested the reported annoyance of 98 subjects, using four continuous fan noises at 80, 250, 500, and 1000 Hz as noise sources. The results (fig A

IV-6) show that the low-frequency noise is most annoying, which was in accordance with their literature review. Following from this, they conclude that the dB(A) scale underestimates the negative perception that people have for low-frequency noise.

Similarly, Fuchs (2013) argues that the perception of the low-frequency spectrum in noise dominates, especially in the more remote vicinity around the source. The A-weighting conceals this problem, as humans might not detect low-frequency sound at equal loudness, yet perceive it as more annoying. This is illustrated by the equal annoyance contour (Persson and Björkman, 1988). Additionally, sound absorbing materials and insertion losses are usually measured down to 125 Hz, which results in overestimated single-number ratings, such as the weighted absorption coefficient (aw). Such averages do not account for human noise perception (Fuchs, 2013).
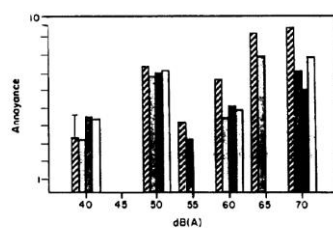

Figure 2. The average value of the 1–10 annoyance scale, related to the dB(A) level of the exposure noises. ▨, 80 Hz; ▦, 250 Hz; ▧, 500 Hz; □, 1000 Hz.
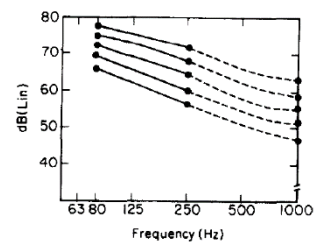
Figure 5. Curves of equal annoyance.

Fig A IV-6 – LF annoyance, from Persson & Björkman, 1988

To illustrate the concealing effect, suppose the application of the A-, B-, and C-scales on the linear SPL results as found by Can et al. (2010). The measurement results from microphone position 1 (see fig A IV-3) and the frequency weighted results are depicted in fig A IV-7. From this comparison, it can be observed that the low-frequency representation (up to 1000 Hz) is substantially divergent, to the point that the A-weighted results show only a peak in the 1000 Hz octave band.

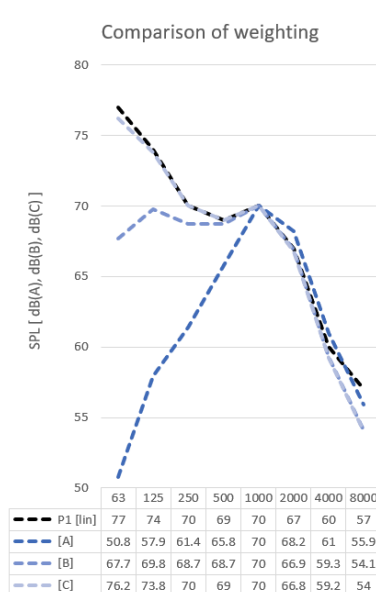|	63	125	250	500	1000	2000	4000	8000
P1 [lin]	77	74	70	69	70	67	60	57
[A]	50.8	57.9	61.4	65.8	70	68.2	61	55.9
[B]	67.7	69.8	68.7	68.7	70	66.9	59.3	54.1
[C]	76.2	73.8	70	69	70	66.8	59.2	54

Fig A IV-7 – Applied weighting on linear sound levels

The archetype of the urban street canyon

Urban environments are globally characterized by a city fabric in which population and traffic density are relatively high. A common example of such an environment is the urban street canyon. This term is defined by a narrow street with the facades of buildings lined up continuously along its sides (Vardoulakis et al., 2003). The geometrical ratios of such urban street canyons determine its type. The height of the canyon walls H can be related to the width of the street W, known as its aspect ratio. If this ratio is < 0.5, it is known as an avenue canyon; if it is equal to 1 it is a regular canyon; and if the ratio is > 2 it is a deep canyon. Theoretically, urban street canyons can have infinite length. However, in practice, the canyon has a finite length L as defined by its endpoints at two major intersections.

Noise in urban street canyons

Krimm (2018) has researched the architectural possibilities on how to resolve high noise levels in urban street canyons. Two strategies exist for reducing the noise levels:

1. Adding angled reflective surfaces that can reflect sound waves away, e.g. towards the sky
2. Adding sound absorption to reflective facades

Sanchez et al. (2016) have numerically tested the effects of e.g. inclined facades, adding balconies, low barriers, and substantial facade prominences. They conclude that the building shape can reduce noise levels in urban street canyons. However, Krimm (2018) argues that these interventions do not represented the daily practises of architects and engineers. Unusual shapes requiring customized production methods are costly to apply, especially for retrofitting projects. For example, a facade shape cannot simply be retrofitted so that it will incline. In the case that it is possible, the inward inclination would be at the expense of usable/rentable floor area. Realistically, angling facade surfaces in urban street canyons is a solution that is out of scale with the actual noise problem. Instead, the application of acoustically absorbing materials to a facade is realistically the best solution for retrofitting projects. Adding acoustically absorbing materials to the urban street canyon can make a substantial difference in noise levels. This is because the materials that are usually applied to facades, are mostly close to acoustically rigid (Davis et al., 2017; Thomas et al., 2013). The table below shows the absorption coefficients of some of the most common facade materials (Van der Linden et al., 2011):

Material	α per octave band [Hz]					
	125	250	500	1000	2000	4000
Concrete (unfinished)	0.02	0.03	0.03	0.03	0.04	0.07
Masonry brickwork	0.05	0.04	0.02	0.04	0.05	0.05
Cement plaster on masonry wall	0.02	0.02	0.03	0.04	0.05	0.05
Ceramic tiling	0.01	0.01	0.01	0.02	0.02	0.02
Glazing 6 mm	0.10	0.06	0.04	0.03	0.02	0.02
Hardwood panelling on 25 mm cavity	0.30	0.20	0.15	0.10	0.10	0.05

Because of these highly reflective parallel surfaces, sound continuously propagates in the canyons as a result of multiple reflections (Thomas et al., 2013). These multiple reflections increase reverberation times and sound levels in and around the canyon. Compared to free-field conditions, the multiple reflections amplify the sound levels (Van Renterghem et al., 2012). This is due to time-weighted sound levels (Leq), which are determined using equation IV-1:

$$L_{eq} = 10 \log_{10} \frac{1}{\Delta_T} \int_{0}^{\Delta_T} \left(\frac{L_p(t)}{P_0} \right)^2 dt \qquad \text{(IV-1)}$$

Where ΔT is the time interval and L_p is the instantaneous sound pressure level. Thus, the time interval which is chosen determines for a large part the resulting L_{eq}. This fact is of interest for the measurement of sound pressure levels in reverberant spaces, such as urban street canyons. For example, consider two similar urban street canyons A and B with similar sound sources on the street level. Canyon A has acoustically reflective materials on the surfaces, while canyon B has substantial amounts of acoustic absorption on its canyon walls. Noises in canyon A will continuously reflect and therefore do not decay quickly. Meanwhile, noises in canyon B will be absorbed quickly and continuously reflect to a smaller extent. A time interval must be determined for L_{eq}-measurements in the canyons. Relating the different continuous sound levels in both canyons to the same time interval, yields a higher L_{eq} in canyon A, and a lower L_{eq} in canyon B.

An additional phenomenon that can occur, is the effect of standing waves. When a sound wave, or multiples thereof, fit exactly in the canyon width, standing waves or modes occur. This happens when the sound waves continuously reflect, and interfere with the opposite travelling wave. At the positions where the opposite traveling waves are in phase, amplified peaks occur. Where they are 180 degrees out of phase, the net result is zero due to destructive interference. When standing on the positions of the nodes, and the low-frequency sound level will be over-emphasized (Salter, 1998). This effect of traffic noise in urban street canyons with reflective materials is a serious problem (Vladimir and Madalina, 2019), since the amount of noise pollution is not expected to decrease.

Why continuous reflections cause higher sound levels

When a continuous sound is emitted by a source, such as the noise of an air conditioning, the sound pressure levels (SPLs) are stable. However, most noise sources in the urban environment are dynamic, and the SPLs fluctuate. For instance, it is complicated to read the real-time SPL when measuring the sound of children yelling at a playground. To yield a more practical SPL measurement, time weighting is done (Salter, 1998). Using time weighting, a short but loud sound can yield the same SPL as a subdued sound that sustains for longer. Similarly, two sounds of equal loudness but with different decay times yield two different time-weighted SPLs. Whereas L_p represents instantaneous SPL, L_{eq} is the equivalent continuous sound pressure level which corresponds to the received sound energy, averaged over a time window (LAeq when A-weighted).

Concluding: How does traffic noise affect people in and near urban street canyons?

- Noise pollution is a major health problem in places where a high number of people are exposed to high traffic density, such as in the urban street canyon. It represents a narrow street with the acoustically hard facades lined up along its sides.
- The noise can propagate to neighbouring canyons by 'bending' over roof edges, due to diffraction.
- Here, the major noise source is low-velocity vehicular traffic. The noise is mainly generated by the propulsion systems, generating a broadband noise, primarily low-frequency with a peak between 50-100 Hz.
- Meanwhile, the human hearing has maximal sensitivity for frequencies between 200-5000 Hz. The A-weighting is generally applied to compensate for this sensitivity. However, although humans perceive lower frequency sounds as being less loud, lower frequency sounds are more annoying than higher frequency sounds. Hence, applying an A-weighting on low-velocity vehicular traffic noise obscures the relative probability of annoyance.
- To solve the noise problem, architectural interventions can be taken. For instance, the shape of a building can be inclined so that it reflects the traffic noise towards the sky. However, constructing these unusual shapes are costly. Alternatively, the application of acoustically absorbing materials to a facade is a relatively low-cost measure.
- Replacing reflective materials by absorbing materials decreases reverberation times. When regarding time-weighted sound pressure levels, a shorter decay time yields lower sound levels.
- Concluding, high traffic flows in urban street canyons cause substantial levels of low-frequency noise, which continuously reflects in the canyon and propagates to nearby canyons by diffraction. The high noise levels cause noise annoyance in residents and pedestrians, and in turn increase long-term health problems.

Appendix V - Reflection

Reflection

1. How is your graduation topic positioned in the sustainable design studio?

Noise pollution is the second largest environmental cause of health problems. In this graduation project, an architectural product is designed that can lower the burden of environmental noise. Hence, increasing the acoustic absorption of vertical greening systems is a topic that that fits in the scope of the design studio.

2. How did the research approach work out? And did it lead to the results you aimed for?

The objective of the approach was to become acquainted with the most used methods in acoustics research. That is: developing a Matlab script to predict the acoustic absorption, performing impedance tube measurements, performing reverberation room measurements, and running acoustic simulations. Even though combining all these different approaches meant a tight schedule, it worked out. The advantage is that the different approaches increased the reliability. For example, the impedance tube measurements yielded useful results to improve the Matlab script.

Ultimately, the low-frequency absorption of a VGS was improved. However, not to the extent that I hoped for. The research proofs that absorbing frequencies, particularly <100 Hz, is extremely hard.

3. What is the relationship between the methodical line of approach of the graduation studio and your chosen method?

The chosen method in this research is mostly a quantitative process, where concept designs are developed and consequently evaluated. That is in line with the approach of the graduation studio.

4. How are research and design related?

Research and design are closely related. Reviewing the literature has formed the basis for the list of product criteria, and also inspired the hypothesis. When the concept designs did not work out, a new design hypothesis was formed, based on more literature research. The methods of validation also originated from literature research.

5. Did you encounter ethical issues or dilemmas during the process?

The best way to solve a problem is to tackle the issue at the source. In the case of noise pollution, it would be best if vehicular traffic would generate less noise. However, solving this would require solutions on a legislative scale. That is not within the reach of the architectural engineer.

6. To what extent are the results applicable in practice?

The results from the Matlab script and the acoustical simulation are directly applicable in practice. These results describe the performance of the product that can be applied to facades. The experimental measurements were primarily performed to prove whether certain phenomenon would occur. For example, in the reverberation room test, the prototype did not have the materials and layer thicknesses

of the final product (rockwool thickness was 50 mm, while the final product would have a hydroponic rock wool of 100 mm with an Aqua Breath geotextile layer). The results only described whether or not the resonators would yield a combined absorption with the substrate layer.

7. **To what extent has the projected innovation been achieved?**

    Prior to the final design, it was still unknown to what extent the low-frequency noise could be absorbed. It turns out that absorbing in lower frequencies (<100 Hz) becomes increasingly more difficult, since Helmholtz resonator dimensions become increasingly large. There therefore is a limit for absorbing in the LF-spectrum. It was found that an absorption of $\alpha>0.5$ could only be yielded for approximately $f>80$ Hz.

8. **Does the project contribute to sustainable development?**

    Yes, the project presents a product that can help in solving many environmental issues in the urban fabric (urban heat island, low biodiversity, high noise levels, etc.).

9. **What is the socio-cultural and ethical impact?**

    The objective of the project is to redesign a vertical greening system into an even more multi-disciplinary solution. By doing so, vertical greening might become more popular. Hence, it promotes building owners to apply vertical greenery to their facades.

10. **How does the project affect architecture and the built environment?**

    The project presents a VGS design that can be applied to the exterior of buildings. It is primarily designed for facades of an urban street canyon. The project promotes facade greening in this context.

11. **How did you translate the feedback of your mentors into your work?**

    The mentors have given useful feedback in all stages of the process. The first mentor was consulted on a weekly basis, and gave most guidance on all facets of the graduation project. The mentors have consulted a lot on the methods, and proposed me to read certain literature.

12. **What have you learned in the graduation process?**

    I am happy that I have developed as a building physics engineer, and extremely thankful for the experiments that I was able to perform. In the process, I have learned not to be scared of difficult mathematical formulas. They often seem more difficult than they actually are.